SEISMIC DELINEATION OF THE SOUTHERN MARGIN OF THE MIDDLE DEVONIAN PRAIRIE EVAPORITE IN THE ELK POINT BASIN, SOUTH-CENTRAL SASKATCHEWAN

A Thesis Submitted to the College of

Graduate Studies and Research

in Partial Fulfillment of the Requirements

for the Degree of Master of Science

in the Department of Geological sciences

University of Saskatchewan

Saskatoon

By

Haitham I. Hamid

PERMISSION TO USE

In presenting this thesis in partial fulfillment of the requirements for a Postgraduate degree from the University of Saskatchewan, I agree that the Libraries of this University may make it freely available for inspection. I further agree that permission for copying of this thesis in any manner, in whole or in part, for scholarly purposes may be granted by the professor or professors who supervised my thesis work or, in their absence, by the Head of the Department or the Dean of the College in which my thesis work was done. It is understood that any copying or publication or use of this thesis or parts thereof for financial gain shall not be allowed without my written permission. It is also understood that due recognition shall be given to me and to the University of Saskatchewan in any scholarly use which may be made of any material in my thesis.

Requests for permission to copy or to make other use of material in this thesis in whole or part should be addressed to:

Head of the Department of Geological Sciences

114 Science place

University of Saskatchewan

Saskatoon, Saskatchewan S7N 5E2

ABSTRACT

The present study focuses on delineation of the southern edge of the middle Devonian Prairie Evaporite (PE) in south-central Saskatchewan. The purpose of this work was to improve the accuracy and resolution of subsurface mapping by including additional information from well logs and seismic data not included in the previous studies.

Approximately 330 km of 2-D seismic data were integrated with horizon picks from 1334 well logs to improve the delineation of the southern margin of the PE. Thirteen seismic lines were re-processed with an emphasis on high-frequency imaging. The resulting seismic sections show marked improvement in the accuracy and resolution of mapping of the PE salt edges, with the estimated depth resolution improved to ~15 m. Seismic data indicate that salt dissolution structures were created by multistage processes. Salt collapses were identified within the body of the Prairie Evaporite and off-salt.

Well log data were combined with seismic results and gridded to create an updated map of the Prairie Evaporite. Different gridding methods provided different interpolations of the data set, particularly where the salt layer is thin near its margin. Incorporation of seismic interpretations resulted in 2-9 km changes in the positions of the salt edges derived earlier from well log and limited seismic interpretations. Therefore, integration of the seismic and well log data should increase the accuracy of the positions of the salt edge.

In order to evaluate the effects of the basin fill on regional gravity signatures and to determine whether the effect of the salt edge could be observed in gravity data, two gravity profiles crossing the salt collapse margin and the Trans-Hudson Orogen and the

Wyoming Structural Province were analysed. Regional-scale gravity modeling showed that the transition from the Trans-Hudson Orogen to Wyoming Province was marked by deep-seated structures within the basemen. Detailed gravity modeling of a shorter profile well-constrained by seismic data showed that the salt collapses contribute ~0.4 mgal to the total anomaly of about 4 mgal. Although a direct observation of salt edge by gravity appears hardly feasible, performing high-resolution gravity survey with station interval ~100 m might still be useful to constrain the overburden and thereby help detect salt collapses.

ACKNOWLEDGEMENTS

This research was made possible through financial support from the Saskatchewan Industry and Resources and the University of Saskatchewan. I express my gratitude to my thesis supervisor Dr. Igor Morozov for his invaluable advice, encouragement, support, and guidance. I thank Drs. Z. Hajnal, D. Gendzwill, B. Pandit (U of S), K. Kreis, and C. Gilboy (Saskatchewan Industry and Resources) for many valuable discussions. Dr. Hajnal's support was also critical in obtaining the seismic data and formulating the initial goals of the project. Special thanks to Kim Kreis for providing the borehole data set. Thanks also extend to Brian Reilkoff for computing services during processing and interpreting the seismic data. This work was facilitated by software grants from Landmark Graphics Corporation, Schlumberger Limited and Hampson-Russell Limited. GMT programs (Wessel and Smith, 1995) were used in preparation of some of the illustrations.

LIST OF CONTENTS

PERMISSION TO USE ii

ABSTRACT iii

ACKNOWLEDGEMENTS v

TABLE OF CONTENTS vi

LIST OF TABLES viii

LIST OF FIGURES viii

1. INTRODUCTION 1

1.1 Objectives of this Study 1

1.2 Methods 4

1.3 Geological Background 5

1.3.1 Regional Setting 8

1.3.2 Precambrian Geology 12

1.3.3 Phanerozoic Geology 14

1.4 Formations of Interest 18

1.5 Subsurface Salt Dissolution 23

1.5.1 Salt Dissolution Mechanisms 26

1.5.2 Salt Dissolution Age 26

1.5.3 Causes and Limiting Factors of Salt Dissolution 29

1.6 Collapse Examples 34

2. SEISMIC DATA ANALYSIS 37

2.1 Seismic Data 37

2.2 Seismic Processing 39

2.3 Seismic Resolution 56

2.4 Tuning Effects 61

2.4.1 Wedge Model 62

3. INTERPRETATION 68

3.1 Seismic Interpretation 68

3.2 Subsurface Map Interpolation 86

3.3 Gravity Inversion and Interpretation 93

3.3.1 Regional Gravity Profile A-A’ 93

3.3.2 Detailed Gravity Profile B-B’ 98

4. CONCLUSIONS 104

REFERENCES 106

APPENDIX A 112

APPENDIX B 126

APPENDIX C 132

LIST OF TABLES

Table 2.1	Seismic lines and acquisition parameters.	38
Table 2.2	Seismic data processing steps.	40

LIST OF FIGURES

Figure 1.1	Study area in south-central Saskatchewan.	2
Figure 1.2	Formations of Elk Point Group.	7
Figure 1.3A	Schematic diagram showing how a reservoir can be structurally closed around a salt edge.	9
Figure 1.3B	Four stages of structural reservoir closure closed over a salt remnant.	9
Figure 1.4A	Sketch of a reservoir deposited within a subsidence resulting from the salt dissolution.	10
Figure 1.4B	Sketch of a reservoir preferentially preserved in a salt dissolution low.	10
Figure 1.5	Regional setting of the Elk Point Basin.	11
Figure 1.6	Major Precambrian basement structures within the study area.	13
Figure 1.7	Stratigraphy and litholgy of south-central Saskatchewan.	15
Figure 1.8	Stratigraphic subdivisions of the Elk point and Manitoba Groups.	20
Figure 1.9	Facies distribution in the Elk Point Basin.	21
Figure 1.10	Stratigraphic relationship of the middle Devonian Winnipegosis Formation and lower Prairie Evaporite.	24
Figure 1.11A	Development f the salt dissolution area at Early Mississippian.	28
Figure 1.11B	Development f the salt dissolution area at Middle Jurassic.	28
Figure 1.11C	Development f the salt dissolution area at Late Cretaceous.	28
Figure 1.11D	Development f the salt dissolution area at Present day	28

Figure 1.12	Proposed model based on seismic, drilling and mining data suggest water circulation through mounds.	31
Figure 1.13	Schematic illustration of the dissolution of salt and resulting subsidence due to regional faulting and/or fracturing.	33
Figure 1.14	Distribution of local salt collapses, position of the salt dissolution edge and Major Precambrian basement features in Saskatchewan.	35
Figure 2.1	Raw shot gather from shot point 66, Line J.	42
Figure 2.2A	Receiver Refraction statics shifts computed by GRM (seismic line H).	44
Figure 2.2B	Shot Refraction statics shifts computed by GRM (seismic line H).	44
Figure 2.3	A shot gather prior to F-K filter from shot point 12, Line F.	46
Figure 2.4	A shot gather after using F-K filter from shot point 12, Line F.	47
Figure 2.5A	Shot gather No. 24, Line F before applying predictive deconvolution.	48
Figure 2.5B	Shot gather No. 24, Line F after applying predictive deconvolution.	48
Figure 2.6	Velocity analysis (Line H) before multiples suppression.	50
Figure 2.7	Velocity analyses (Line H) after applying Radon filter.	51
Figure 2.8	Stacked section (Line E) before using Radon filter.	52
Figure 2.9	Stack section after multiples suppression (Line E).	53
Figure 2.10	Principles of horizontal resolution of seismic method.	57
Figure 2.11	Final stack from line E (by Olympic Seismic) without spectral whitening applied.	59
Figure 2.12	Final stacked section from line E with post stack spectral whitening and F-X deconvolution applied.	60
Figure 2.13A	Events illustrate vertical resolution of Reflection coefficients of the same polarity.	63
Figure 2.13B	Events illustrate vertical resolution of reflection coefficients of opposite polarity.	63

Figure 2.14	Event from a faulted reflector with a fault offset indicated as fraction of the wavelength.	63
Figure 2.15	A segment of seismic line J shows a tuning effect.	64
Figure 2.16A	Wedge model.	65
Figure 2.16B	Synthetic seismogram.	65
Figure 2.16C	Synthetic amplitude versus distance.	65
Figure 2.16D	Original amplitude versus distance.	65
Figure 3.1	A synthetic seismogram compare to a segment of seismic line J.	70
Figure 3.2	A synthetic seismogram compare to a segment of seismic line M.	71
Figure 3.3	Correlation of synthetic seismogram of well no. 01/08-05-002-14W2/0 with seismic line J.	73
Figure 3.4	Correlation of synthetic seismogram of well no. 01/12-33-005-23W2/0 with seismic line M.	74
Figure 3.5	Salt-dissolution induced subsidence that did not affect strata shallower than about ~980 ms (seismic line E).	75
Figure 3.6	Effect of a salt collapse on seismic events (Line G).	77
Figure 3.7	Seismic Line H showing conventional section of Regina Trough. P.E. – Prairie Evaporite	78
Figure 3.8	Seismic Line M displays both regional and local salt dissolution of the Prairie Evaporite formation.	79
Figure 3.9	Strata slumping due to salt removal, basement uplift and several deep faults (Line J).	82
Figure 3.10	Line K shows salt collapse that may have occurred in Mesozoic.	83
Figure 3.11	Composite cross-section from seismic lines E and B.	84
Figure 3.12	Composite cross-section from seismic lines G and B.	85
Figure 3.13	Prairie salt maps interpolated using two values of spline tension (T_B =0 and T_B =0.5.)	88

Figure 3.14	Prairie salt maps interpolated using two values of spline tension (T_B = 1 and T_B =1.0.)	89
Figure 3.15	Interpolated isopach maps of the Prairie Evaporite Formation using both well and seismic data.	91
Figure 3.16	Bouguer anomaly map of Saskatchewan.	94
Figure 3.17	Gravity model along the cross-section A-A'.	96
Figure 3.18	Bouguer anomaly map of the study area.	99
Figure 3.19	Gravity model along the ~33 km gravity profile B-B' across the salt collapse.	100
Figure 3.20	Sonic log, density log, and location of the formation tops of well no. (01/08-05-002-14W/0)	102
Figure A.1	Seismic Line A.	113
Figure A.2	Seismic Line B.	114
Figure A.3	Seismic Line C.	115
Figure A.4	Seismic Line D.	116
Figure A.5	Seismic Line E.	117
Figure A.6	Seismic Line F.	118
Figure A.7	Seismic Line G.	119
Figure A.8	Seismic Line H.	120
Figure A.9	Seismic Line I.	121
Figure A.10	Seismic Line J.	122
Figure A.11	Seismic Line K.	123
Figure A.12	Seismic Line L.	124
Figure A.13	Seismic Line M.	125
Figure C.1	Interpolated isopach map of the Prairie Evaporite using GMT programs with spline tension parameter = 0.0.	133

Figure C.2	Interpolated isopach map of the Prairie Evaporite using GMT programs with spline tension parameter = 0.5.	134
Figure C.3	Interpolated isopach map of the Prairie Evaporite using GMT programs with spline tension parameter = 0.75.	135
Figure C.4	Interpolated isopach map of the Prairie Evaporite using GMT programs with spline tension parameter = 1.	136
Figure C.5	Interpolated isopach map of the Prairie Evaporite using both well log and seismic data.	137

1. INTRODUCTION

1.1 Objectives of this Study

This project focuses on improved delineation of the southeastern dissolution edge of the Prairie Evaporite Formation in south-central Saskatchewan (Figure 1.1). In its utilization and interpretation of seismic and well datasets, the project ties in with regional 2D seismic studies (Hajnal, 2003, personal communication) and subsurface geological mapping (Kreis et al., 2003) conducted as part of the International Energy Agency Weyburn CO_2 Monitoring and Storage Project. Our objectives are to correlate areas of salt dissolution with the underlying structural features, such as basement highs, Winnipegosis mounds, faults etc., and to document their potential relationships. The four specific objectives of this work were:

1) To use the available 2D and 3D seismic data acquired by industry to improve delineation of the southeastern margin of the Prairie Evaporite Formation south of Regina.
2) To develop processing and interpretation approaches to help identify thin salt beds and collapses near the dissolution edge and seismically evaluate the underlying strata, with particular attention to the Precambrian basement. In particular, this could help recognize structural features that may have influenced the location of the present-day salt edge.

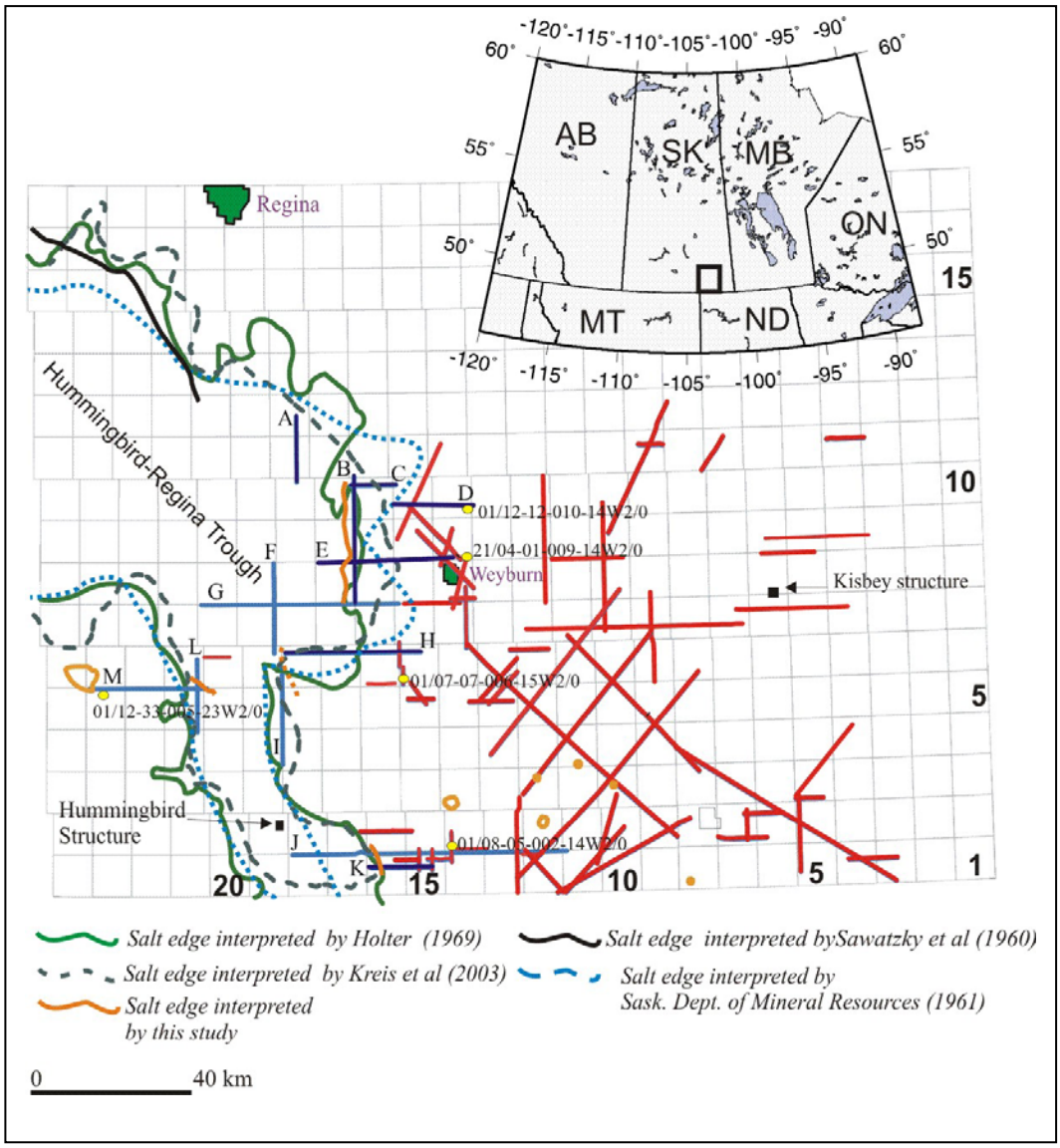

Figure 1.1 Study area in south-central Saskatchewan. The seismic lines are shown in blue, and red indicates other seismic lines analyzed in the International Energy Agency Weyburn CO2 Monitoring and Storage Project (Dr. Z. Hajnal, Univ. of Saskatchewan). Labeled green and black contours indicate the positions of the Prairie Evaporite edge interpreted from the previous studies, and brown contours are the results of the present study. The areas out lied in brown indicate the locations of local salt dissolution. Yellow dots indicate the boreholes used in seismic interpretation. Note the differences in the previous mappings of the southern margin of the Prairie Evaporite Formation, and also their differences from the present results. Numbers along the edges of the plot indicate townships and ranges. Black box in the inset shows the location of the study area in Canada.

3) To evaluate the effects of different mapping (spatial interpolation) techniques on determination of the positions of salt edges.

4) To explore the potential application of gravity methods to delineation of salt edges.

The southern edge of salt beds was defined from earlier composite seismic anomaly maps summarized by Holter (1969). The precise location of the Prairie Evaporite edge is uncertain, as it is irregular and complex. In the study area, additional well logs and seismic data have been used to improve the southern margin of the Prairie Evaportite.

In addition to improved delineation of the edges, our objective is to study the nature of the contacts between the Prairie Evaporite and both of its underlying and overlying formations. The contact between the Prairie Evaporite and Red Beds of the overlying Dawson Bay is generally sharp (Holter, 1969; Fuzesy, 1982), whereas the vertical transition between Prairie Evaporite and underlying Winnipegosis Formation is complicated and gradational (Fuzesy, 1982). At the Prairie Evaporite depth (1600-2500 m below the surface), high seismic frequencies are attenuated because of the absorption and scattering effects of the earth. Therefore, accurate mapping of both formation contacts and salt edges requires high-resolution seismic imaging with special attention to high-frequency enhancement during re-processing of the seismic data.

1.2 Methods

This study is based on integration of three general methods critical in subsurface mapping:

1) Two-dimensional (2D) seismic processing and interpretation.
2) Spatial interpolation of well log and seismic data.
3) gravity interpretation. As the area of the study is large and only sparsely covered by heterogeneous datasets (Figure 1.1), no single geophysical technique as able to provide a unique and definitive answer; however, a combination of this approaches leads to significantly more precise and complete understanding of the structure of the Prairie Evaporite.

Achieving sufficiently high seismic frequencies is the key factor in detection of thin beds and salt dissolution edges of the Prairie Evaporite Formation. Broadly, my efforts in the analysis of the seismic datasets focused on: 1) their uniform re-processing, 2) improving their resolution and enhancing high frequencies, and 3) their integration with gravity and subsurface mapping results.

In order to create a map of the Prairie Evaporite Formation, depth horizon picks from well logs and seismic sections need to be interpolated into a regular grid. The interpolation results may be not unique and depend on the methods employed. This is particularly important in poorly constrained areas, and particularly where the data need to be extrapolated, such as the salt edge of this study. Thus, integration of seismic

information, well log data and robust interpolation techniques would increase the accuracy of the position of the salt edge of the Prairie Evaporite.

In addition to the higher-resolution subsurface mapping studies above, I also apply gravity methods to explore the regional basement features, investigate the nature of the tectonic boundary between the Trans-Hudson Orogen and the Wyoming Province. Finally, at a significantly smaller scale length, I use a combination of detailed 2D seismic and gravity interpretations to determine whether the salt edge could be observed on gravity data available from the national Canadian gravity database.

1.3 Geological Background

The Middle Devonian Prairie Evaporite Formation is among the key economic targets in southeastern Saskatchewan. Three main potash members are recognized within the upper part of the Prairie Evaporite: the Esterhazy, Belle Plaine, and Patience Lake (Holter, 1969). The Devonian carbonates of the Williston basin host numerous oil plays. In the recent years, the focus of attention has shifted towards the deeper carbonates of the underlying Devonian Winnipegosis Formation through to the clastics of the Middle Ordovician Winnipeg Formation. Positive paleotopographic features on the Precambrian basement are spatially related to structural trapping of hydrocarbons in overlying strata (Kreis and Kent, 2000).

Accurate mapping of the salt margin is necessary for understanding of the processes of salt dissolution, the nature of basement control, and its impact on hydrocarbon production. Structures created by salt collapses may influence oil entrapment, reservoir enhancement, and migration of fluids. Thus, knowledge of the distribution and nature of salt collapses would also aid hydrocarbon exploration.

Deposits of the Elk Point Group contain the largest amount of salt in the Western Canada Sedimentary Basin, with salt volume of ~10^6 km^3 (Zharkov, 1988). Most of the salt is located within four formations of the Elk Point Group: 1) Lotsberg; 2) Cold Lake; 3) Prairie Evaporite; and 4) Dawson Bay (Meijer Drees, 1986) (Figure 1.2). The middle Devonian Prairie Evaporite is the most widespread of these deposits, lying beneath much of the southern Saskatchewan with salt up to 220 m thick (Holter, 1969). In some parts of the study area, the Prairie Evaporite is dissolved and removed either partially or completely by ground water (Holter, 1969). Salt can be dissolved from the top or bottom or from both sides (Gendzwill and Martin, 1996).

Salt dissolution and collapse structures are considered the most prominent geological features of the Phanerozoic subsurface of Saskatchewan. Knowledge of the locations and dimensions of salt collapse structures is essential for mining, as it is hazardous to mine those areas and it is also to evaluate the hydrocarbon exploration potential. Salt dissolution and the resulting subsidence could be the most important hydro-carbon-trapping mechanisms in western Canada (Edmund, 1980).

The salt dissolution and collapses are extremely important to the explorationist for the following reasons (Anderson, 1992; Anderson et al., 1988; Anderson and Brown, 1991, 1992):

1) Reservoir facies can be developed in high-energy environments such as topographic highs that are controlled by the salt edge or remnants resulting in forming structural traps over the salt edge (Figure 1.3A).
2) Structural traps can be initiated where reservoir facies are draped along salt remnants or collapse structures (Figure 1.3B).

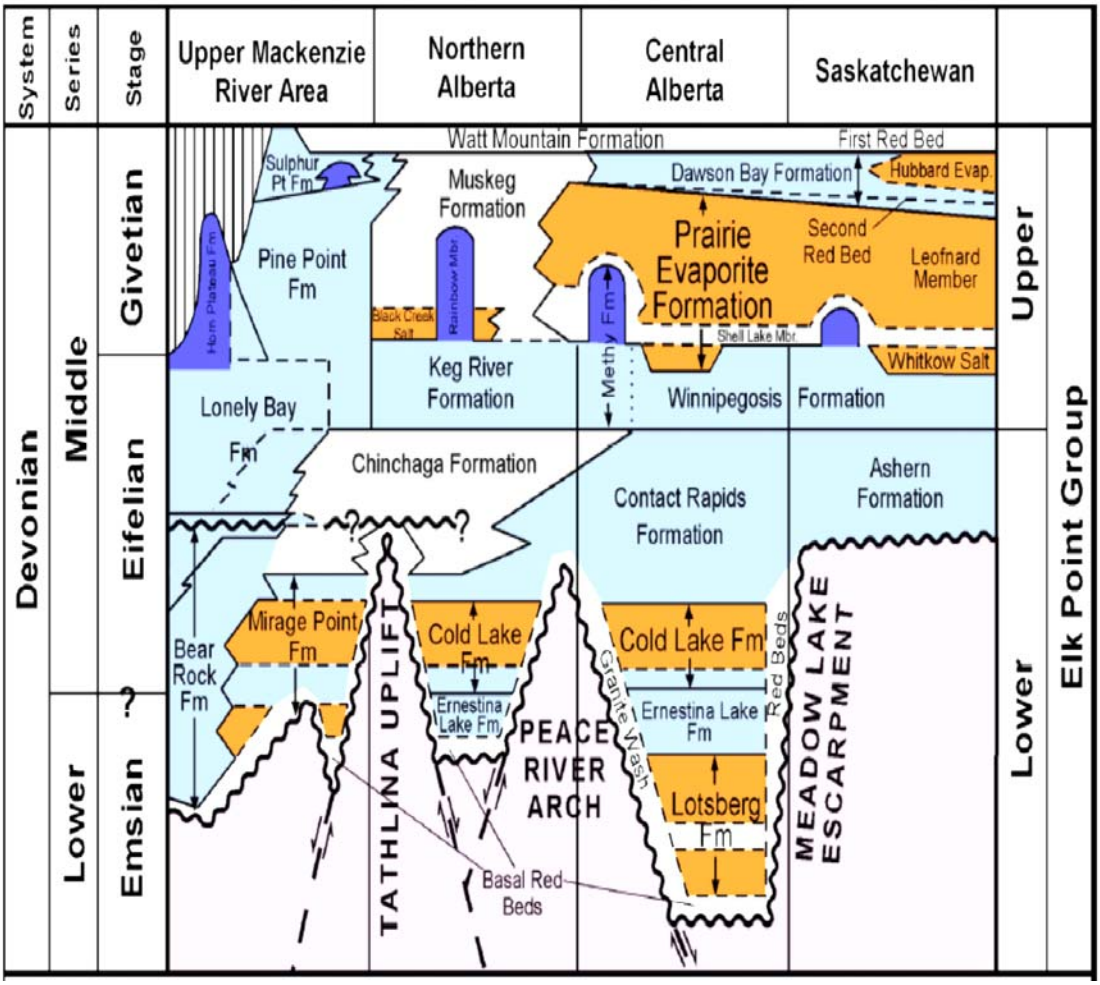

Figure 1.2 Formations of the Elk Point Group (modified after Meijer Drees, 1986).

3) Stratigraphic traps can develop where reservoir facies are deposited in salt dissolution lows (Figure 1.4A) or highs (Figure 1.3) or preferentially preserved in salt dissolution lows (Figure 1.4B). In the study area, collapse structures may be multistage and located off salt where all salt has been removed (e.g., the Hummingbird structure) or on-salt within the Prairie Evaporate itself, such as the Kisbey structure (Figure 1.1).

1.3.1 Regional Setting

During the Devonian, Manitoba and Saskatchewan were a part of a large basin called the Elk Point Basin (Figure 1.5). The Elk Point Basin covered the present-day Northwest Territories, northeastern British Columbia, Alberta, Southern Saskatchewan, southwestern Manitoba and extended into the Dakotas. The basin is bounded to the north by the Canadian Shield and to the west and south by the Western Alberta Arch and the Central Montana uplift respectively. In addition to the elements that define the Elk Point Basin, there were two major positive elements, the Peace River Arch and the Meadow Lake Escarpment, which divided this elongate NW-SE trough into three sub-basins. These sub-basins are the Northern Alberta, Central Alberta and Saskatchewan, shown in Figure1.5 (Grayston et al, 1964).

The sediments of the Elk Point Basin are mainly evaporitic and exist in three sub-basins. The Devonian sea transgressed from a narrow inlet to the northwest (Grayston et al., 1964; Holter, 1969 and Porter et al., 1982) to flood the Central Alberta sub basin where the Lotsberg Formation was deposited. Subsiding and downwarping of the basin permitted the sea to flood the Northern Alberta sub-basin; as a result, Ernestina

A)

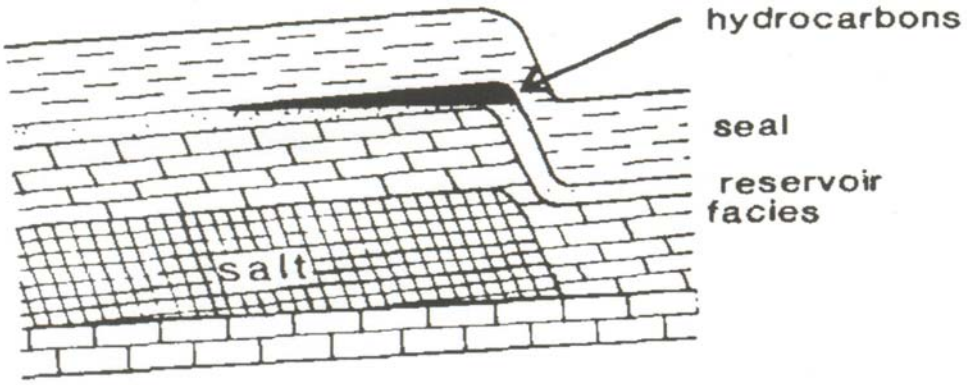

B)

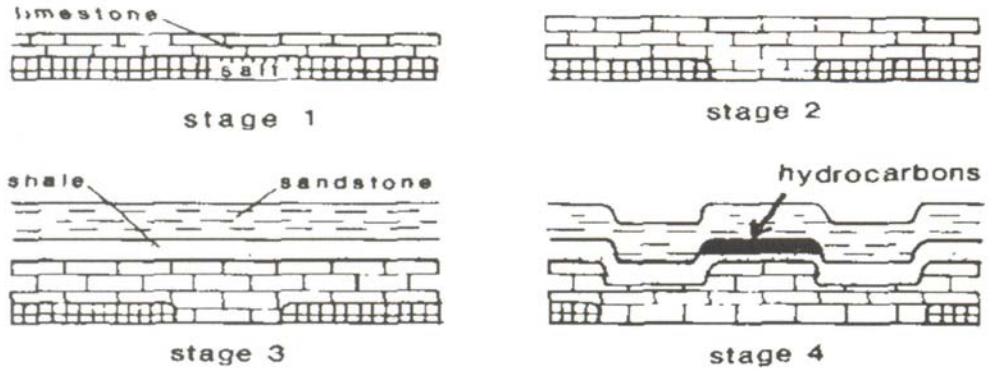

Figure 1.3 (A) Schematic diagram showing how a reservoir can be structurally closed around a salt edge due to the salt dissolution. (B) Four stages of structural reservoir closure closed over a salt remnant due to progressive leaching of salt (Anderson, et al, 1988).

A)

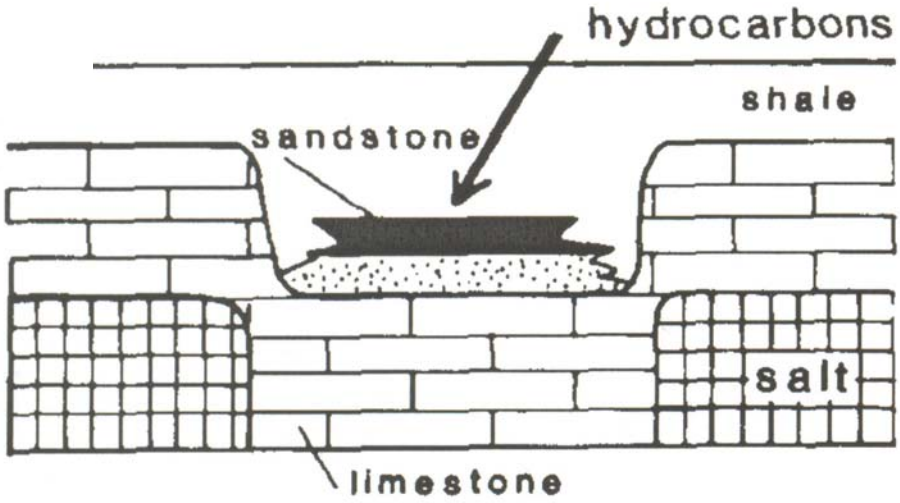

B)

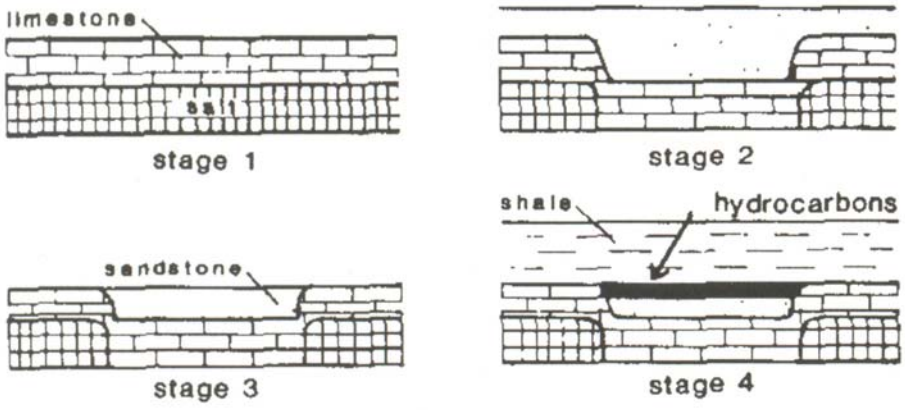

Figure 1.4 Sketches of: (A) a reservoir deposited within a subsidence resulting from salt dissolution; (B) a reservoir preferentially preserved within a salt dissolution low (Anderson, et al, 1988).

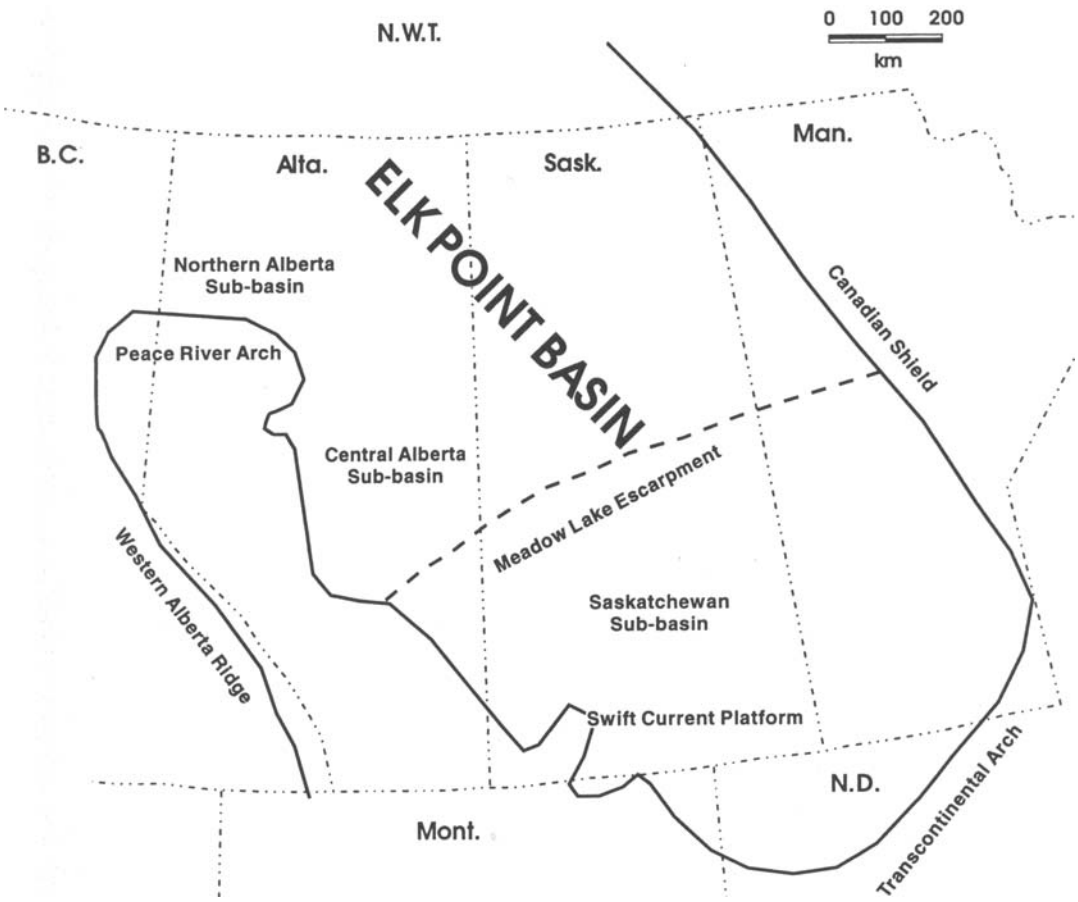

Figure 1.5 Regional setting and major tectonic elements of the Elk Point Basin (modified from Grayston et al., 1964)

Lake and Cold lake formations were deposited. Later, the sea breached the Meadow Lake Escarpment to flood the southern portion of Elk Point Basin.Sequential filling of the sediments of the Central Alberta sub basin, followed by filling of the Saskatchewan sub basin, defined the boundary between the lower and upper Elk Point Group. The lower Elk Point Group was found in the northern and central Alberta sub basins, and with breaching of Meadow lake Escarpment, the upper Elk Point group was deposited in all three sub-basins (VanHees, 1956).

1.3.2 Precambrian Geology

Basement rocks of the Williston Basin area belong to three major tectonic regions, which are, from the east to the west: the Archean Superior Province; the Trans-Hudson Orogen (a Proterozoic collision belt); and the Wyoming province (Figure 1.6). These provinces are recognized from regional magnetic data in the Williston Basin (Green et al., 1985a, 1985b; Baird et al, 1995; Gibson, 1995, and Kreis et al, 2000).

The Archean Superior Craton outcrops in mid-eastern Canada and extends westward beneath the Phanerozoic sediments into the Dakotas (Lidiak, 1971) and the northwest corner of Iowa (Bickford et al, 1987). The Wyoming Craton is located on the west side of Williston Basin and is separated from Proterozoic rocks in Colorado to the south by a major crustal suture zone called the Cheyenne belt (Houston et al, 1979).

The Trans-Hudson Orogen (THO) is considered by Hoffman (1981) to be one of the world's major early Proterozoic orogenic belts. It is exposed in west-central Canada and extends within the subsurface southward to South Dakota (Sims and Peterman, 1986). THO is composed of four major tectonic domains (Lewry, 1981; and Lewry and Collerson, 1990):

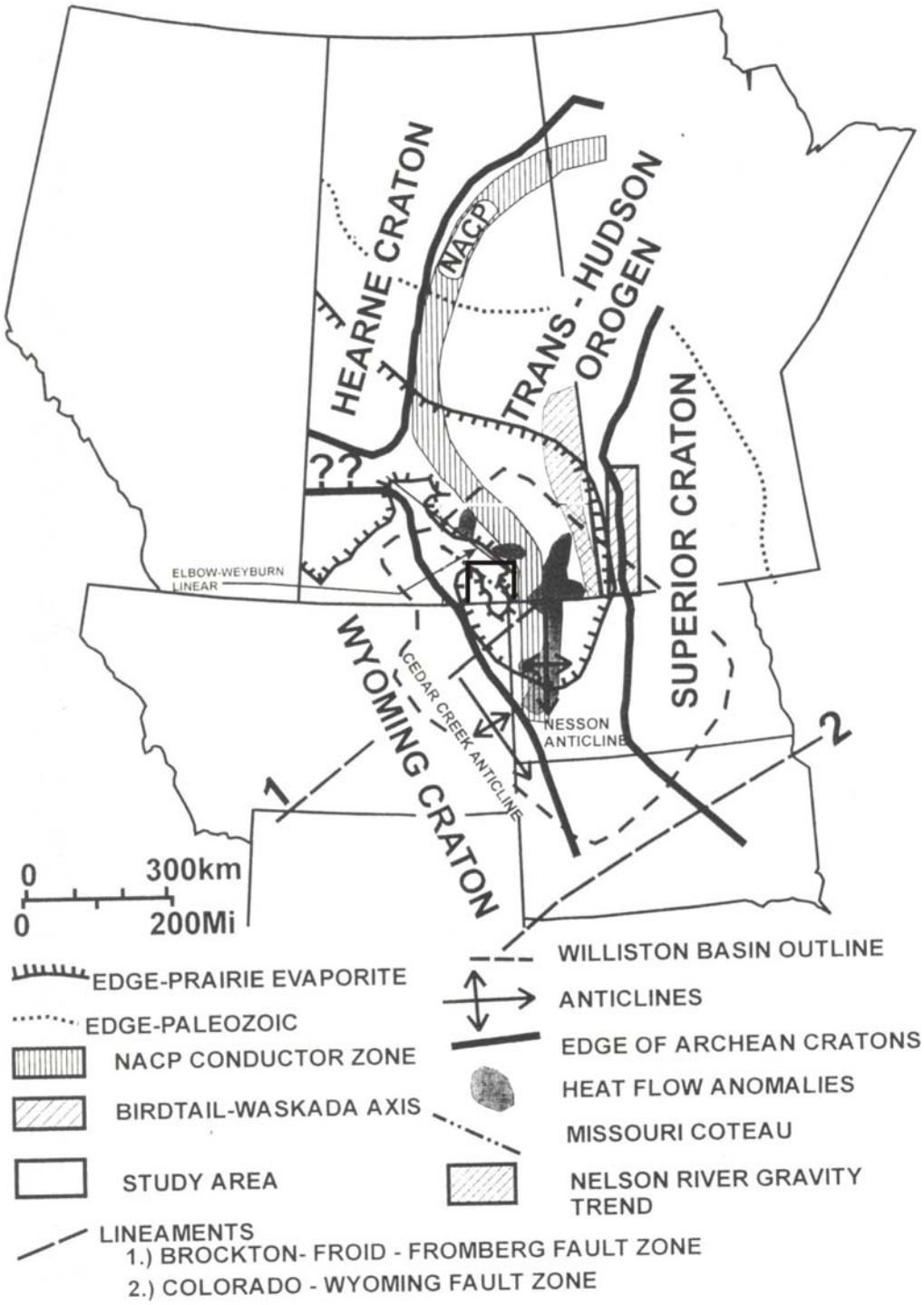

Figure 1.6 Major Precambrian basement structures and lineaments within the study area (modified from Kent, 1987; Majorowicz et al., 1988; and Baird et al., 1995).

1) Thompson Belt, a narrow eastern foreland boundary zone with Superior province
2) Reindeer Zone, a broad collage of imbricated magmatic, arc marginal basin and collisional basin belts;
3) Wathaman-Chipewyan batholith, an Andean-type continental margin batholith.
4) Wollaston Domain, a reworked hinterland of the Hearne Craton.

1.3.3 Phanerozoic Geology

The following is a brief summary of stratigraphic relationships of the sedimentary rocks in the study area, following Smith and Pullen (1976), Simpson (1982), Kries et al. (2003) and Gordon (1979). Stratigraphic column of the study area is shown in Figure 1.7.

Cambrian deposits

Cambrian clastics cover the western half of the Williston basin but are missing from its eastern part. Cambrian sediments show no evidence of a depositional Williston basin. Cambrian rocks are characterized by sandstone shale sequences (Deadwood Formation), which reflect shallow shelf deposition during marine transgression from the west. Strata of the Deadwood Formation provide the first clue of a marine incursion over the Williston Basin and Western Canada Sedimentary Basin. It comprises the entire interval from the upper Precambrian rocks to the unconformity at the top of the Deadwood Formation Deadwood Formation ranges in thickness from ~70 to ~ 110 m in the study area.

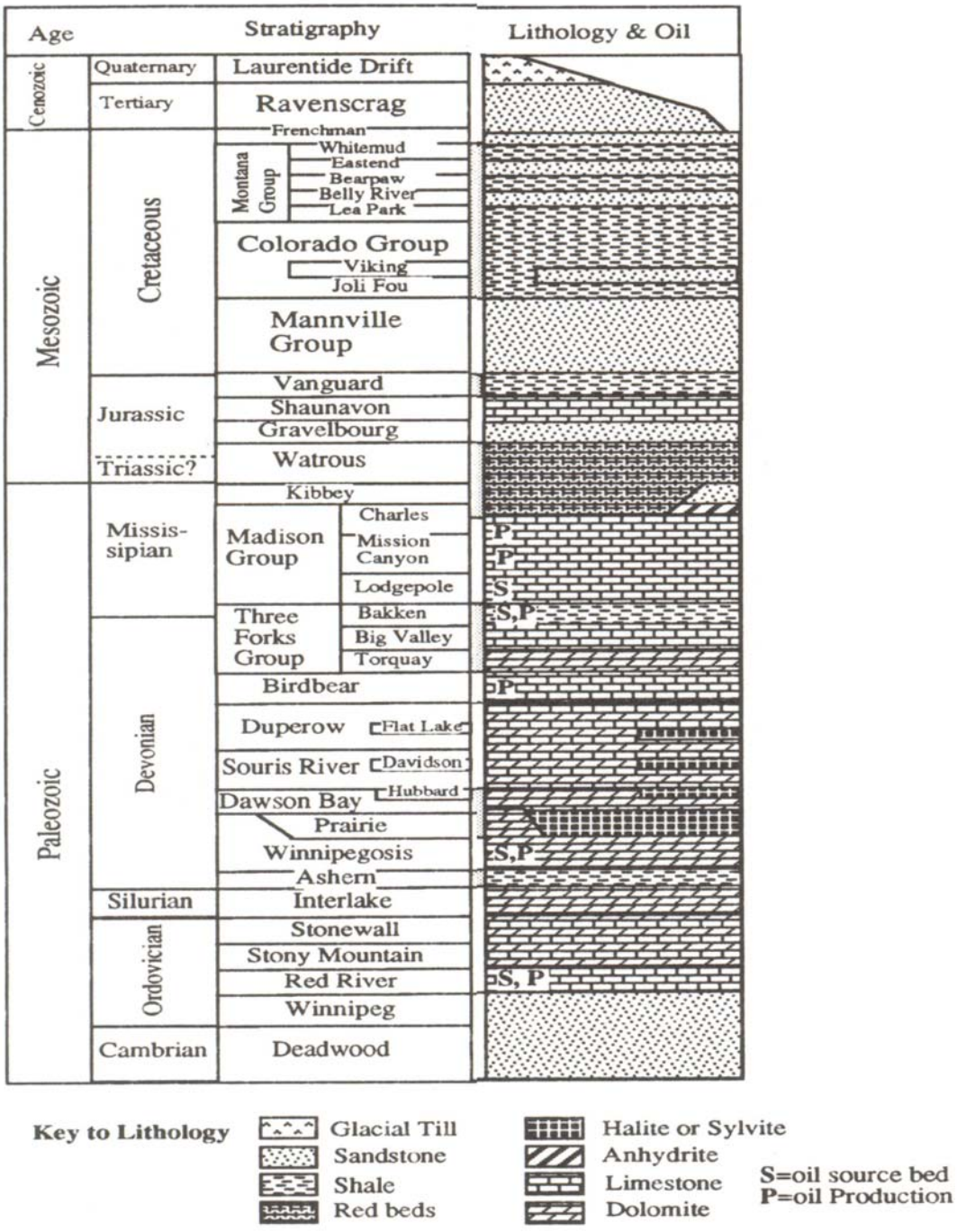

Figure 1.7 Stratigraphy and litholgy of south-central Saskatchewan (modified from Toop and Toth, 1995).

Ordovician and Silurian deposits

The Ordovician and Silurian sequences are subdivided into three main stratigraphic units within the Williston basin: 1) basal sandstone-shale sequence of the Winnipeg Formation; 2) open marine carbonate overlies by carbonate-anhydrite sequence (Big Horn Group) made of Red River (dolomites), Stony Mountain (dolomites) and Stonewall (dolomites) formations; and 3) Interlake dolomite group. Ordovician and Silurian deposits thicken toward the centre of the Williston basin reaching a maximum thickness of ~606 m near Williston, North Dakota. These sediments recorded a series of transgression-regression episodes with complete carbonate-evaporite cycle found in the centre of the basin.

The Devonian rocks

The Devonian rocks are subdivided into three main stratigraphic units:

1) A lower carbonate platform reef of complex overlain by evaporates of the Elk Point Group. It includes Ashern Formation (dolomite shales), Winnipegosis Formation (sucrosic, anhydritic dolomite-limestone) and Prairie Evaporite Formation (anhydrite and salt members).
2) An overlying carbonate-evaporite-shale sequence of Manitoba and Saskatchewan Groups. Manitoba Group comprises the Dawson Bay Formation (calcareous, anhydrite, dolomite-limestone) and Souris River Formation (limestone, dolomite, and anhydrite). Dolomite shale at the base of Dawson Bay Formation is known as the Second Red bed member; while dolomitic shale deposit at the base of the Souris River is know as First Red Bed member. The Saskatchewan Group is made up of the Duperow Formation (anhydritic dolomites) and Birdbear Formation (dolomites).

3) An upper clastics sediments with partial carbonate and anhydrite sediments (Three Folk Group). It is comprised of Torquay (siliciclastics and dolomites) and Big Valley (limestone and shale) formations.

Devonian sediments do not thicken toward the basin centre, but they are related to the Western Canada Sedimentary Basin, which extended from South Dakota to North West Territories during the Devonian. The maximum thickness of the Devonian succession in the Williston Basin located in north of Regina, Saskatchewan, where ~ 667 m of sediments are present. Devonian Rocks are interpreted to reflect complex conditions associated with transgression, regression and evaporite of an ancient sea.

Mississippian, Pennsylvanian and Permian deposits

During these periods, the subsidence rate of the Williston Basin exceeded that of the surrounding shelf area, which is indicated by thickening of the sediments of these periods. The maximum thickness of these deposits in the Williston Basin is ~870 m. Mississippian rocks composed of four main stratigraphic units: 1) basal sandstone-shale sequence (Bakken Formation); 2) open-marine carbonate sequence (Souris Valley and Lodge-Pole Formations); 3) carbonate-evaporite sequence with some clastics (Mission Canyon, Charles Formations); and 4) upper clastic sequence (Big Snow Group). Pennsylvanian and Permian sediments composed mainly of clastic with minor carbonate. Although they are present in the central Williston Basin, they are absent in the study area, either because they were not deposited or eroded in Saskatchewan.

Mesozoic-Cenozoic deposits

Triassic and Jurassic sediments also thicken into the Williston Basin while some Tertiary-Cretaceous and younger sediments do not show subsidence of the Williston Basin. The Mesozoic-Cenozoic sequence consists of mainly clastic with minimal amounts of carbonates. One of the most important formations in the Mesozoic period is Watrous Formation. It is overlying immediately sub- Mesozoic unconformity and forms one of the trap systems in the study area. Watrous Formation consists of a lower unit (siltstone shales and minor sandstone) reflecting continental to restricted marine redbeds while the upper unit (dolomitic shales, dolomites and anhydrite) representing restricted marine depositional environment. The maximum thickness of these deposits is ~ 83 m in the study area.

1.4 Formations of Interest

The Winnipegosis and Prairie Evaporite formations form the major part of the Middle Devonian Elk Point Group in Saskatchewan. They provide an opportunity to examine the transition from marine to brine environment in the ancient intracratonic basin. These formations have been extensively studied due to the hydrocarbon potential of the Winnipegosis carbonate and high-grade potash sediments of the Prairie Evaporite. Knowledge of the distribution and thickness of these formations is required to evaluate the potential hydrocarbon exploration and potash mining.

Prairie Evaporite Formation

Bailie (1953) introduces the term “Prairie Evaporite” for the evaporites found between the Winnipegosis Formation and Second Red Bed of the Dawson Bay

Formation of Manitoba group (Figure 1.8). Prairie Evaporite Formation lies beneath eastern Saskatchewan into Alberta, where it is called the Muskeg Formation. In the Northwest Territories and British Columbia, Prairie Evaporite grades into Carbonates of the Presqu'ile Formation (Holter, 1969) (Figure 1.9). The middle Devonian Prairie Evaporite of the Elk Point Basin is composed mainly of halite, potash, anhydrite and minor carbonates. The formation has an average dip of 2 to 7 m/km southwest with maximum thickness of 210 m (Holter, 1969). The Prairie Evaporite is subdivided (bottom to top) into Whitkow, Shell Lake and Leofnard members (Jordan, 1968; Meijer Drees, 1986; Reinson and Wardlaw, 1972).

The Whitkow member consists of halite with anhydrite interbeds and basal dolomitic anhydrite. It is forming the intermound and mound capping strata overlying Winnipegosis. Whitkow member thickness varies from 6 m on mounds to 106 m in basinal areas adjacent to the mounds (Reinson and Wardlaw, 1972).

The Shale Lake member is composed predominantly of a sequence of dolomites and anhydrites. However, a thin carbonate unit occurs within this member. This unit is referred to as the Quill Lake marker bed. Where the Whitkow is absent, the base of the Prairie Evaporite is represented by the Shale Lake member, witch has a maximum thickness of 35 m between mounds and is absent over mounds (Reinson and Wardlaw, 1972).

The Leofnard member includes the carnallite- and sylvite-rich Esterhazy, White Bear, Belle Plaine and Patience Lake sub-members (Meijer Drees, 1986). These sub-members were previously named the Upper Prairie Evaporite (Holter, 1969). In Saskatchewan, the evaporites of the Prairie Formation represent the final stage of a major depositional cycle.

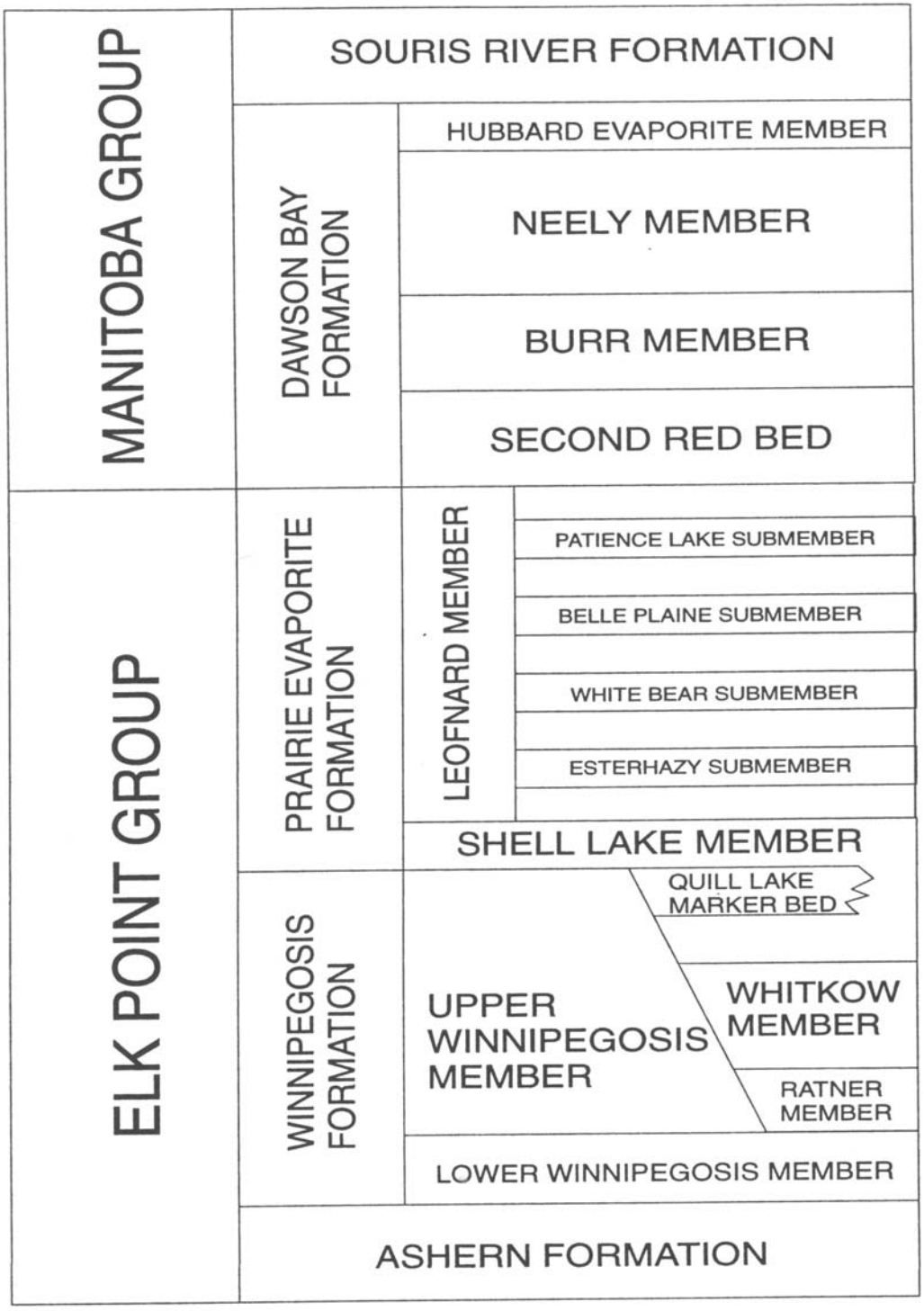

Figure 1.8 Stratigraphic subdivisions of the Elk point and Manitoba Groups (modified from Meijer Drees, 1986).

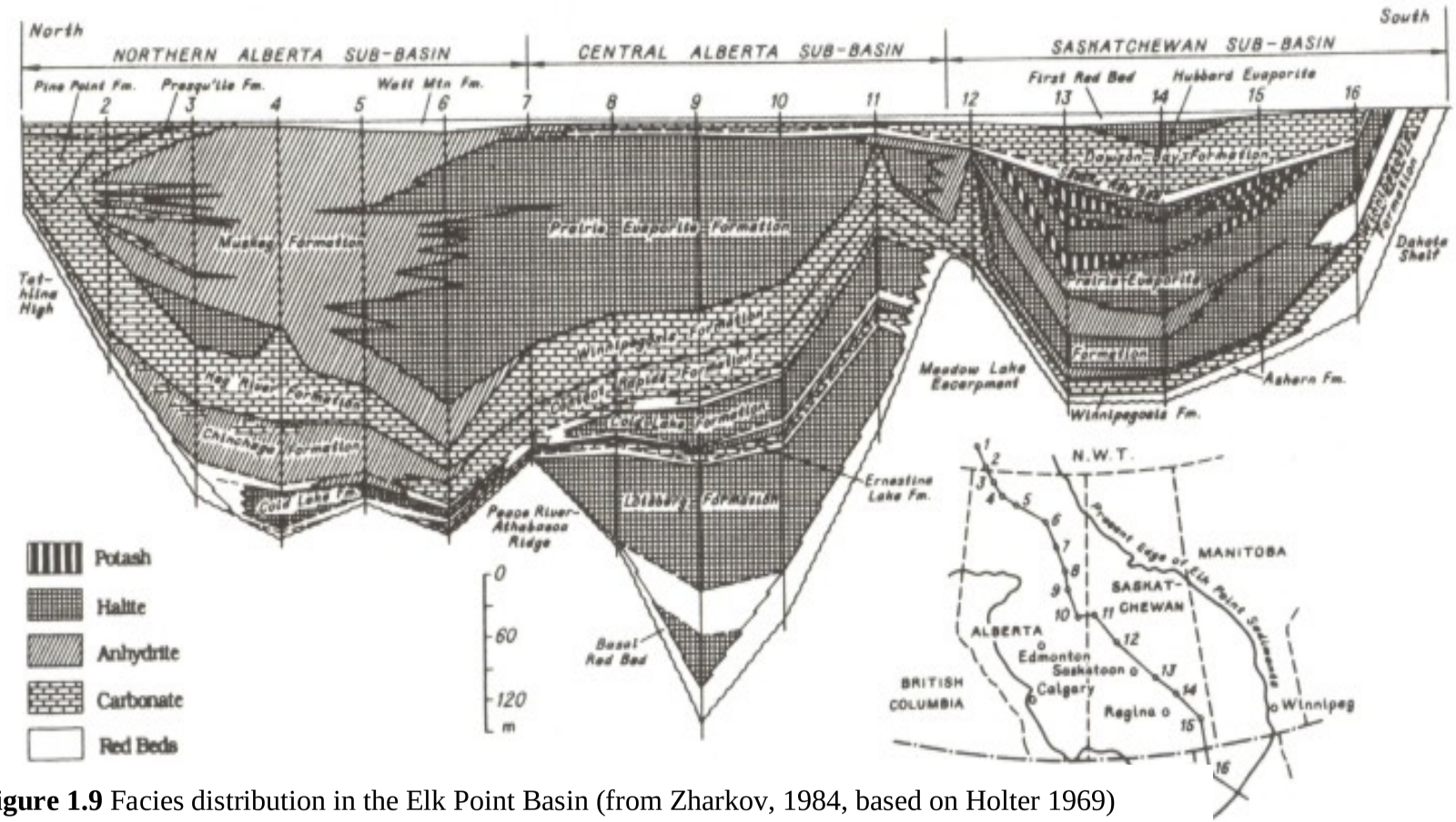

Figure 1.9 Facies distribution in the Elk Point Basin (from Zharkov, 1984, based on Holter 1969)

At the onset of this cycle, a major drop in the sea level occurred leaving most of the basin desiccated and exposed the Winnipegosis mounds. As a result of an increasing salinity in this inland sea, the carbonate banks were covered by evaporates deposited in thin anhydrite beds, followed by a thick sequence of halite and later on, as the concentration increased, – by sylvite and carallite, respectively (DeMille et al., 1964).

Winnipegosis Formation

The Winnipegosis Formation extends from North Dakota to southern Saskatchewan and crops out in Manitoba. It is equivalent to Keg River carbonate in northeastern British Columbia and Alberta as well as it is correlated to the Resistant member of the Methy Formation along the border between Saskatchewan and Manitoba (Norris et al., 1982) (Figure 1.9). The Winnipegosis Formation is subdivided into three members:

1) The lower platform member (or the lower Winnipegosis member) composed of mottled, highly dolomitized fossilferious packstone that varies in thickness from 6 m to 15.5 m. The lower member lies unconformably on eroded Precambrian or Palaeozoic rocks.
2) The Rater member on and off-reef mound, consisting of lamination with maximum thickness of 16 m.
3) The upper member (up-reef mound units) commonly referred to as carbonate banks because of the lack of frame-building organisms, which might also qualify them as reefs (Wradlaw and Reinson, 1971; Bailie, 1953; Jones, 1965).

Wilson (1984) subdivided the upper Winnipegosis (mound lithology) into peloidal grainstone, laminated mudstone, organic, and fringing cap members (Figure 1.10).

From seismic and well data, Gendzwill (1978) suggested the term “mound” to refer to the upper Winnipegosis which is composed of small steep-sided structures with thickness of up to 105 m and ranging from 0.5 to 6 km in diameters. These build-ups have undergone several phases of subsequent diagenesis that have commonly obliterated their depositional textures. The maximum thickness of the mounds is over 90 m, which appeared to be clustered in Saskatoon area (Wilson, 1985). Recent work on sequence stratigraphy of the Winnipegosis – Prairie Evaporite transition and diagenesis of Winnipegosis has been done at the University of Regina (Fu, 2005).

1.5 Subsurface Salt Dissolution

Subsurface dissolution was first recognized by Bailie (1953) and Bishop (1954). Bailie (1953) described the solution collapse breccias of the middle Devonian sediments in Manitoba and Saskatchewan. Bishop (1954) suggested that dissolution in the Venn area of western Saskatchewan occurred mainly during pre-Jurassic and post-Cretaceous.

Subsurface dissolution of the Prairie Evaporite is a major structural disturbance of the Phanerozoic strata. Dissolution or removal, either partial or complete, of evaporite beds from any of the Palaeozoic salt-bearing units within the Williston Basin may result in fracturing, collapse or subsidence of the overlying strata. The removal of the salt is compensated by local thickening of the sediments at the surface at the time the salt dissolved. Initially, subsurface dissolution was believed to be created during one collapse event of evaporite removal that resulted in thickening of sediment deposited during the time of salt dissolution.

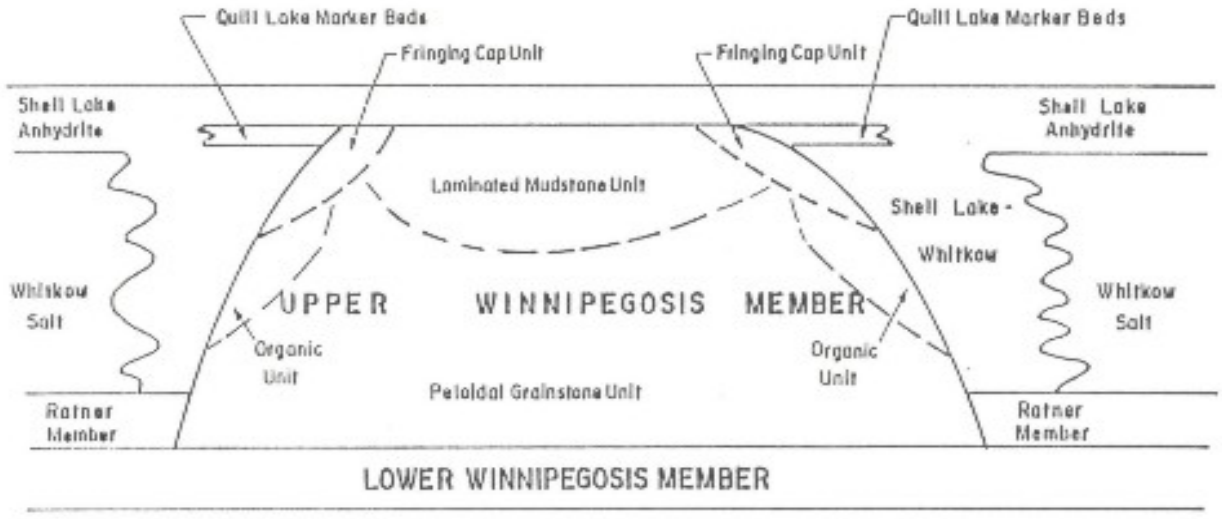

Figure 1.10 Stratigraphic relationship of the middle Devonian Winnipegosis Formation and lower Prairie Evaporite (Wilson, 1984).

Within the Hummingbird oil field, Smith and Pullen (1976) suggested that salt dissolution is a multistage process generating a complex localized dome structure. They demonstrated that the dome could lead to a structural trap formed due to local salt dissolution of the middle Devonian Prairie Evaporite balanced by thickening of the Devonian and Mississippian strata. Figure 1.3B shows the stages of creating such a complex localized dome structure caused by multistage salt dissolution. In a study of the upper Devonian strata of western Saskatchewan, Kent (1968) suggested that dissolution features originated as narrow local solution channels in the Prairie Evaporite perpendicular to the present-day salt dissolution edge. The channels grew wider with time and coalesced to produce escarpments at the present salt edge. Christopher (1961) suggested that solution channels moved laterally because they were blocked by collapse breccias. Parker (1967) suggested that initiation of salt dissolution and the resulting collapse structures required the presence of two factors: 1) the existence of an aquifer beneath the salt beds with sufficient hydrostatic pressure leading to its dissolution and removal through the sedimentary layers to the sea floor; and 2) the presence of sufficient faulting or fracturing created as a result of tectonic movements and permitting the entry of water from the aquifer upward to the salt and then to the ocean floor. Both requirements can be met in most of the southern dissolution areas, where porous and thick Winnipegosis Formation with sufficient hydrostatic head could serve as an aquifer beneath the middle Devonian Prairie Evaporite Formation (Holter, 1969).

In south-western Saskatchewan, close relations between localized salt dissolutions and the underlying Precambrian uplifts have been observed. Basement highs could be responsible for localized salt dissolution during rejuvenation of small basement

structures. In the process of such rejuvenation, faulting of Precambrian rocks and vertical movement of water could be expected (Sawatsky et al., 1960).

1.5.1 Salt Dissolution Mechanisms

A number of models have been proposed to explain the mechanisms of Prairie Evaporite salt dissolution (summarized by Holter, 1969). All models require that unsaturated fluids coming into contact with the salt section and transporting saline fluids away from the dissolution site either through regional or local fluid movements. Many models require faulting or fracturing in the Precambrian basement (Sawatsky et al. 1960; Christopher, 1961) resulting from tectonic movements and providing communication with the salt section. Others suggest dissolution of the salt by low-salinity fluids in areas where it overlies porous and permeable facies of the subjacent Winnipegosis Formations (Gendzwill, 1978). DeMille et al. (1964) considered a model that included both tectonic movements and fluid flow through the underlying permeable Winnipegosis strata.

1.5.2 Salt Dissolution Age

Several methods can be used to determine the times of the episodes of salt dissolution and the ages of the resulting collapse structures in the Williston basin. Methods commonly used to provide the evidence and determine the time of salt dissolution are seismic and structural mapping of the overlying strata on the basis of salt removal from the middle Devonian Prairie Evaporite. Salt removal produces not only disturbance of the Phanerozoic column but also causes the overlying strata to become locally thickened. A comprehensive study of such mapping procedures and determination of the salt removal times was given by MacTavish (1990).

Subsurface dissolution and removal of the Prairie Evaporite started soon after the deposition of Prairie Formation and continued to the post-Pleistocene. Isopach maps of Dawson Bay and Souris River show a positive thickness anomaly. Salt dissolution apparently began during the middle Devonian and continued into the early part of Late Devonian. Interpretation of the structural, isopach, and residual maps indicates that west of the study area (106° W longitude), the Prairie Evaporite was not deposited, at least not in large amounts (MacTavihs, 1991).

During the Early Mississippian and at the beginning of Madison Group deposition, the salt dissolution edge was very close to its original position with only minor areas of salt free in the extreme northwest and along the western margin of the Roncott Remnant. Thinning of the salt beds was observed throughout the Hummingbird and south Regina Troughs (Figure 1.11A). During Mississippian to Jurassic time and between deposition of the Madison Group and Watrous Formation, Prairie Evaporite was entirely removed from large parts of Regina and southern Hummingbird Troughs (Figure 1.11B).

During the deposition of Late Cretaceous Second White Speckled Shale, Prairie Evaporite was completely removed from the northern part of Hummingbird Trough (Figure 1.11C) (MacTavish and Vigrass, 1987). Subsidence on the eroded surface of Tertiary and Cretaceous sediments, which is in filled by Quaternary deposits, is common in the southern Saskatchewan. Many of these depressions are related to the subsurface dissolution of Prairie Evaporite during Pleistocene or more recent epochs (Christiansen, 1967, 1971a, 1971b).

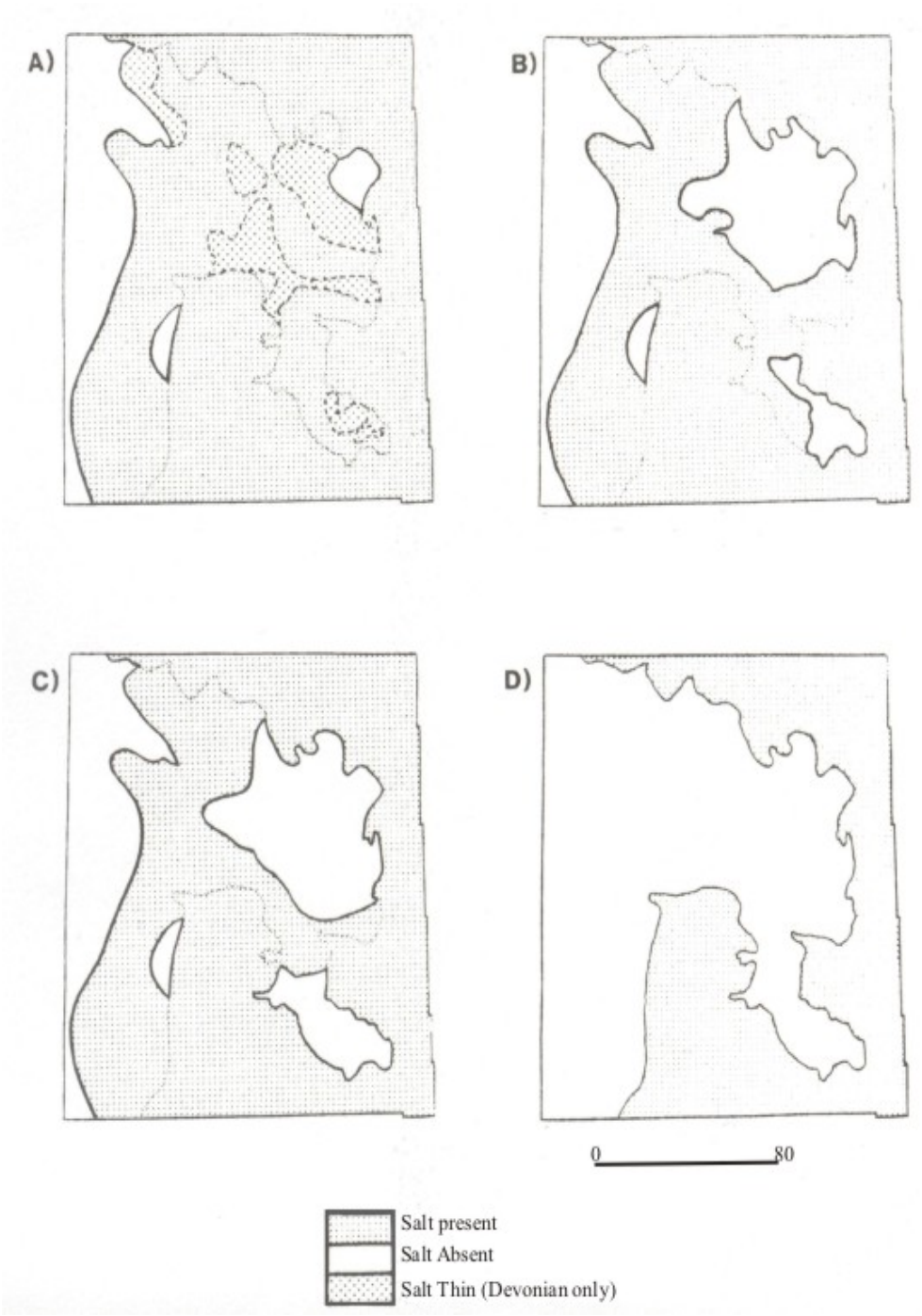

Figure 1.11 Development of the salt dissolution area at A) Early Mississippian (Madison Group); B) Middle Jurassic (Watrous Formation); C) Late Cretaceous (second White Speckled Shale); and D) Present day (MacTavish and Vigrass, 1987).

1.5.3 Causes and Limiting Factors of Salt Dissolution

Salt dissolution can appear as localized features, as series of dissolution lenses, as channel-like structures, or as dissolution edges. The shapes of salt dissolution edges or collapse structures may provide clues to the processes of their formation (Lefever and Lefever, 1995). Salt dissolution can be attributed to the intersection of faults, such that the concentration of fractures and increase of permeability make such areas more vulnerable to dissolution (Smith and Pullen, 1967). Faulting and fracturing are common mechanisms used to explain dissolution and removal of the Prairie Evaporite (Holter, 1969). More recent work suggested that the removal of Middle Devonian Prairie Evaporite occurred at both the top and base of the formation (Gendzwill, 1978; Oglesby, 1986) preferentially over Winnipegosis carbonate mounds.

Basement Relations

Many researchers attribute initiation of salt dissolution to the effects of basement structures. Figure 1.6 shows large-scale basement features, which may affect the salt dissolution in Saskatchewan. Dietrich and Magnusson (1998) pointed out that the location and origin of subsurface dissolution of Prairie Evaporite appears linked to the differential movement of the adjoining crustal block. Activation of these movements probably affects the regional hydrodynamic system in the Williston basin and areas of salt dissolution. Kent (1987) showed the North American Central Plains (NACP) anomaly to be linked: 1) to Regina-Hummingbird Trough, Venn, Saskatoon and Bladworth lows; and 2) to the northern margin and northern solution trend of the Embayment of Swift Current. Close relation between the NACP anomaly and salt dissolution suggests periodic reactivation of the anomaly causing fracturing of the

sedimentary rocks. Fractures provided conduits between the evaporite strata and the adjacent aquifers resulting in dissolution of the evaporite beds of the middle Devonian Prairie Evaporite and younger Devonian salt. Camfield and Gough (1977) reported that NACP structure is seismically active at certain locations. Canadian Seismological Observatory has observed four earthquakes near the NACP anomaly.

Positive gravity anomaly indicated that topographic uplifts on the Precambrian surface are parallel to the early dissolution trends in Hummingbird and localities up north (Wilson et al., 1963). In the southwestern Saskatchewan, a close relation between local salt dissolution and Basement uplifts has been noticed. Precambrian high could be responsible for local salt dissolution in the area, particularly during the periods of rejuvenation of Precambrian high when faulting and vertical movements are expected (Sawatzky et al 1960).

Mounds

DeMille et al (1964) suggested that areas of subsurface dissolution could be related to porous and permeable formations beneath the salt, which provides the pathways for fresh water migrating into the salt bed and for saline water transported out of it. Bishop (1954) and Gendzwill (1978) suggested that permeable Winnipegosis carbonate mounds were responsible for salt dissolution of the Prairie Evaporite (Figure 1.12). According to their studies, groundwater flowing through the carbonate mounds during the Middle and Upper Devonian caused subsurface dissolution at the base of the Prairie Evaporite. Salt dissolution was limited by the release of insoluble material blocking mound pores and stopping fluid circulation. Mossop (1972) showed that the subsidence over the Redwater

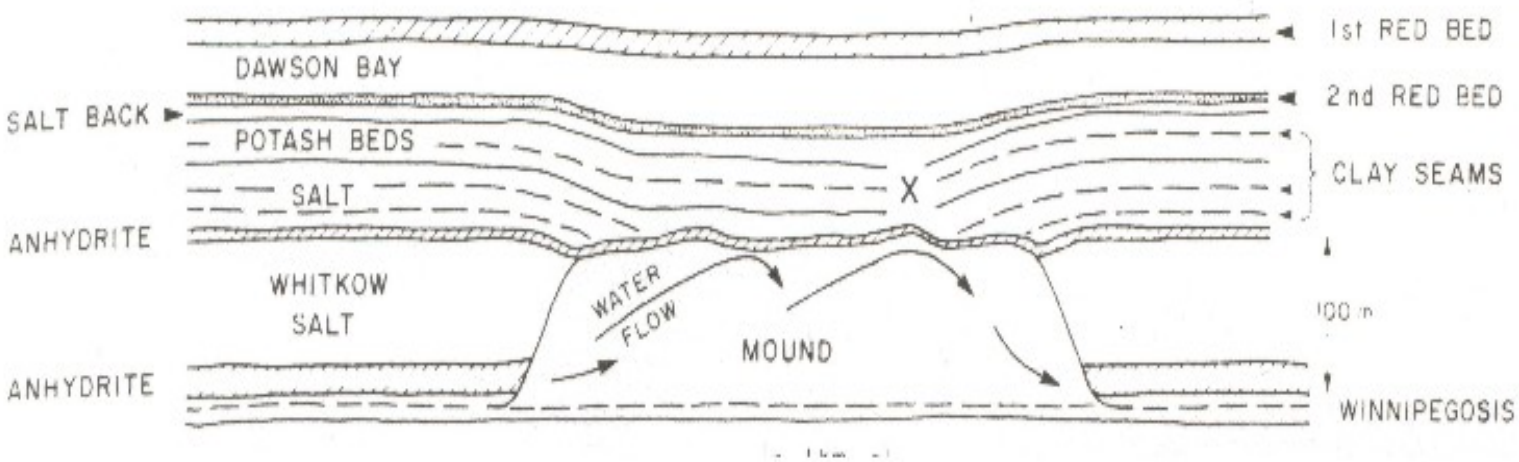

Figure 1.12 proposed model based on seismic, drilling and mining data suggest water circulation through mounds, slumping as result of salt dissolution and removal directly over the mound (Gendzwill (1978)

reef complex in central Alberta was caused by pressure solution of the carbonate material in the reefs. He estimated that a minimum of 700 m of overburden pressure was required to cause the depression at Redwater Reef.

Fractures and Joints

McTavish and Vigrass (1987) attribute the initiation of salt removal to factors other than basement topography and carbonate mounds. These factors should have been responsible for the widespread subsurface dissolution observed above the Winnipegosis marginal shelf. In the study area, a large part of subsurface dissolution may be attributable to groundwater movement along fractures, which interconnects porous and permeable strata that exist at the base and the top of Prairie Evaporate (Figure 1.13).

Some fractures penetrating the sedimentary column may reflect ubiquitous jointing in the underlying Precambrian rocks. These fracture systems are comprised of two fracture sets with northwest and northeast directions and appeared at the surface by photo lineaments (McTavish and Vigrass (1987). Davis (1972) believed that two major sets of lineaments with NE and NW trends within the Williston basin. These lineaments may be related to continental-scale block wrenching and were periodically reactivated. Kent (1974) indicated that salt dissolution structures could be associated with extensive fracturing along the two groups of lineaments. Vertical transport of water could occur along these fractures and caused subsurface salt dissolution of the middle Devonian Prairie Evaporite. In the Saskatoon area, deep crustal movement could allow fresh water from Second Red Bed to flow down into Prairie Evaporite and assist in its dissolution.

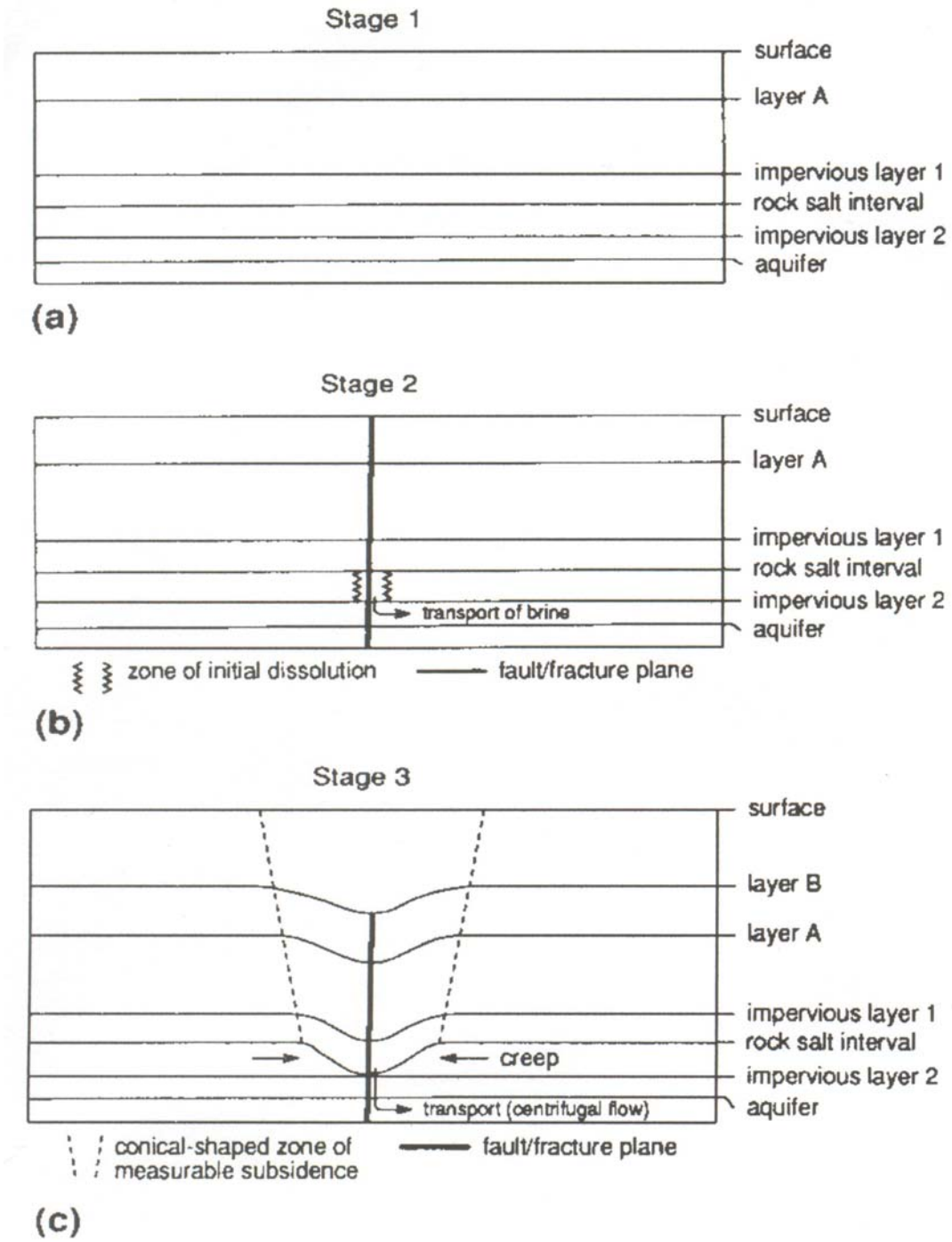

Figure 1.13 Schematic illustration of the dissolution of salt and resulting subsidence due to regional faulting and/or fracturing (Anderson and Brown, 1992).

Anderson and Cederwall (1993) proposed that post-glacial dissolution occurred as a result of glacial loading and unloading causing fractures, which are developed along pre-existing planes of weakness.

1.6 Collapse Examples

Numerous salt dissolution structures have been studied in the past 50 years. A brief summary of some of these dissolutions structures is given below. Figure 1.14 shows the locations of these collapses (of these, only the Regina-Hummingbird Trough, is within my study area in Figure 1.1).

Regina-Hummingbird Trough

Regina-Hummingbird Trough is believed to be a result of multi-stage salt dissolution (Smith and Pullen, 1967). It extends southward from Regina for ~160 km. Smith and Pullen (1967) argued that dissolution forming a structural trap could be a result of local subsurface dissolution of the Prairie Evaporite with thickening of Devonian and Mississippian strata. Similar dissolution with thickening of the post-Mississippian occurred in the surrounding area. The structure was believed to be caused by permeable Winnipegosis carbonates aiding formation water moving along high-angle basement-controlled fault or the intersection of two such faults. Each period of dissolution and removal of the salt coincided with movement along a basement fault, which could not be seen in the seismic data because of the masking effect of the collapse or its small vertical offset. DeMille et al (1964) proposed that the Regina-Hummingbird Trough is a result of basement activity associated with the northern extension of Nemo-Estes Trend, which is characterized by gravity and magnetic gradients corresponding to lithological and structural variations in the basement rocks.

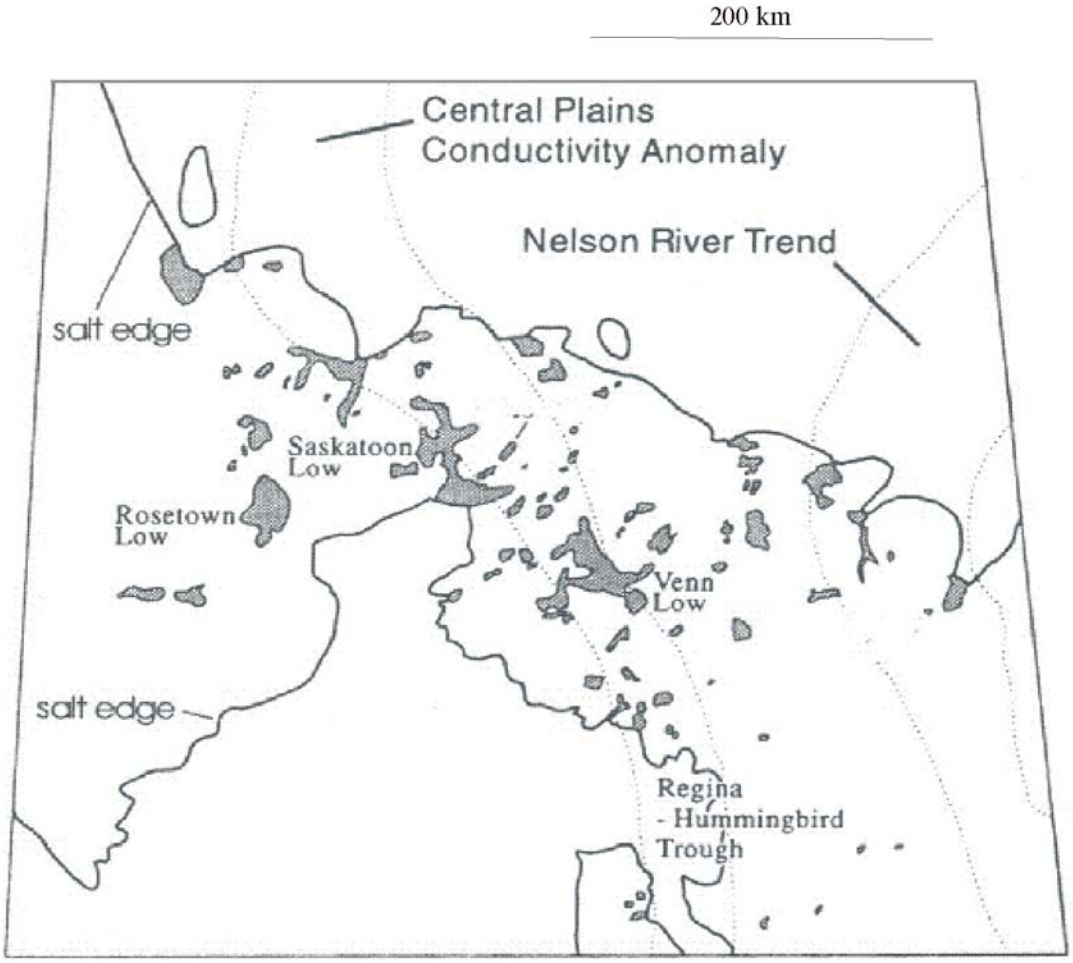

Figure 1.14 Distribution of local salt collapses, position of the salt dissolution edge and Major Precambrian basement features in Saskatchewan (modified from Macdonald and Broughton, 1980; and Fuzesy, 1982).

Rosetown Low

The Rosetown Low collapse was observed only from seismic data before it was drilled. It covers 373 km^2 within an area that would normally be expected to contain 120 m of salt. The collapse depth is about 114 m, which is approximately equal to the salt expected in this region. The southwest flank of this structure shows an extension fringe reef, which is partially overlapped by the upper strata of the middle Devonian Prairie Evaporite. The permeability of the flanking reef may have aided the transportation of water and dissolved the overlying evaporate (DeMille et al, 1964).

Saskatoon Low

The Saskatoon Low is a structural depression, which is believed to result from dissolution of the Prairie Evaporite. Two phases were identified in this structure. The first phase represented the initial 40 m of depression in the Saskatoon Low occurred after deposition of the Ardkenneth member of Bearpaw Formation and either before glaciation or during a pre-Illinoian glaciation. The second phase represented the final 70 m of collapse and took place in the Saskatoon Low during the Battleford (Late Wisconsinan) glaciation (Christiansen and Sauer, 2001).

Venn low

The Venn low is a result of salt removal from above localized and thick Winnipegosis. It is a long north-northwesterly oriented solution channel feature extending from Range 24, Township 24 west of the 2^{nd} meridian to Range 22, Township 25, west of 2^{nd} meridian (Holter, 1969).

2. SEISMIC DATA ANALYSIS

In the study area, the depth of the Prairie Evaporate varies from 1600 to 2500 m, with thickness ranging from 0 to 220 m. At this depth, the higher frequencies are significantly attenuated because of absorption and scattering effects of the earth, and also are contaminated by noise. Therefore, the primary goal of re-processing seismic data was to recover sufficiently high seismic frequencies to identify thin beds and map the salt dissolution edge of the Prairie Evaporite. In order to increase the resolution and consistency of seismic imaging, all data were re-processed in a uniform manner, with emphasis on high-frequency image enhancement.

2.1 Seismic Data

Seismic observations are critical for the present study because they provide detailed and continuous coverage for correlation with surface and subsurface geological mapping and well logs. This study used thirteen seismic lines covering a total of ~330 km, acquired from 1979 to 1984 and donated for research at the University of Saskatchewan by Encana Corporation, Petro-Canada, Olympic Seismic Ltd., and Kary Data Consultants Ltd. The data were acquired using different recording systems and a variety of dynamite and air gun sources. A list of acquisition parameters is given in Table 2.1. Both sources provided high-quality records.

Line Name.	Company	Length Km	Field	Date of Shooting M – Y	Station Interval (m)	Shot Interval (m)	Channel	Source Type Dynamite/Air gun	Instrument Type	Record Length	Sample Rate
H	Petro Canada	31.750	Roughbark	Nov 83	25	125	120	Dyn.	DFSV	3	2
D	Petro Canada	18.9	Weyburn North	Dec 83	30	90	120	Dyn.	DFSV	3	2
C	Encana	11.250	North Tatagwa	Nov 84	25	75	120	Air gun	DFSV	3	2
K	Encana	5.69	Flat Lake	Aug 85	25	75	120	Air gun	DFSV	3	2
J	Olympic Seismic	64.454	Estevan	Nov 79	67	134	48	Dyn.	DFSV	3	2
E	Olympic Seismic	31.758	Weyburn	Jun 80	67	134	48	Dyn.	SE338B	3	2
G	Olympic Seismic	48.240	Weyburn	Jul 80	67	134	48	Dyn.	DFSV	3	2
F	Olympic Seismic	21.375	Weyburn	Nov 84	25	125	120	Dyn.	DFSV	3	2
B	Encana	29.7	North Tatagwa	Nov 84	25	125	120	Air gun	DFSV	3	2
A	Encana	14.025	North Tatagwa	Sep 84	25	75	120	Air gun	DFSV	3	2
I	Simonson	19.8	Weyburn North	Mar 83	33	132	96	Dyn.	DFSV	3	2
M	Sourcex	26.6	Bunch Lake	Aug 79	50	200	96	Dyn	DFSV	3	2
L	Encana	15.54	Hardy	Jul 78	67	134	48	Dyn	DFSV	3	2

Table 2.1 Seismic lines and acquisition parameters

2.2 Seismic Processing

The processing procedure was similar for all lines and both types of sources (Table 2.2). However, to compensate for the different source types, the lines acquired with air gun sources required modification of some processing parameters. In particular, in order to attenuate the stronger air waves contaminating the air-gun source data, surface noise attenuation was applied, and different cut-off frequencies were used in designing the time-variant spectral whitening band (6-10-60-100 Hz; Table 2.2). For dynamite data, *f-k* filter was used to eliminate the ground roll in shot gathers and the pass-band frequencies in time-variant spectral whitening was 6-10-100-130 Hz. Dynamite data generally lead to better defined reflections than the equivalent air gun sources. Stacked and migrated sections from all seismic lines processed in this study are shown in Appendix A.

The processing steps can be subdivided into five groups:

1) Pre-processing, including SEG-Y-input, geometry, trace editing, and refraction statics.
2) Pre-stack processing steps that include *f-k* filtering, deconvolution, residual statics and Radon filter.
3) Normal moveout correction (NMO), and CMP stacking the data.
4) Post-stack processing, including time migration.
5) Additional image enhancement steps including Time-Variant Spectral Whitening (TVSW) and F-X deconvolution.

Process	*Purpose*
SEG-Y input	Data input from field records.
Geometry	Providing the geographic reference; correcting logging errors.
Trace editing	Removing bad traces, reversing polarity as necessary, and muting.
Refraction static	Time correction for shallow subsurface.
f-k filter	Attenuating the ground roll in shot gathers.
Deconvolution	Compressing the input pulse and attenuating reverberations.
NMO correction	Removal of reflection time moveout.
Residual static correction	Removing the residual small time shifts of reflected arrivals.
Radon filter	Suppression of multiple reflections.
CMP stacking	Increasing signal to noise ratio.
Time migration	Plotting events and diffraction at their true locations.
Time-variant spectral whitening	Equalize and flatten the amplitude spectrum.
f-x deconvolution	Reducing random noise and improving image coherency.

Table 2.2 Seismic data processing steps

Pre-processing

Field data were received on compact discs in SEG-B and SEG-Y formats and re-processed using PROMAX software (®Landmark Graphics). In order to process seismic data properly, geometry and surveying information was applied to the data sets. Most of the observer's notes were provided in a paper form. These observer's notes were checked and entered manually. Sometimes errors in the notes required checking the raw records in order to correct mistakes. Figure 2.1 shows the records from shot number 66 of seismic line J. Data quality is good with clear reflection from the basement ~ 1800 ms to the surface. Ground roll contaminated part of the data.

The next pre-processing step was trace editing. Bad and noisy traces were removed and in some cases, channel polarities were corrected to account for geophone or cable wiring errors.

First breaks were picked from the data and later used for generating refraction statics. Depending on the source types and the near-surface conditions qualities of the first arrivals varied resulting in occasionally less reliable picks. Figure 2.1 shows a shot gather with clear first-arrival onsets. Deviation from the linear trend of the first break arrivals was mainly attributed to the surface topography variations along the seismic line. Refraction statics inversion uses the first-arrival times to determine the velocities and depth of the upper geological strata (Sjogren, 1984). Due to their interferences with the shallow reflections and NMO stretching, the first arrivals were muted further in reflection processing; this operation is also based on first-arrival travel-time picks. Refraction statics were used to compensate for the effects of variation in source, receiver

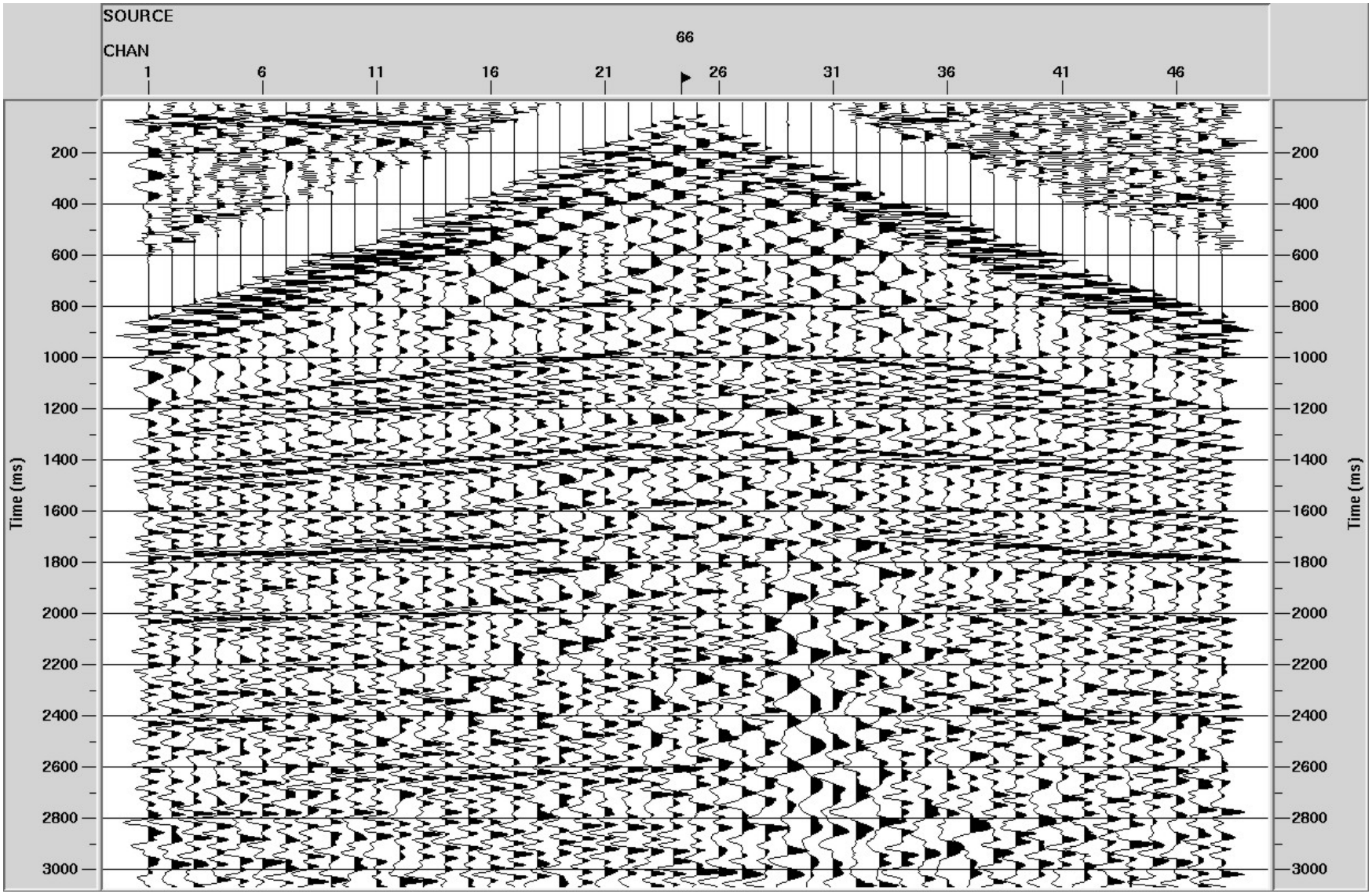

Figure 2.1 Raw shot gather from shot point 66, Line J. Note that data quality is good, with clear reflections from the Paleozoic strata at ~1800 ms to the surface.

elevation and weathering layer thickness above the datum level. Magnitudes of these corrections are based on the chosen datum and the first breaks arrival-picking values. Many methods are available for deriving statics solutions. In this study, the Generalized Reciprocal Method (GRM) was used. A two-layer model with weathering velocity V_w = 700 m/s, replacement velocity V_r = 2300, and datum level of 500 m above the sea level were used in implementing the GRM for all lines. After applying the static corrections computed by GRM, the data were transformed to the common datum, and the effects of the weathering layer were removed. GRM generated files of shots and receiver statics shifts (Figure 2.2), which (ideally) remove the effects of elevation as well as velocity and structural variations within the weathering layer. The statics corrections were applied to each trace as the sum of the corresponding receiver and shot time shifts.

Pre-Stack Processing

In this work, the purpose of using the *f-k* filter (frequency-wave number, dip, or velocity filter) is to remove the low-velocity events such as the ground roll. The discrete two-dimensional Fourier transform is given by (Hatton *et al*., 1986):

$$U_{fk} = \frac{1}{M}\sum_{q=0}^{M-1} e^{\frac{-2i\pi fq}{M}} \cdot \left[\frac{1}{N}\sum_{r=0}^{N-1} u_{qr} e^{\frac{-2i\pi kr}{N}} \right] \qquad (2.1)$$

$f = 0, 1, 2 \ldots M-1,$

$k = 0, 1, 2 \ldots N-1,$

where u_{qr} is the discrete space-time domain record, U_{fk} is its *f-k*domain representation, f and k are the temporal and spatial frequencies, respectively, q and r are

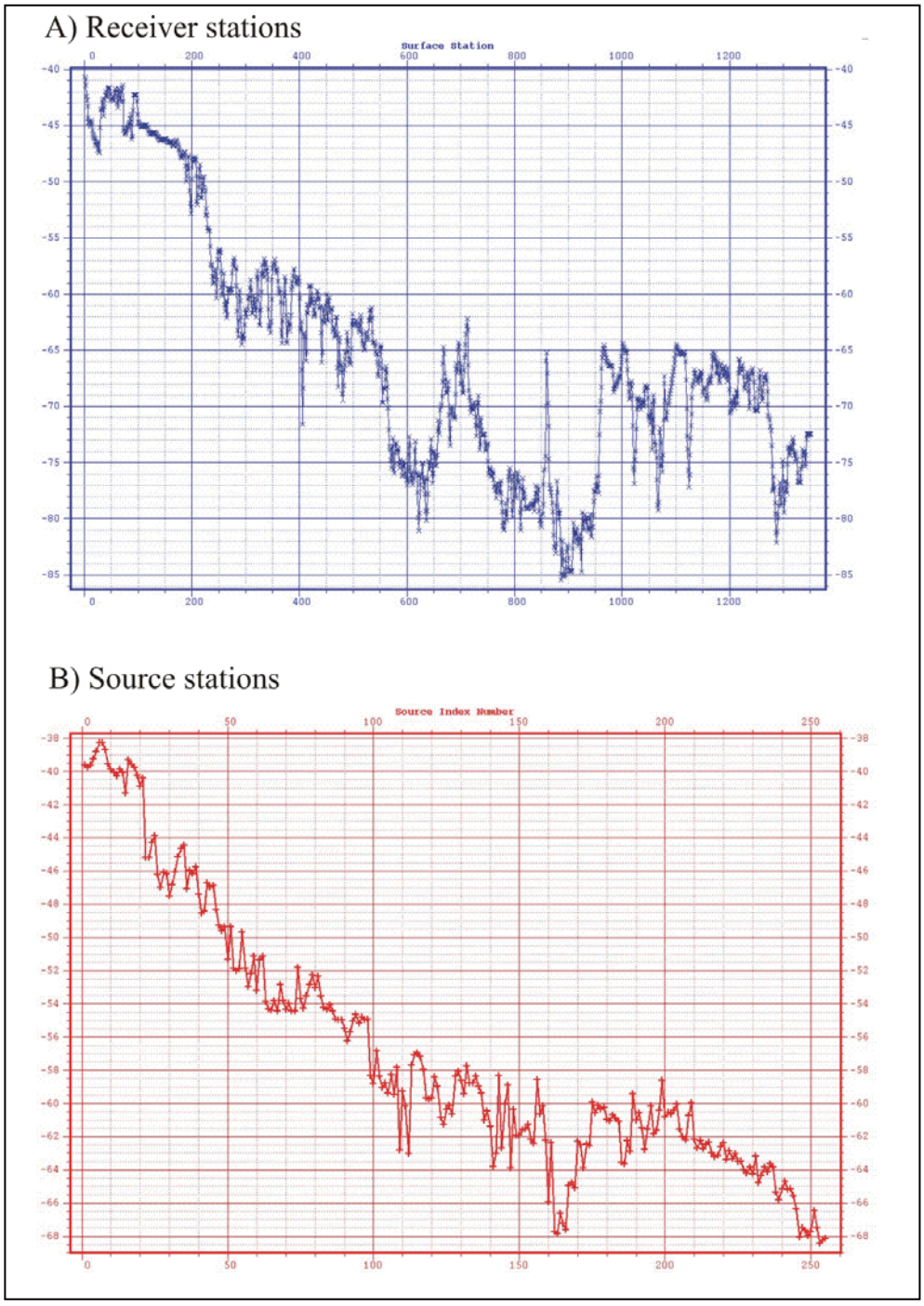

Figure 2.2 Receiver (A) and shot (B) refraction statics shifts computed by GRM (seismic line H, Figure 1.1).

the corresponding temporal and spatial increments, N is the number of time samples, M is the number of spatial positions, and i denotes $\sqrt{-1}$. Figure 2.3 shows an example of ground roll, which has an overlapping frequency band with that of the primary reflections. Thus, a Bandpass filter can not be adopted very effectively for ground roll attenuation. A better choice is the *f-k*, *f-k* filter allows the user to pass or reject regions in the f-k domain; the *f-k* filter can efficiently suppress coherent low-velocity events such as the ground roll (Figure 2.4). Prior to the velocity analysis, minimum-phase predictive deconvolution was applied to the records. Two objectives were achieved by this operation: 1) an increase in the resolution of the seismic data, and 2) attenuation of short-period multiple reflections. Prediction filter parameters were determined from the autocorrelation function. Figure 2.5A shows multiples marked in the shot point 66 of seismic line F were attenuated after using the deconvolution (Figure 2.5B).

The primary goal of the velocity analysis was to obtain accurate Normal Move-Out (NMO) correction velocities for all reflections in the seismic data record. Velocity analysis was performed on common mid-point (CMP) sorted data. Note that preprocessed shot gathers show strong multiples below ~1800 ms, corresponding to the depth to the basement. Velocity analysis of these shot gathers are shown in Figure 2.6.

Following statics and NMO velocity analysis, residual statics calculation was applied on the CMP gather. Residual statics corrections were performed by applying small time shift in order to further align events after NMO and prior to stacking, thereby improving the amplitude and coherency of the stack. In addition, improved time alignment of the traces contributes to the ability to retain high frequencies in the stack, which is critical for the present study.

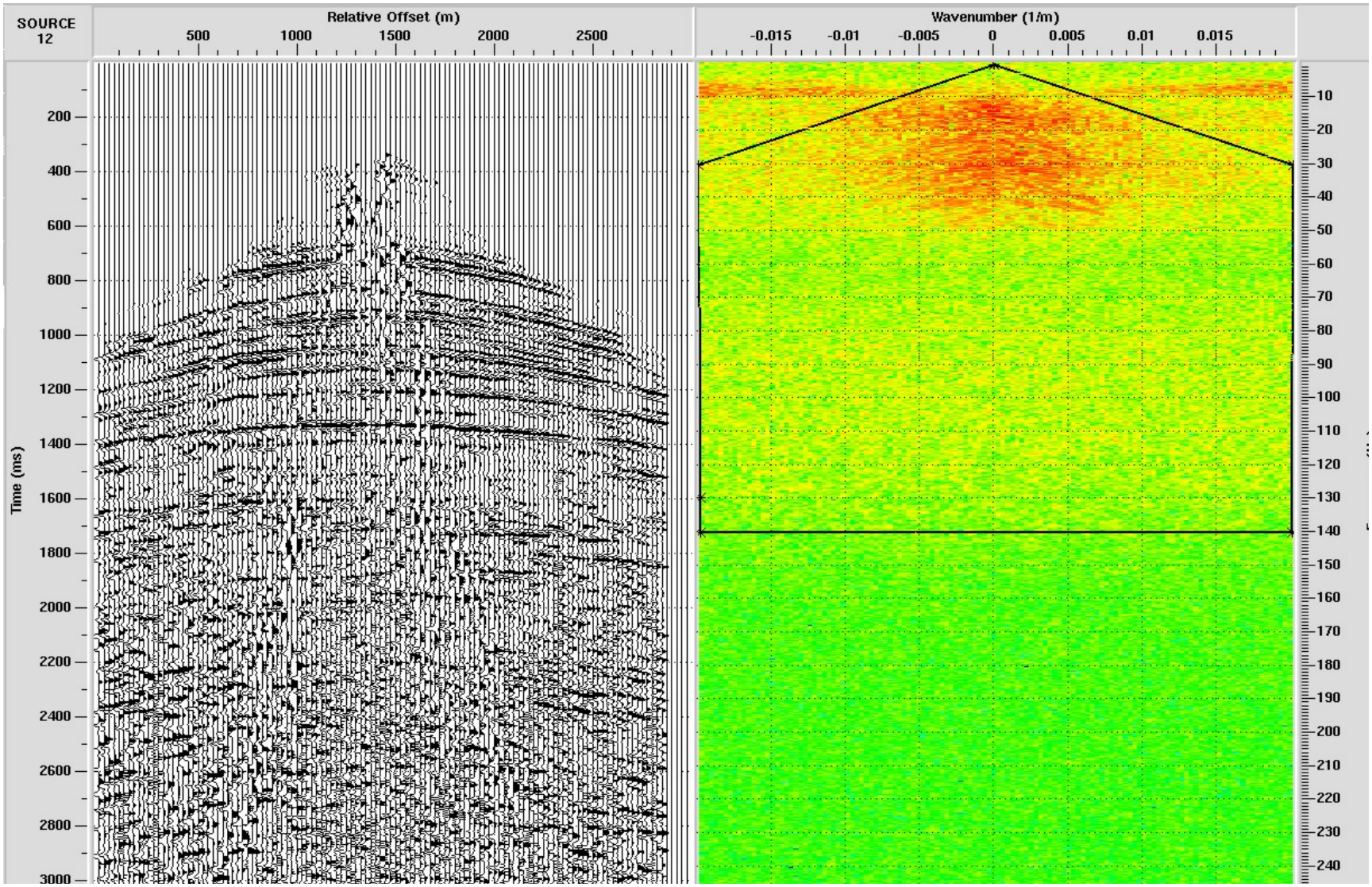

Figure 2.3 A shot gather prior to *f-k* filter from shot point 12, Line F. Ground roll appears as near-horizontal events in the *f-k* panel (right). Polygon in the plot on the right shows the *f-k* filter pass-band.

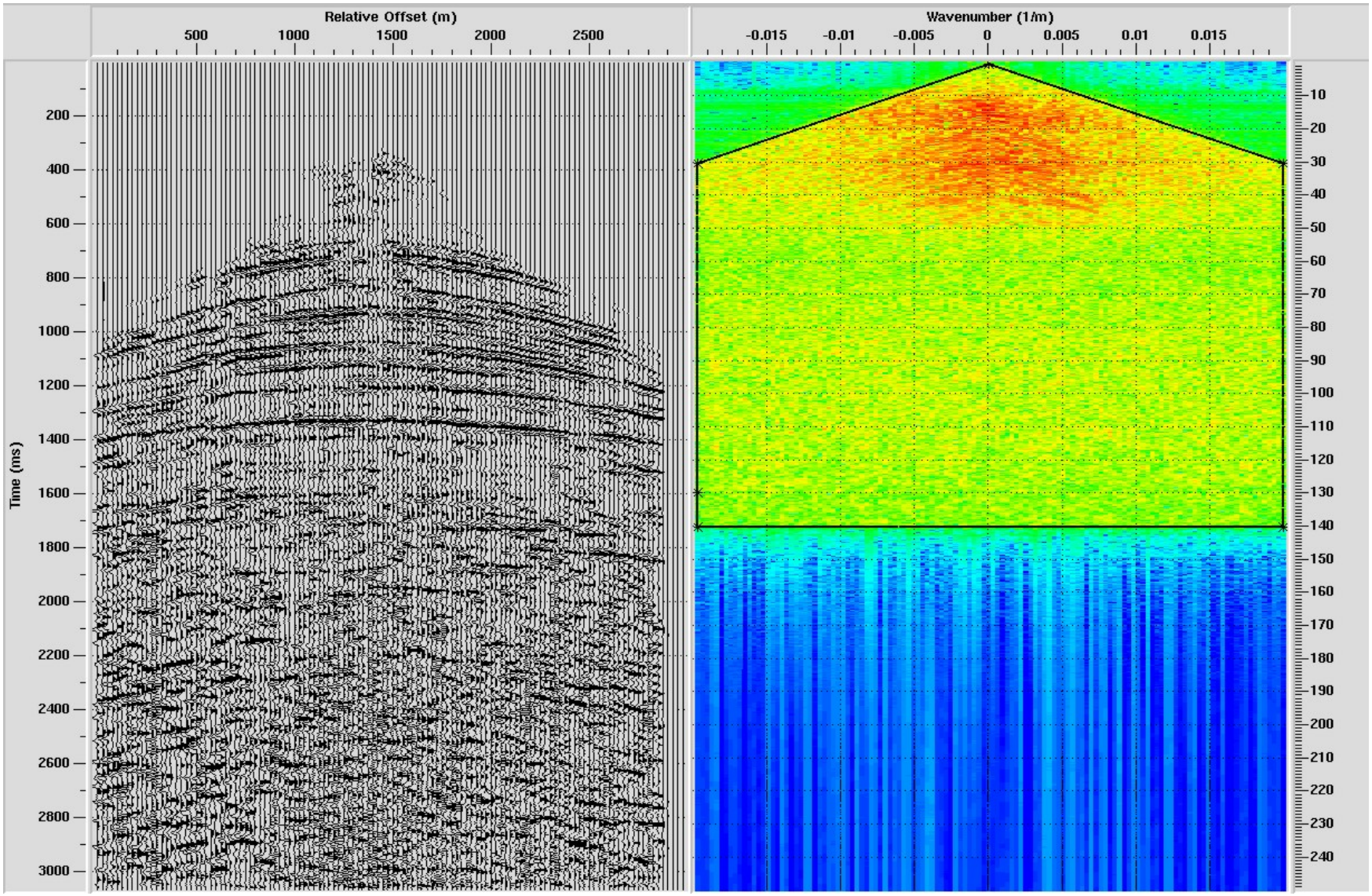

Figure 2.4 The same shot gather as in Figure 2.3 after using the *f-k* filter. Note that ground roll was attenuated.

A)

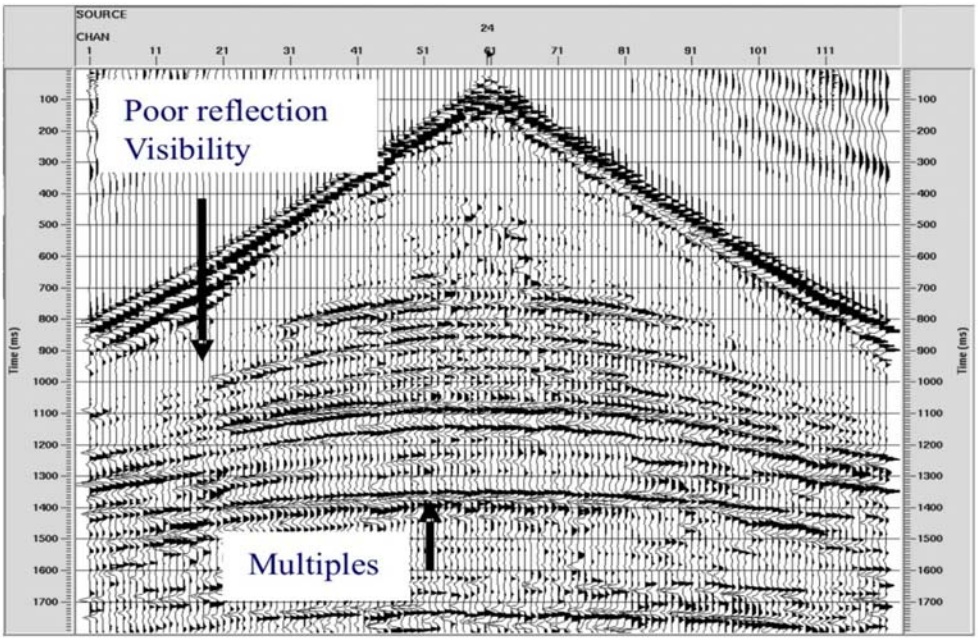

B)

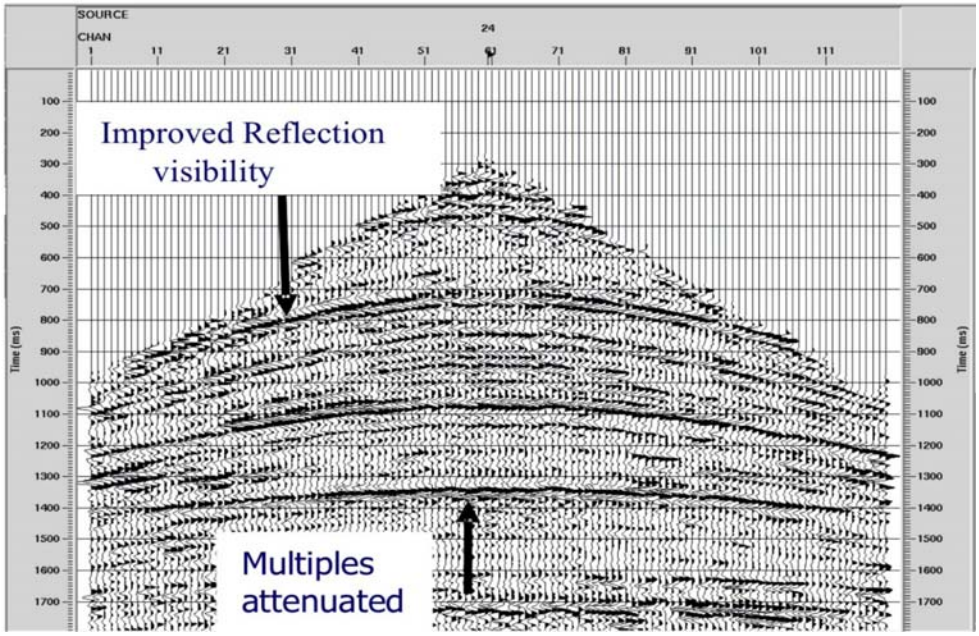

Figure 2.5 Shot gather No. 24, Line F before (A) and after applying predictive deconvolution (B).

There are many techniques for suppressing multiples, such as *f-k* multiple attenuation, Karhunen-Loeve transform and the Generalized Radon transform including, in particular, the τ-p, or slant-stack filter. In this work, the Generalized Radon Transform (GRT) approach was used. The GRT filter transoms the data from the time-space domain into the intercept time (τ) – slowness (p) domain (p=1/v, where v is the apparent velocity).

Separation of the multiples from the primary reflections in this method is based on the difference of their moveouts within different parts of a CMP gather. For NMO-corrected data using correct stacking velocities, all primary reflections have moveouts of around 0 ms whereas the multiples are under-corrected and show larger residual moveouts. Therefore, by removing the events with larger moveouts, the multiples can be attenuated.

Velocity analysis after multiple suppression (Line H; Figure 2.7) shows that multiple reflections were attenuated and the resolution of the shot gather was improved. Ovals in Figures 2.6 and 2.7 indicate the zone contaminated by multiple reflections before and after using the Radon transforms. Figures 2.8 and 2.9 show the stacked section from Line E before and after using the GRT filter.

CMP Stacking

CMP stacking reduces each CMP gather to a single zero-offset trace. Prior to stacking the data, the CMP gather is corrected using the normal moveout correction (NMO) so that the primary reflection energy is horizontally aligned. As a result, stacking process reduces the random noise and additionally attenuates the remaining misaligned multiple energy.

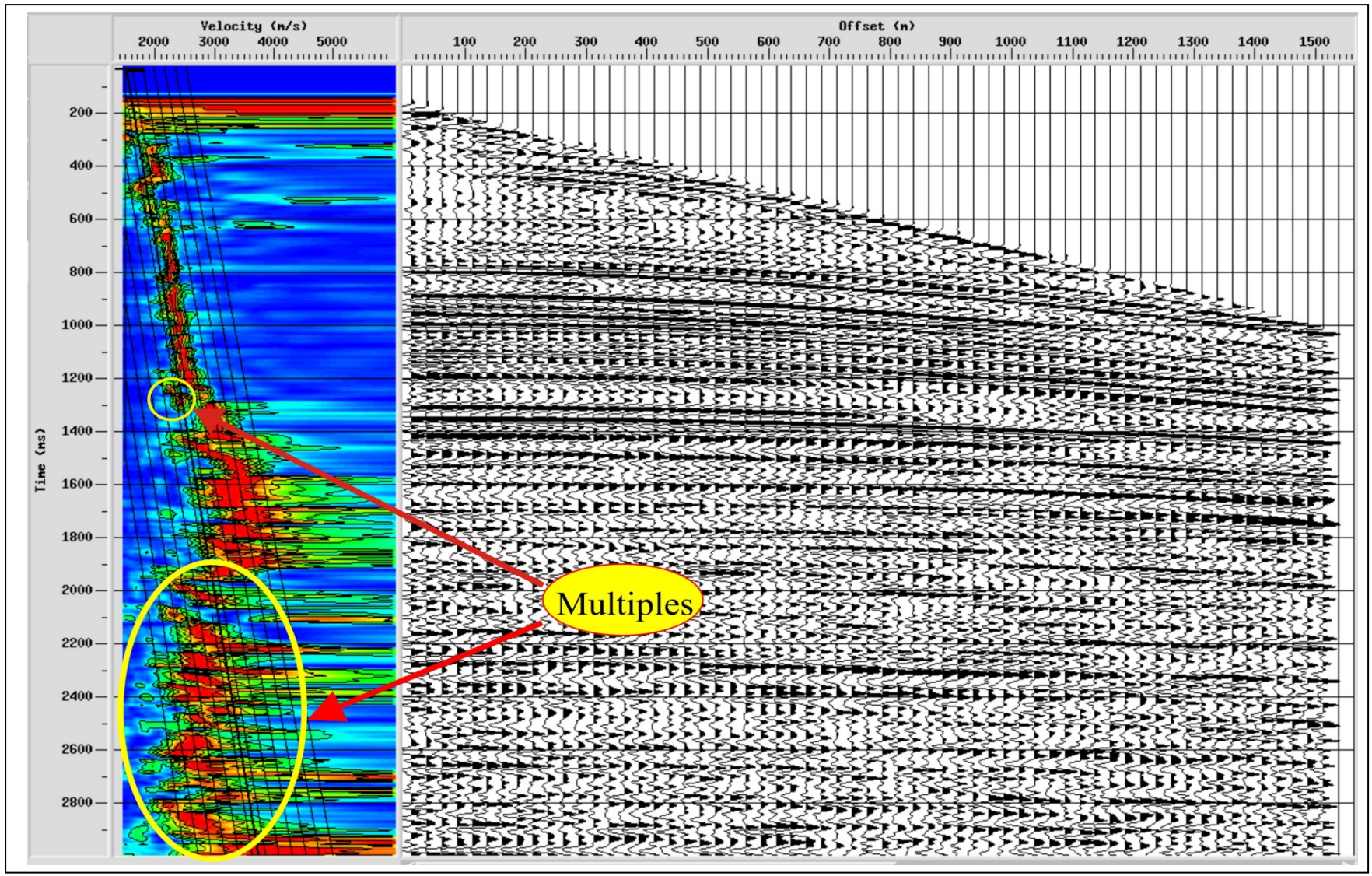

Figure 2.6 Velocity analysis (Line H) before multiples suppression. The arrivals within the ellipses are multiples.

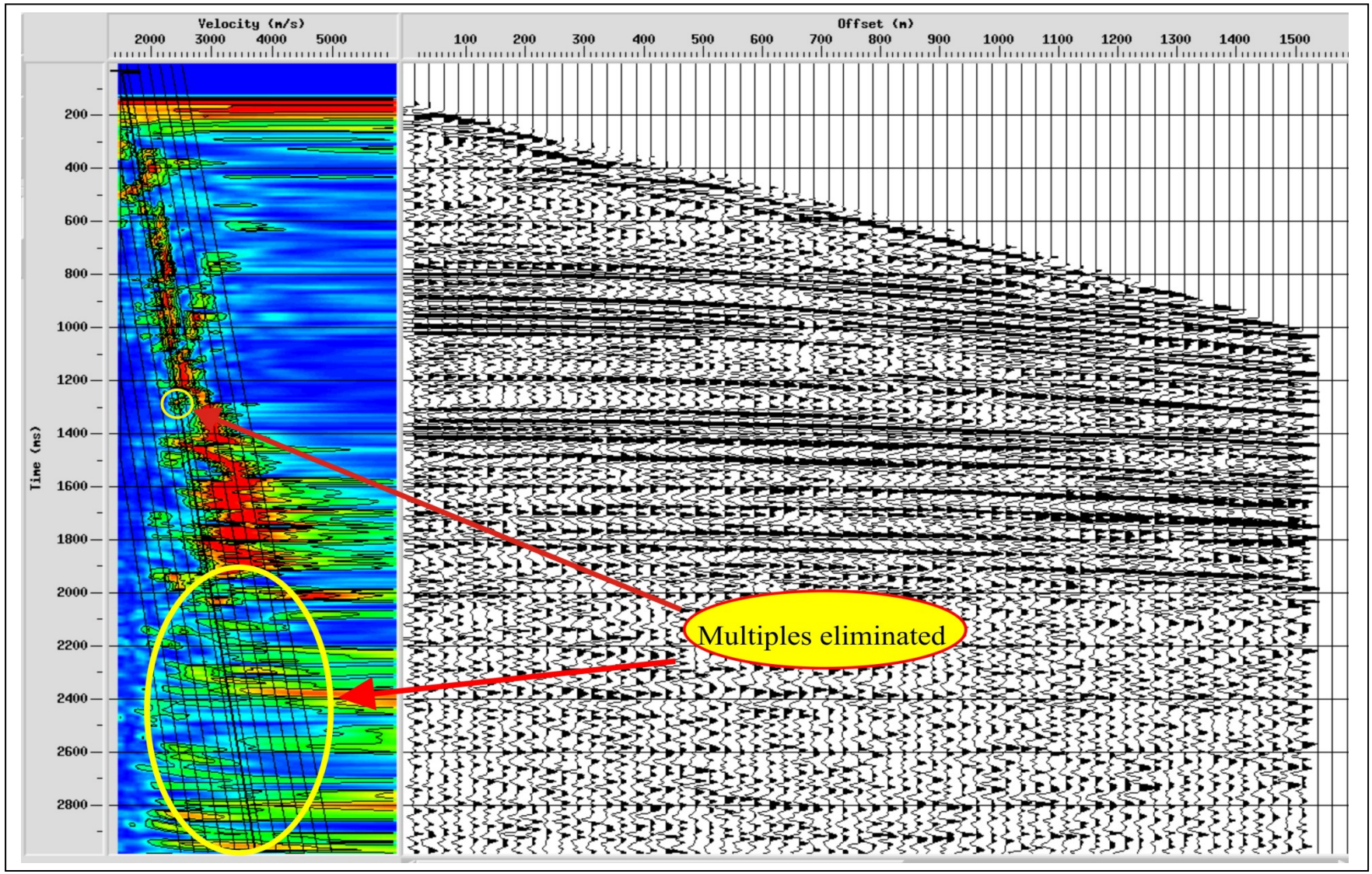

Figure 2.7 Velocity analyses (Line H) after applying Radon filter (Multiple suppressed by Radon filter).

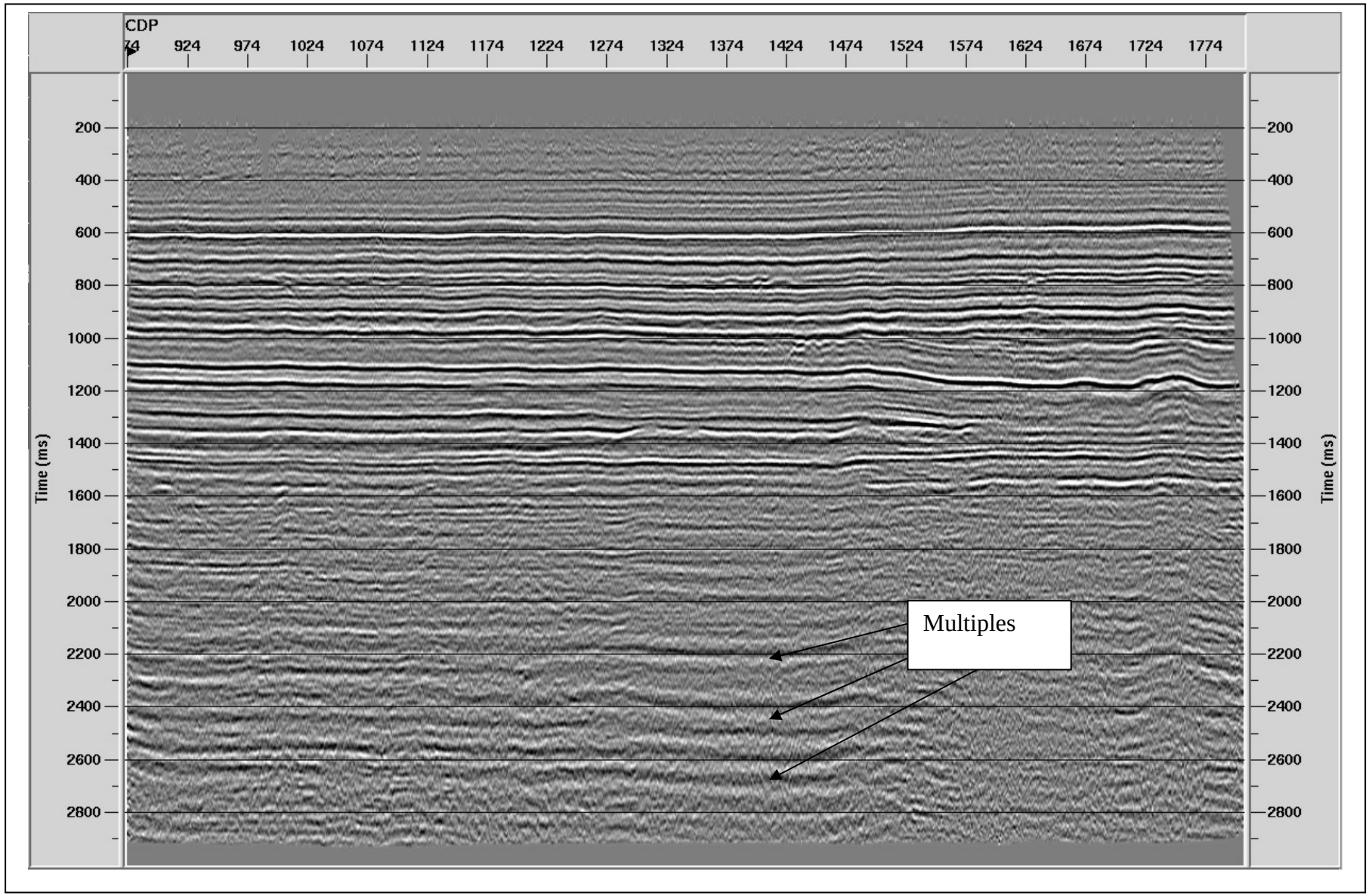

Figure 2.8 Stacked section (Line E) before using Radon filter.

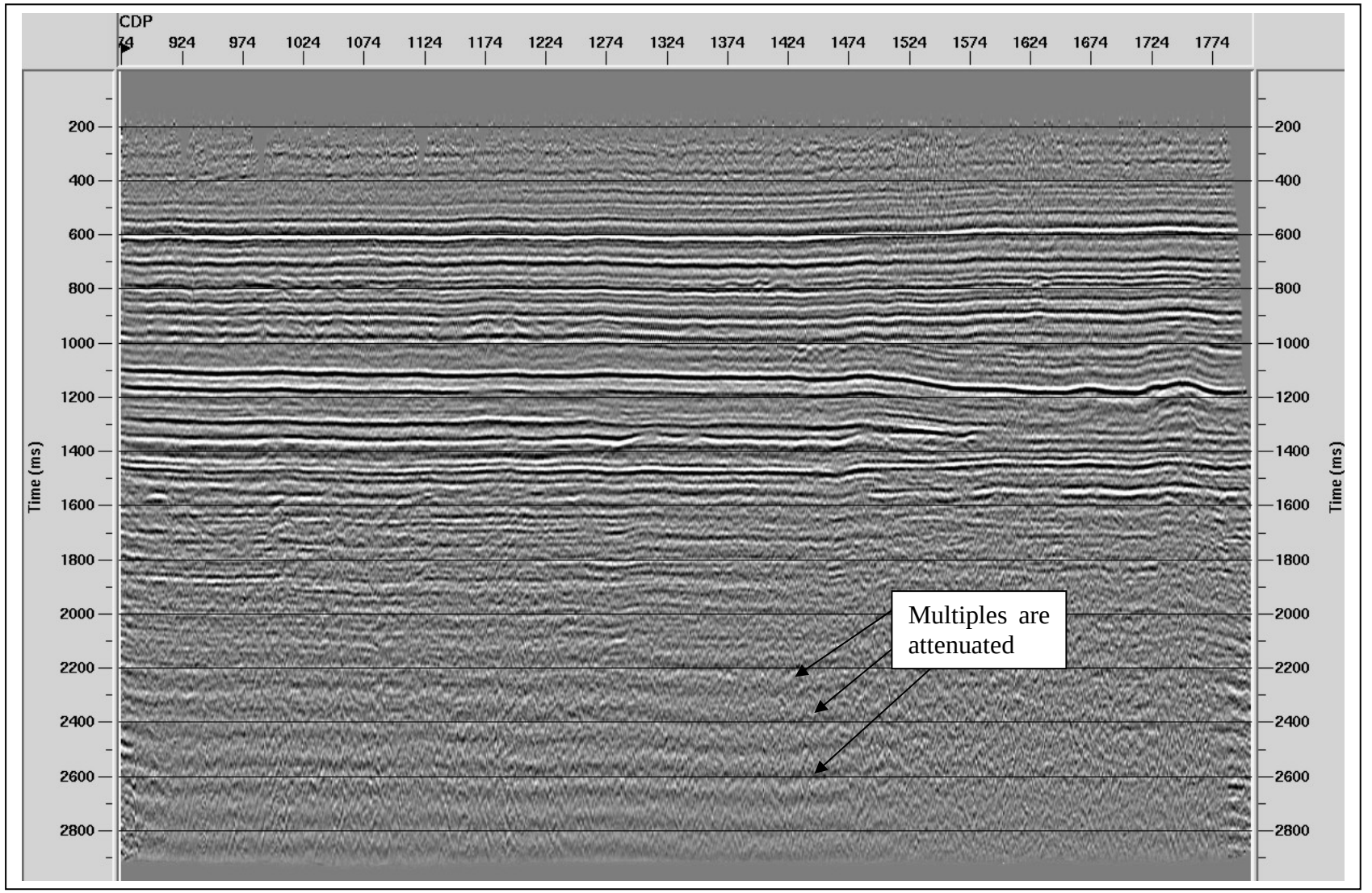

Figure 2.9 Stack section after multiples suppression (Line E) using Radon transform filter.

Migration

Migration is the final step of conventional seismic data processing. It is a tool utilized in seismic processing to produce an accurate depth or time image of subsurface layers. Migration involves geometric repositioning of the reflection events to their true subsurface positions and collapsing diffractions caused by local heterogeneities. At the CMP stacking step, it is assumed that all the reflections appearing on a seismic data occur at interfaces lying directly below the corresponding midpoints (vertical incidence). This is true when the reflecting subsurface boundaries are horizontal. In the case of dipping interfaces, reflected signals may arrive from different locations, which is not directly located below the receiver. To properly image these reflections, migration is required. However, and in the study area, reflecting horizon dips are relatively low, and this aspect of migration is relatively unimportant. A further advantage of migration is in its collapse of diffraction hyperbolas to their apexes and delineating the detailed of seismic discontinuities such as faults planes and layer edges and pinch-outs.

High-frequency signal enhancement

Time-variant spectral whitening (TVSW) was selected as the primary tool for enhancing and normalizing the frequency content of the records. TVSW flattens the spectra within a selected frequency band by applying time-variant band-pass filters compensating the progressive loss of high-frequency energy. Two options for application of TVSW in the processings flow of this study were considered: 1) application before NMO stacking, and 2) using TVSW after the stack. Generally, both TVSW and NMO stacking are approximately linear operations, and consequently the

sequence of these operations should have no influence on the result. The reason for TVSW being typically carried out before stack is in the potential improvement of the quality of velocity analysis and residual statics. However, in this study, both pre- and post-stack TVSW application modes were tried, and the above effect on the velocity analysis was found insignificant. On the contrary, pre-stack application of TVSW boosted the noise levels in the CMP gathers leading to poorer performance of GRT multiple suppression. Thus I chose to apply the TVSW with the stacked records whose improved signal-to-noise ratios allowed the TVSW process to produce less high-frequency noise while allowing good quality control on every processing step.

The TVSW algorithm was designed by specifying several narrow-band filters spanning the frequency band of interest. Each trace was first filtered within each of these frequency bands, and its amplitude was normalized using the Automatic Gain Control (AGC). Both the resulting normalized and filtered traces and the corresponding AGC scalars were summed to produce the "whitened" output trace and an average AGC scalar trace. Finally, to restore the true amplitude, the whitened output trace was multiplied by the time-variant average AGC scalar. A TVSW code was been written to implement this method (see tool "`tvsw`" in http://seisweb.usask.ca/SIA/www/index/index.html; Appendix B). To process the seismic lines of this study, I used a similar method implement in PROMAX software.

In order to further increase the resolution and enhance signal coherency and continuity at high frequencies, TVSW was followed by *f-x* deconvolution. While TVSW was principally responsible for boosting a selected frequency band of the resulting images, the effect of *f-x* deconvolution was in improving the image coherency and reduction of random noise.

2.3 Seismic Resolution

Usually with increasing depth, the high frequencies of seismic data decrease due to the effects of earth absorption and noise while the velocities and wavelengths increase. This means that with increasing depths, the seismic resolution becomes poorer. Two types of resolution are considered – vertical and horizontal resolution, both of which are controlled by the signal bandwidth. In both cases, the resolution criterion requires that the two events (reflections) are separated in time by at least one half of the dominant period of the signal, that is: $\Delta t \geq T/2 = 1/2f$, where f is the dominant frequency. This leads to the important requirement of spatial separation between the two incident wavefronts $\Delta Z \geq \lambda/4$, where λ is the dominant wavelength (Sheriff and Geldart, 1995).

Horizontal resolution is a measure of how close two reflecting points can be located horizontally in order to be seen as two separated points. Lateral resolution in seismic studies is related to the width of the first Fresnel zone (Figure 2.10) (Yilmaz, 1987). The radius of the first Fresnel zone can be calculated to help interpreters determine the minimum structures that can be resolved:

$$R = \sqrt{(Z + \Delta Z)^2 - Z^2} \approx \sqrt{\frac{Z\lambda}{2}} = \frac{V}{2}\sqrt{\frac{t}{f}}\,. \qquad (2.2)$$

Here, R is the Fresnel zone radius, Z is the depth to the reflector, λ is the wavelength, V is the subsurface velocity, time (s), t is the two-way reflection time, and f is dominant frequency of the signal. Any two reflecting points located within the first Fresnel zone are considered undistinguishable using the dominant frequency. With increasing imaging frequency, the Fresnel zone radius would be smaller and the lateral resolution would improve.

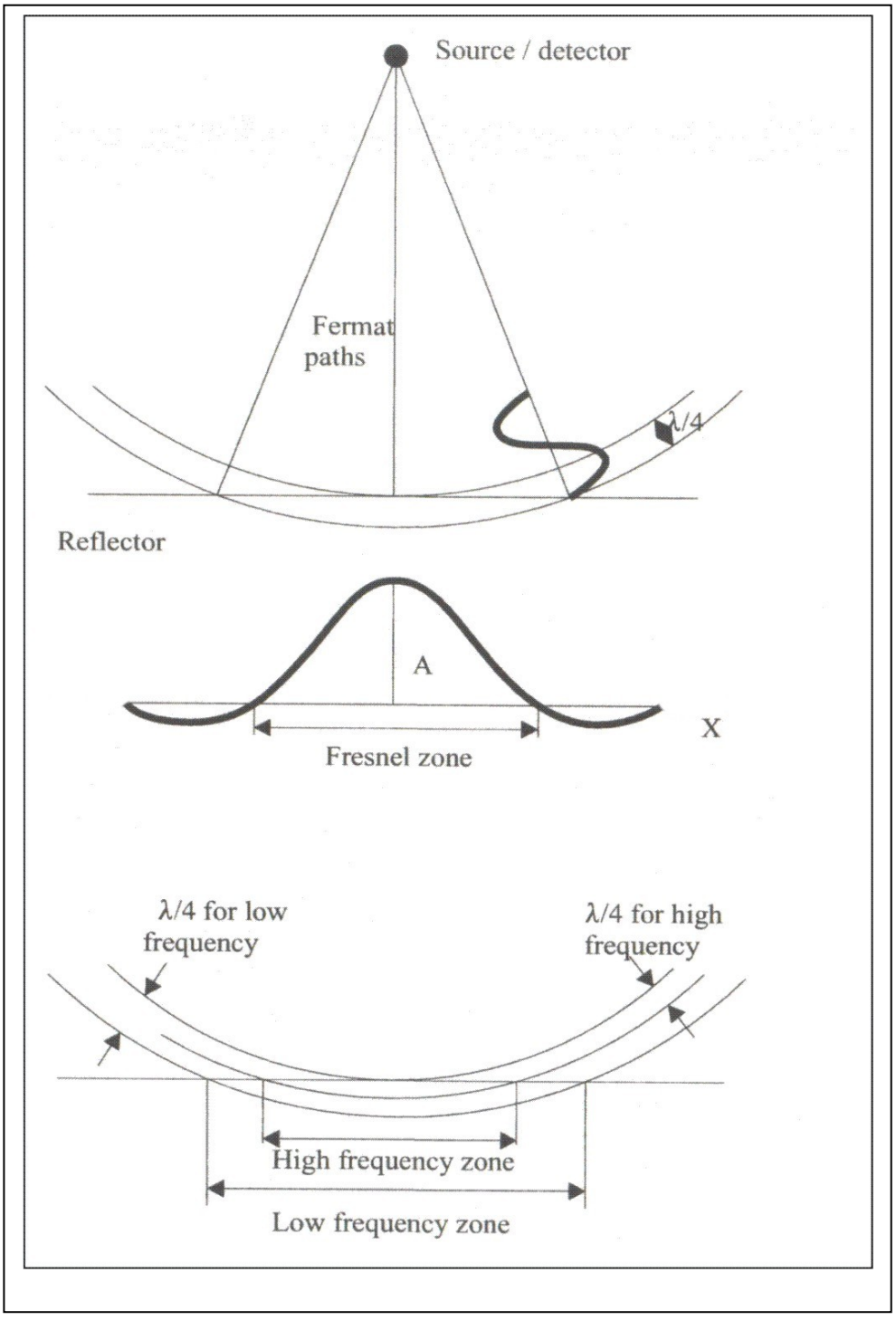

Figure 2.10 Principles of horizontal resolution of seismic method (Emery and Myers, 1996). (A) The reflection ray path and schematic wavelet, (B) amplitude of the reflector as a function of the distance, (C) comparison Fresnel zone at two frequencies.

Vertical resolution in seismic exploration is the minimum separation between reflections that can be resolved on a single seismic trace. For vertical resolution, $\Delta Z=\lambda/4$ is normally considered as the resolution limit unambiguously recoverable bed thickness, In order to improve the resolution, several techniques for enhancement of high-frequency energy were tried as described above. The resulting optimal procedure included a combination of trace equalization (Automatic Gain Control) and *f-x* deconvolution with time-variant spectral whitening.

An example from seismic line E (Figure 2.11) shows that in the raw data, reflection amplitudes near the target depth drop by ~50 dB from 10 Hz to 80 Hz because of the strong absorption and attenuation within the thick sedimentary cover. Without compensation for this attenuation, the dominant frequencies in the final stack are close to 30 Hz, and consequently the $\lambda/4$ vertical resolution limit (with velocities of about 2900 m/s) is ~ 25 m (Figure 2.11).

Salt dissolution causes subsidence of the overlying strata, which can be clearly seen in the western part of the seismic section shown in Figure 2.11. Discontinuities in the seismic reflection events show that several faults exist in the area. However, the fault offsets are difficult to measure from this section and internal thin beds of the Prairie Evaporite and the salt edge are not accurately displayed. The internal thin beds of the Prairie Evaporite appear as inter-mingling events between 1260 and 1330 ms.

Figure 2.12 shows the final migrated stack after applying the frequency-enhancement procedures. The dominant frequencies increased from ~30 Hz to ~50 Hz at the formation depth, thereby improving the estimated depth resolution to ~15 m. The resulting stacked section (Figure 2.12) shows a marked improvement in the detail and

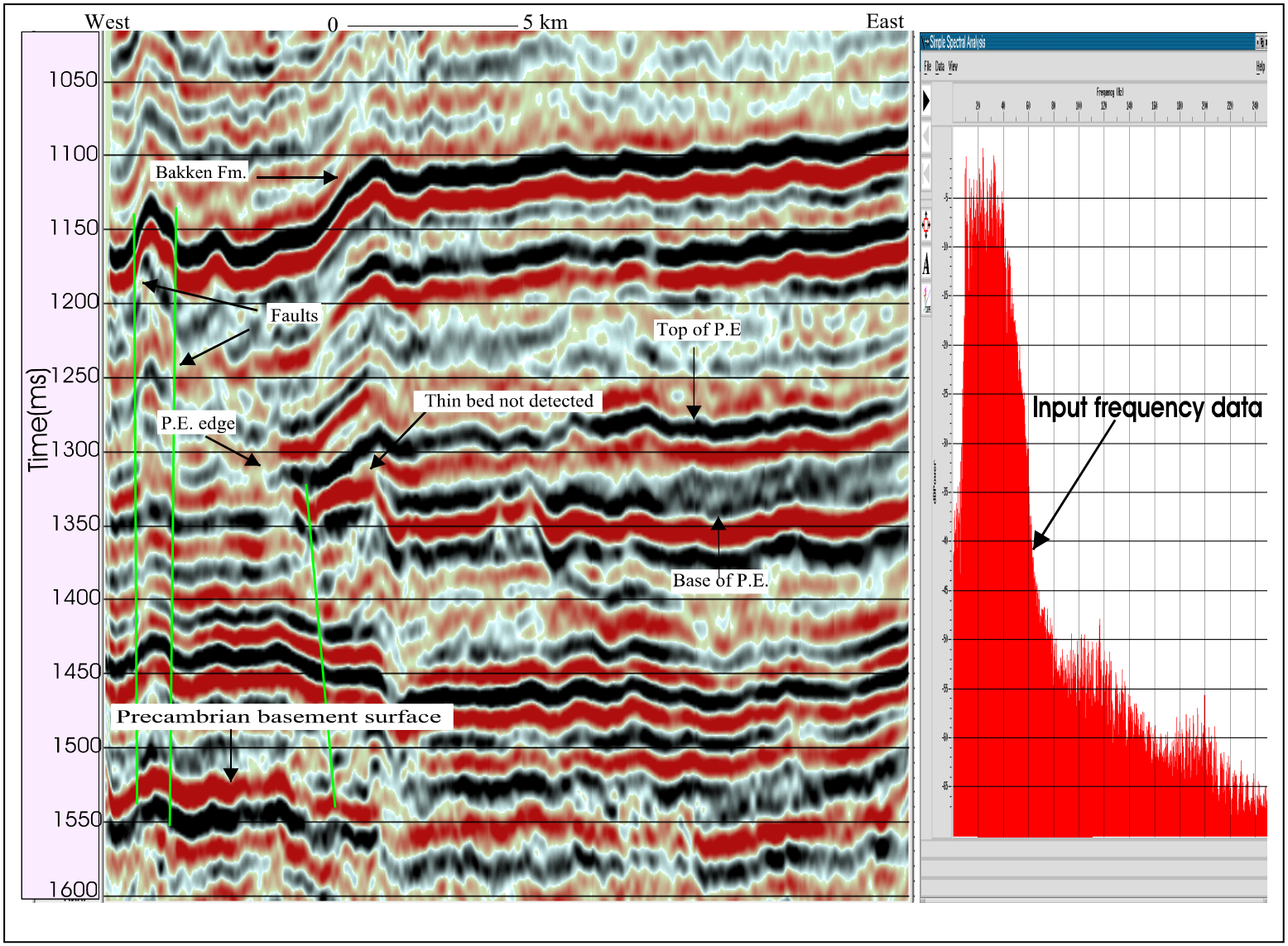

Figure 2.11 Final stack from line E without spectral whitening applied. Note the slumping of the strata caused by salt dissolution in the western part of the section. Also note that the depth resolution of the image is still comparatively low.

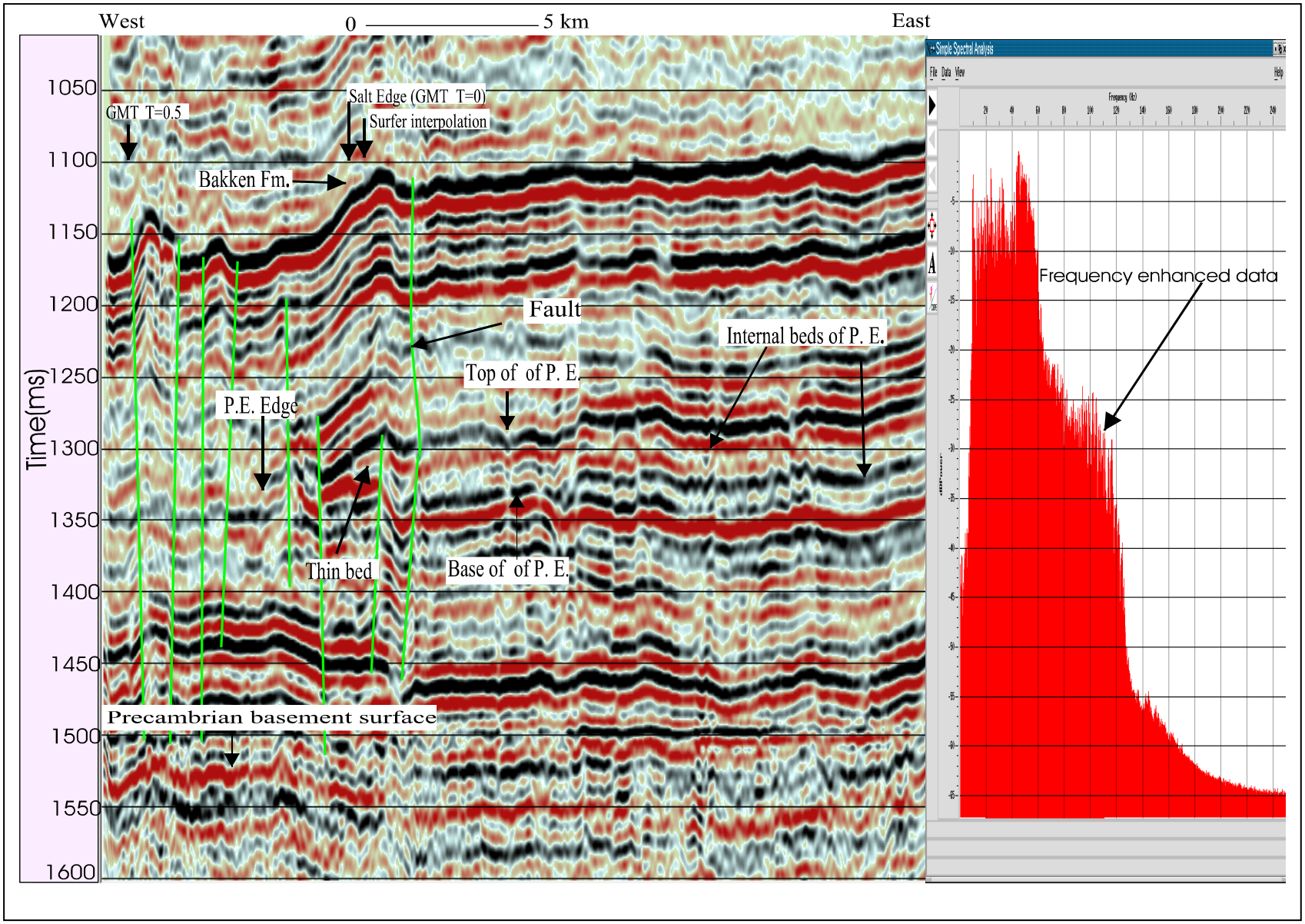

Figure 2.12 Final stacked section from line E with post stack spectral whitening and *f-x* Deconvolution applied. The internal thin beds of the Prairie Evaporite are more visible and are thinning toward the west. Note the interpreted salt collapse that perturbed the strata beneath the Bakken formation.

continuity of the image, and the generally recognizable features include: 1) internal thin beds within the Prairie Evaporite; 2) a more accurately delineated salt edge; and 3) clearer imaged fault displacements that can be measured more accurately from the seismic events. However, accurate resolution of the internal structure of the P.E still requires detailed matching the observed waveform with synthetics.

2.4 Tuning Effects

Tuning effects are caused by constructive or destructive interference of the wave reflected from closely separated boundaries. If the bed thickness is less than $\lambda/4$, events undergo constructive interference and generate a single event of high amplitude. At thicknesses greater than $\lambda/4$, the top and the base of the bed can be distinguished as two separate events. Bed thickness at which two reflections appear indistinguishable in time is known as the tuning thickness. Tuning effects are important in the analysis of hydrocarbon reservoir, hidden trap, cracks, etc.

The Ricker (1953) and Widess (1973) criteria of resolving thin beds are widely accepted. Interpretation of tuning effects from isolated thinning strata is used in estimation the thickness of a thin layer. Based on the velocity, density, thickness and the location of the thin beds in space, tuning effects from interference events could change the wavelet shapes as the bed thins and result in a complex waveform.

Figure 2.13 shows reflections observed in a thinning bed represented by spike of the same and opposite polarities. In addition to the changes in wavelet shapes as the layer thins, high-amplitude anomalies caused by the interference of the top and base reflections are also observed. These anomalies occur near the resolution limit (~12 ms)

in the case of opposite-polarity reflections (Figure 2.13A), and near zero bed thickness in the case of the same reflection polarity (Figure 2.13B).

Similar resolution analysis could be applied to structural features such as faults. Figure 2.14 illustrates a series of faults with varying offsets. The fault can be seen clearly when the displacement is $\lambda/4$ or larger.

Reasnor (2001) indicates that the dissolution edge of the P.E can be reliably identified by the onset of "tuning" in seismic data. Tuning leads to high amplitude observed around the edge the low velocity salt layer where its thickness reaches below the seismic wavelength. Tuning effects has been observed clearly near the edge of the P.E. on seismic line J (Figure 2.15).

2.4.1 Wedge Model

One of the seismic lines of this study (J in Figure 1.1) presents a case in which interference reflection from two closely spaced reflections of the P.E was recorded. As the main objective of this study is to locate the "zero-thickness" edge of the P.E., it is desirable to estimate bed thickness of the P.E thinner than $\lambda/4$. To achieve this, I performed simulations of the P.E. reflection in a simple wedge model in order to relate its amplitude variations to the thickness of the thinning bed. To calculate the seismic response of a thinning P.E bed, a Ricker wavelet with dominant frequency of 50 Hz and 2 ms sample interval was used and convolved with a two-reflector wedge model.

I built the time model that picked the top and bottom of the Prairie (Figure 2.16A) based on seismic and well log information. The velocities of P.E and overlaying (Dawson Bay) and underlying (Winnipegosis) formation are 4475, 5500 and 5600 m/s, respectively. Their respective densities were 2200, 2600 and 2700 kg/m^3. The depth of

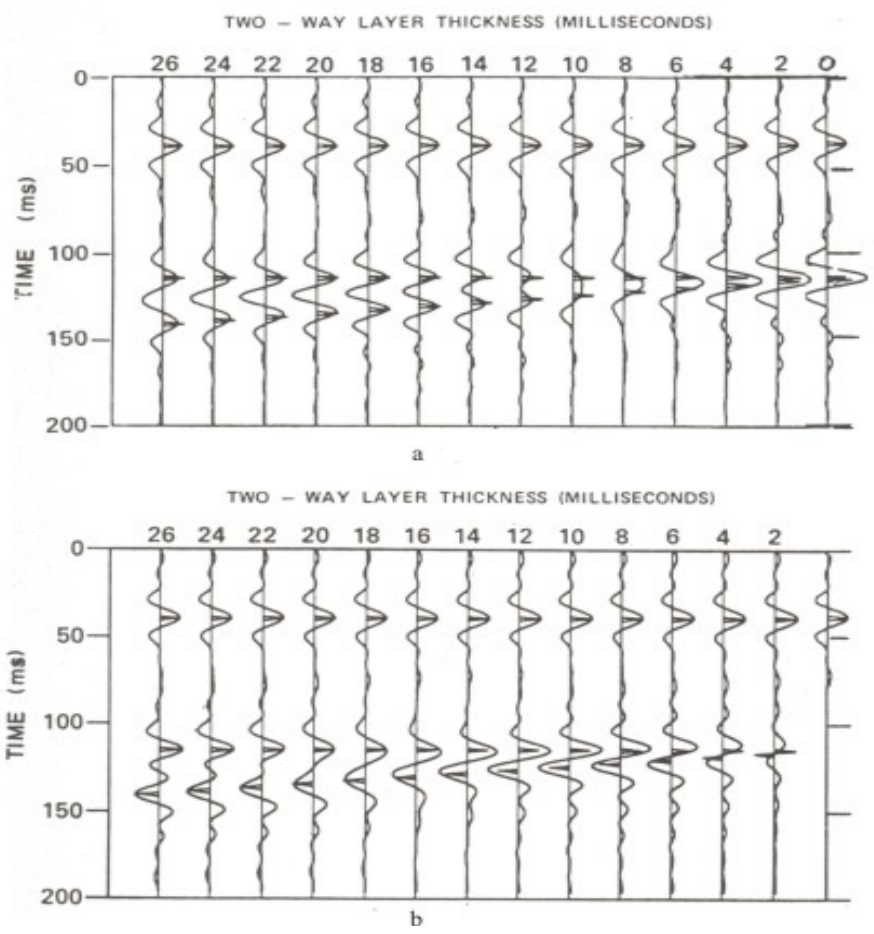

Figure 2.13 Synthetic events illustrating vertical resolution at a thinning bed (from Kalweit and Wood, 1982): (A) reflection coefficients of the same polarity (B) reflection coefficients of opposite polarities. Note the differences in the amplitude near the pinch out.

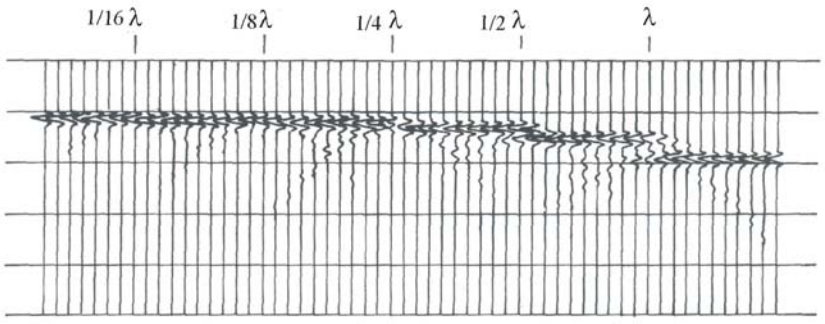

Figure 2.14 Event from a faulted reflector with a fault offset indicated as a fraction of the wavelength (from Sheriff and Geldart, 1995). The fault can be detected at 1/4 λ of the wavelength.

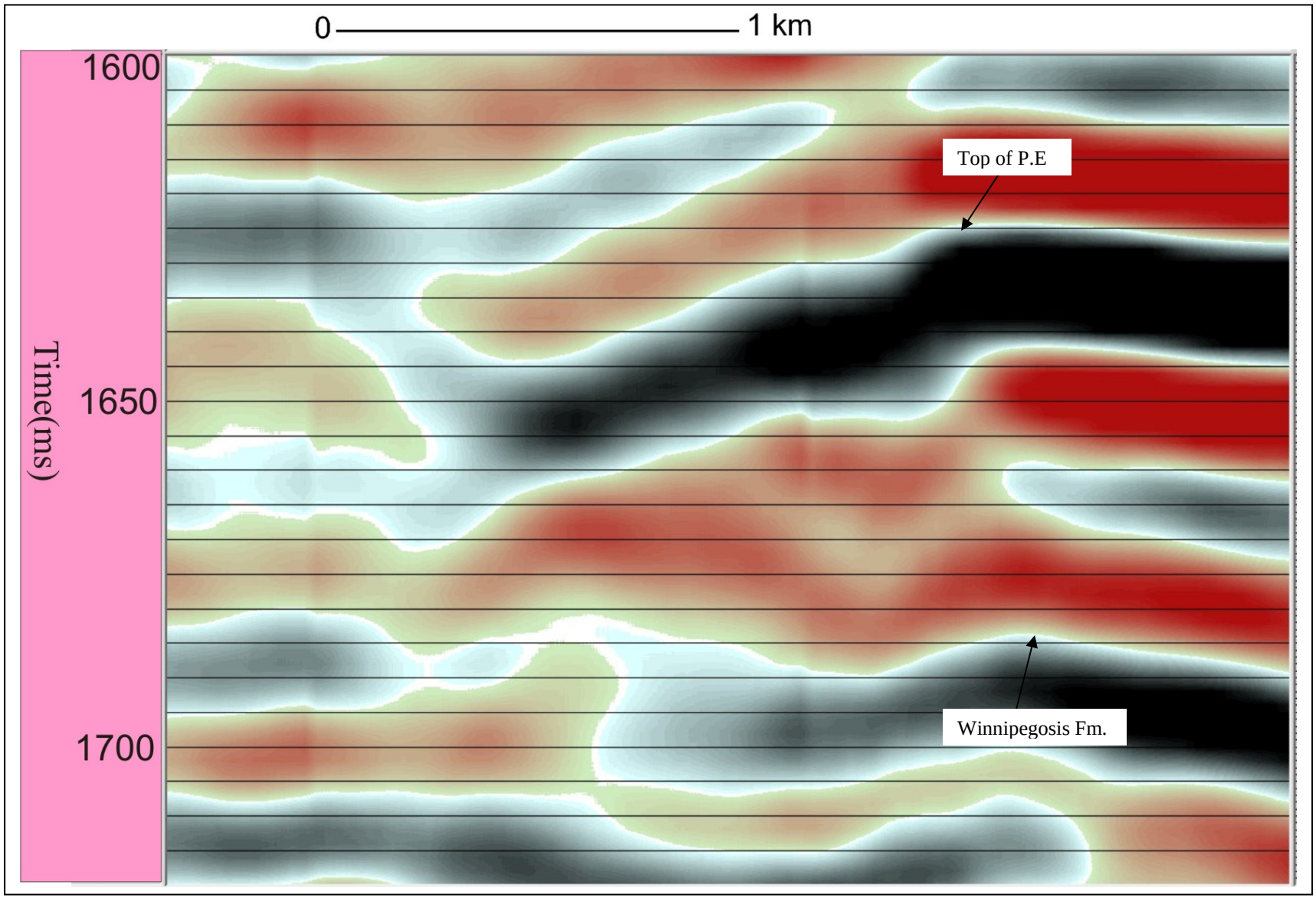

Figure 2.15 A segment of seismic line J showing a tuning effect. Note the unusual high amplitude of closely separated reflections of the Prairie Evaporite -P.E.

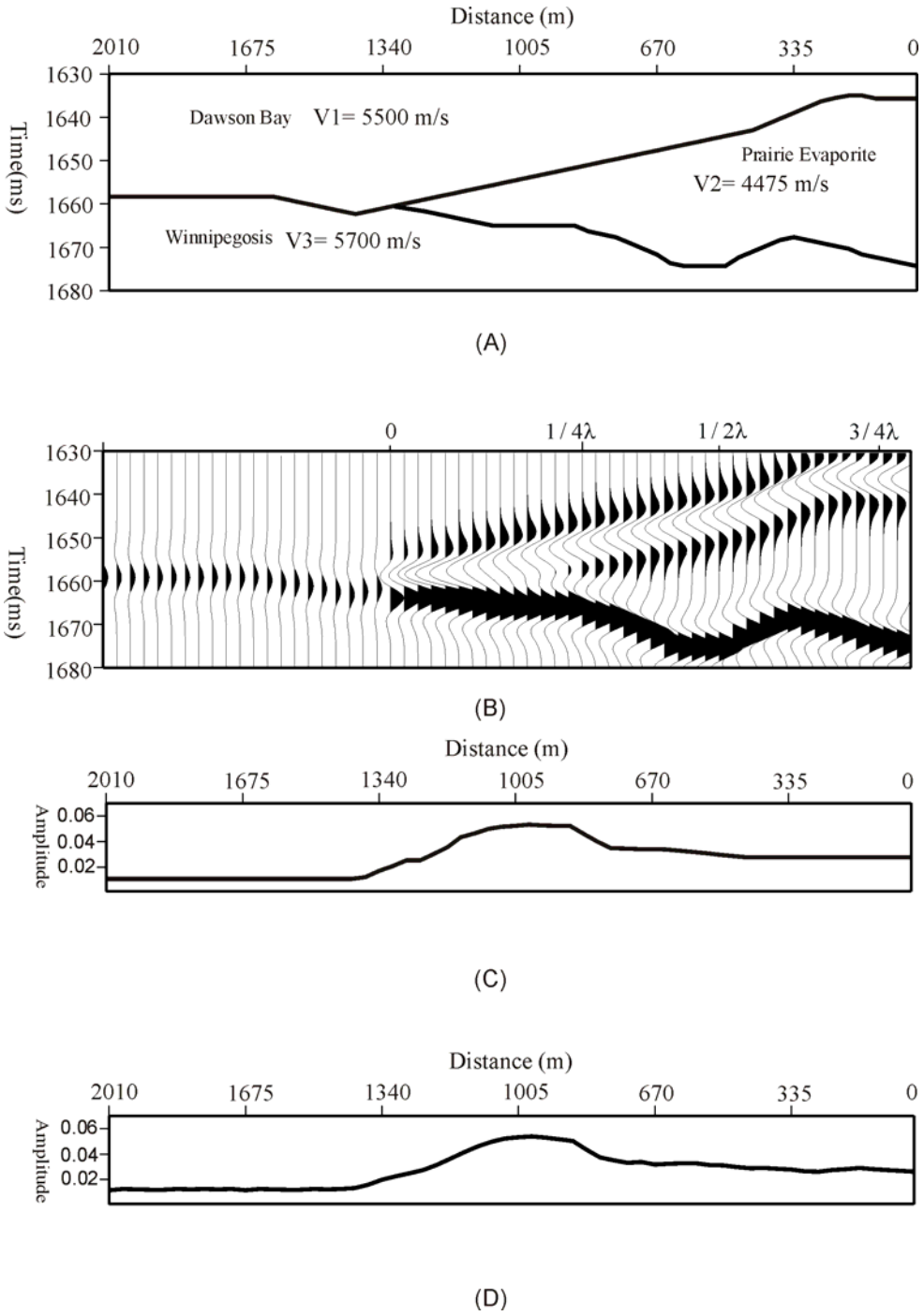

Figure 2.16 (A) Wedge model, (B) synthetic seismogram, (C) synthetic amplitude versus distance, and (D) amplitude versus line distance dependence measured from the data. Note that when the wedge is $\lambda/4$ thick, maximum constructive interference (tuning) and high amplitude are occurred.

the Prairie Evaporite (P.E.) imaged in this study varied from 1600-2500 m and its thickness ranged from 150 to 0 m. The seismic data gathered in this work have a frequency bandwidth from 10 to 120 Hz with dominant frequency of 50 Hz at the target depth. The main object of this model is to demonstrate that the P.E. Formation $\leq \lambda/4$ in thickness can cause a reflection with complex wavelets and to constrain the position of the edge by matching the observed amplitude tuning anomaly with the synthetics.

A synthetic seismogram is shown in Figure 2.16B for the P.E. velocity of 2900 kg/m with dominant frequency of 50 Hz. The maximum constructive interference (tuning) occurs at P.E thickness of $\lambda/4 \approx 15$ m. For P.E thickness below 15 m (tuning thickness), the amplitude of the combined top and base of P.E reflection decreases and the combined events appear approximately as a single reflection (Figure 2.16B). The reflection amplitude is the manifestation of the differences in physical prosperities of the geological formations. The larger the difference in these physical properties, the larger the amplitude of seismic reflections will be recorded from the reflection boundary. From this, it would be natural to expect large amplitude at the boundaries of the formations below (Winnipegosis) and above (Dawson Bay) the Prairie Evaporite due to the large differences in physical prosperities (Figure 2.16B), and small amplitude would be recorded at the reflection surface between Dawson Bay and Winnipegosis caused by small differences in physical properties between them. In order to obtain an accurate model below the tuning thickness, amplitude information must be used. The extracted amplitude of the synthetic and raw data over the thinning layer shows a good correlation along the thinning layer, large amplitude over the tuning thickness and small below it (Figures 2.16C and D). By matching the observed variations in the composite reflection

amplitude (Figure 2.16D) with the modeled one (Figure 2.16C), the position of the pinch-out of the P.E. can be estimated.

Figure 2.15 shows the slope, thickness gradient and the tuning effect of the Prairie Evaporite are clearly detectable. The position of the salt edge of the Prairie Evaporite west of seismic line J can be extrapolated based on the slope of the Prairie Evaporate shown in Figure 2.15. The wedge model (Figure 2.16A) thus leads to an extrapolation of the salt edge west of the zone of observed tuning in seismic line J.

3. INTERPRETATION

The interpreted seismic data were used to correlate the areas of salt dissolution with the underlying structures such as Precambrian basement, Winnipegosis Formation, faults, and other structural features in an attempt to document their potential relationships. Below, I start with the use of seismic results to improve the mapping of the southern margin of the P.E, to explore its correlation with the basement structure, and to constrain the times when salt dissolution occurred. The results of seismic interpretation are further incorporated in subsurface mapping of the Prairie Evaporate, and the effects of several 2D interpolation techniques are discussed. At the end of this chapter, I also investigate whether the salt edge could be observed from gravity data.

3.1 Seismic Interpretation

Identification of the seismic horizons was based on the interpretation of the synthetic seismograms produced by the sonic and density logs available in the study area. Synthetic seismograms play the key role in recognition of position of geological formation tops on seismic data. The synthetic data show the seismic response at well where the geology is known and permit the subsurface well log data to be correlated with seismic horizons. A synthetic seismogram is the convolution of a reflection coefficient series with a source wavelet. If a seismic wave crosses an interface separating two different lithologies, the reflected energy is calculated by the reflection coefficient:

$$R_i = \frac{\rho_{i+1}V_{i+1} - \rho_i V_i}{\rho_{i+1}V_{i+1} + \rho_i V_i}, \qquad (3.1)$$

where V_i and ρ_i are the densities and velocities of the corresponding layers. The product of velocity and density is the acoustic impedance (Telford et al, 1990).

Synthetic seismograms were generated from sonic and density logs from well sites near the seismic lines being interpreted. Well logs were digitized and loaded into synthetic seismogram-generating software (Geoframe). Ricker wavelet was used to generate the synthetic seismograms based on the sonic and density logs available in the study area. The resulting synthetic seismograms were spliced into the seismic section and correlated by moving the synthetic seismogram until the reflection pattern matched the synthetic. Lithologic units producing high amplitude peaks or troughs should match well if the synthetic seismogram and seismic section are correctly tied. Some examples of the synthetics are displayed in Figures 3.1 and 3.2. The figures show the velocity, density, wavelet, synthetic seismogram, identified formation tops, and a segment of a seismic line for comparison.

The sonic logs indicated that Bakken and P.E formations have lower velocities compared to the overlying and underlying formations, while Winnipegosis formation has higher velocity compared to the formations above it. Consequently, reflection coefficients show negative amplitude for Bakken and P.E formations and are therefore indicated by troughs in the synthetic data. Reflection coefficient of Winnipegosis Formation displayed as positive reflection amplitude in all synthetic data.

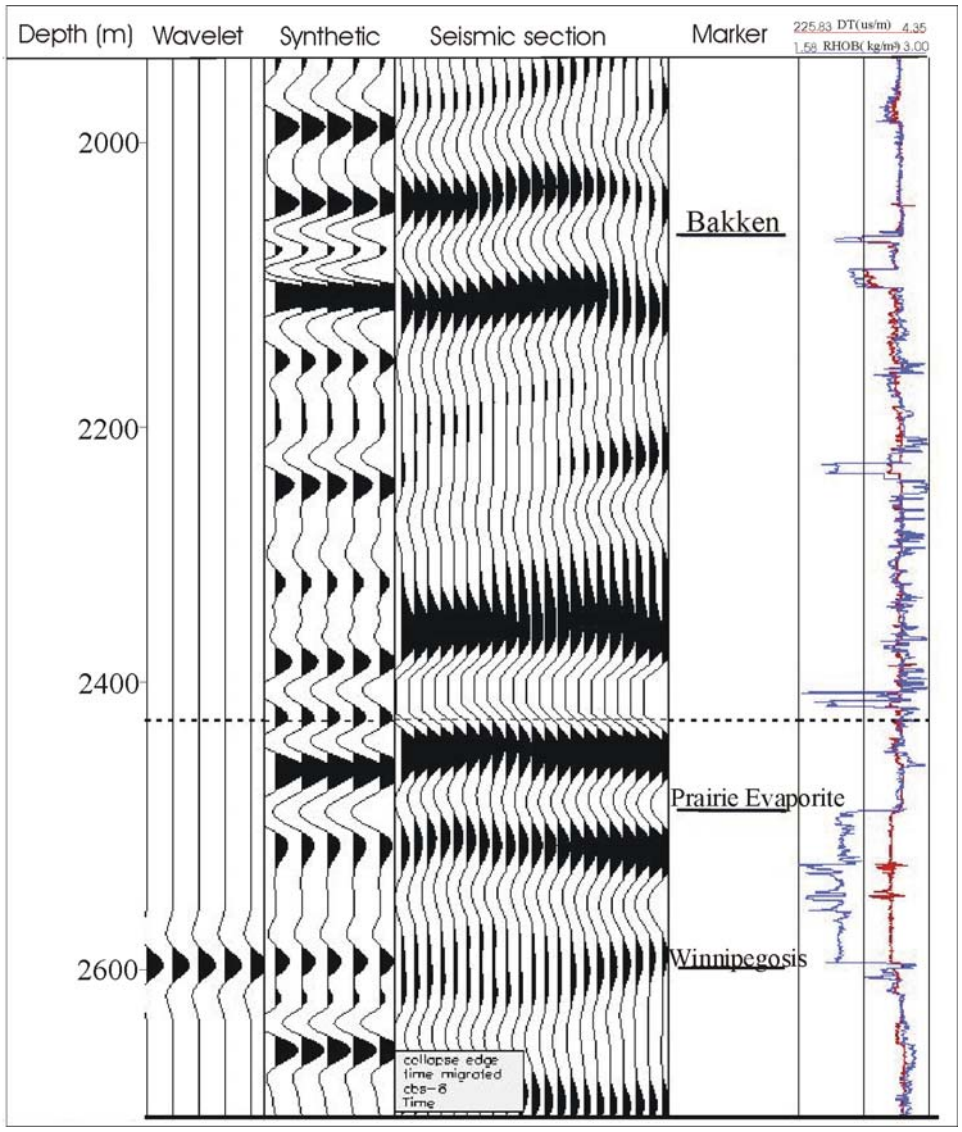

Figure 3.1 Sonic log, density log, wavelet, location of the formation tops of well no. (01/08-05-002-14W/0), and the corresponding synthetic seismogram compared to a segment of seismic line J.

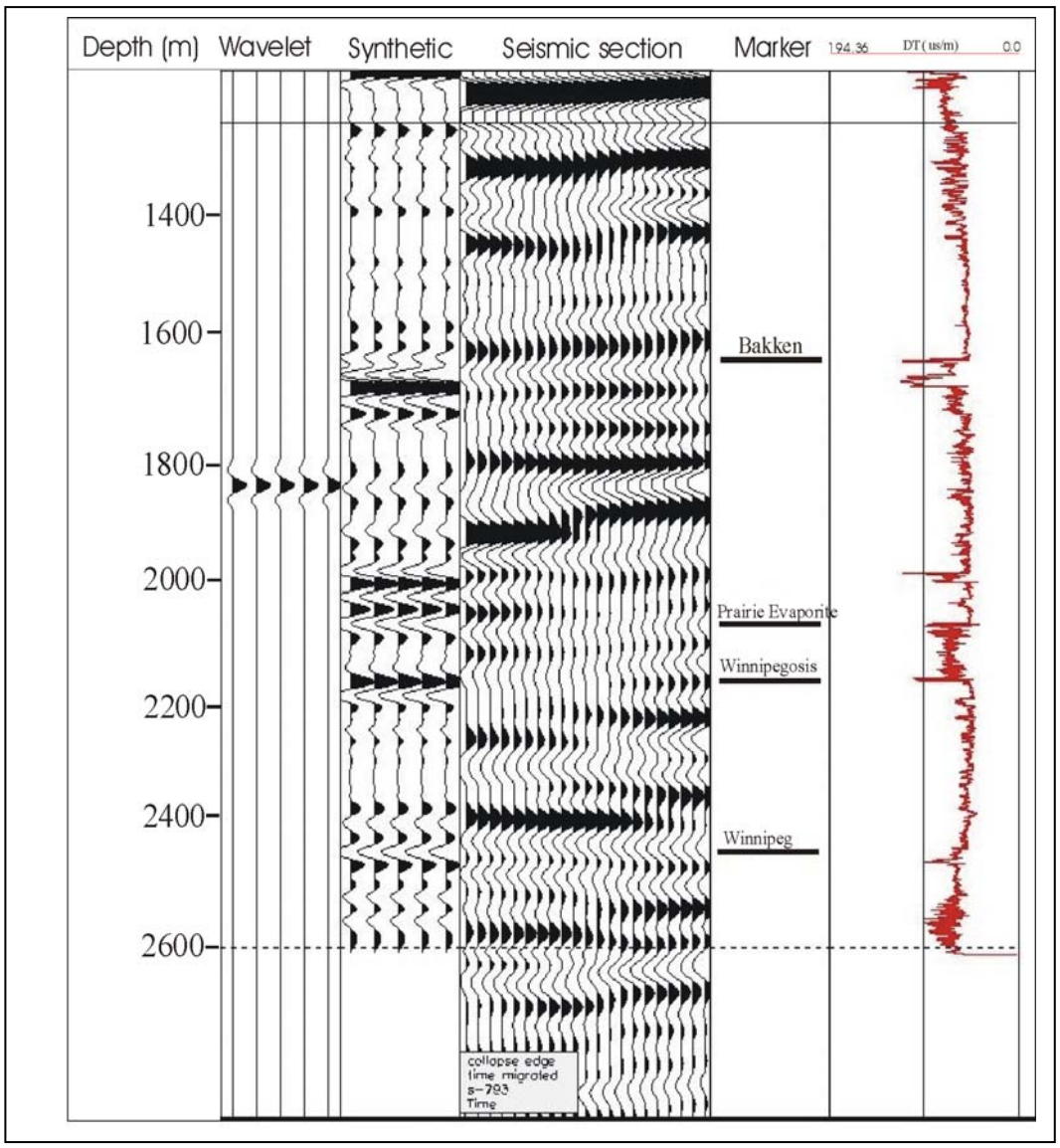

Figure 3.2 Sonic log, wavelet, location of the formation tops of well no. (01/12-33-005-23W/0), and the corresponding synthetic seismogram compared to a segment of seismic line M.

Due to the consistent and characteristic acoustic behaviour of Bakken, P.E and Winnipegosis formations, these geological units were used to tie synthetic data to the seismic lines. The synthetic data were adjusted to the tops of the respective formations. Good correlations were found between the synthetic seismograms and seismic data. Figures 3.3 and 3.4 show seismic lines J and M correlated with the synthetic data for boreholes 01/08-05-002-14W2/0 and 01/12-33-005-23W2/0, respectively.

The main goals of seismic interpretation in this work are to better delineate the P.E. formation, identify subsurface structures that influence the dissolution of P.E, and document the relations between the P.E. and the underlying and overlaying formations. We thus selected seismic lines that mostly either crossed or were located close to the salt edges. In summary, the data (described in detail below) indicated a major salt dissolution of the Prairie Evaporite located off-salt, and local salt dissolution within the Prairie Evaporite. In the study area, seismic sections indicate that salt dissolution occurred in Mississippian, Triassic, Jurassic, and more recently as it disturbs all of the overlying seismic horizons.

Seismic line E (Figure 3.5) shows a salt dissolution that occurred during the Mississippian. Salt dissolution structures, basement uplift and vertical throw faults are well imaged in this line. Some of the faults are deep, rooted in the basement and appear to extend to the surface. Others are shallow and penetrate into the Devonian strata.

The salt dissolution caused subsidence of the overlying sediments. Time structure anomaly was observed within the zone of the subsidence suggesting that extensive faults system is present in the salt collapse zone. The seismic line displays a relatively wide salt edge front of about ~3 km.

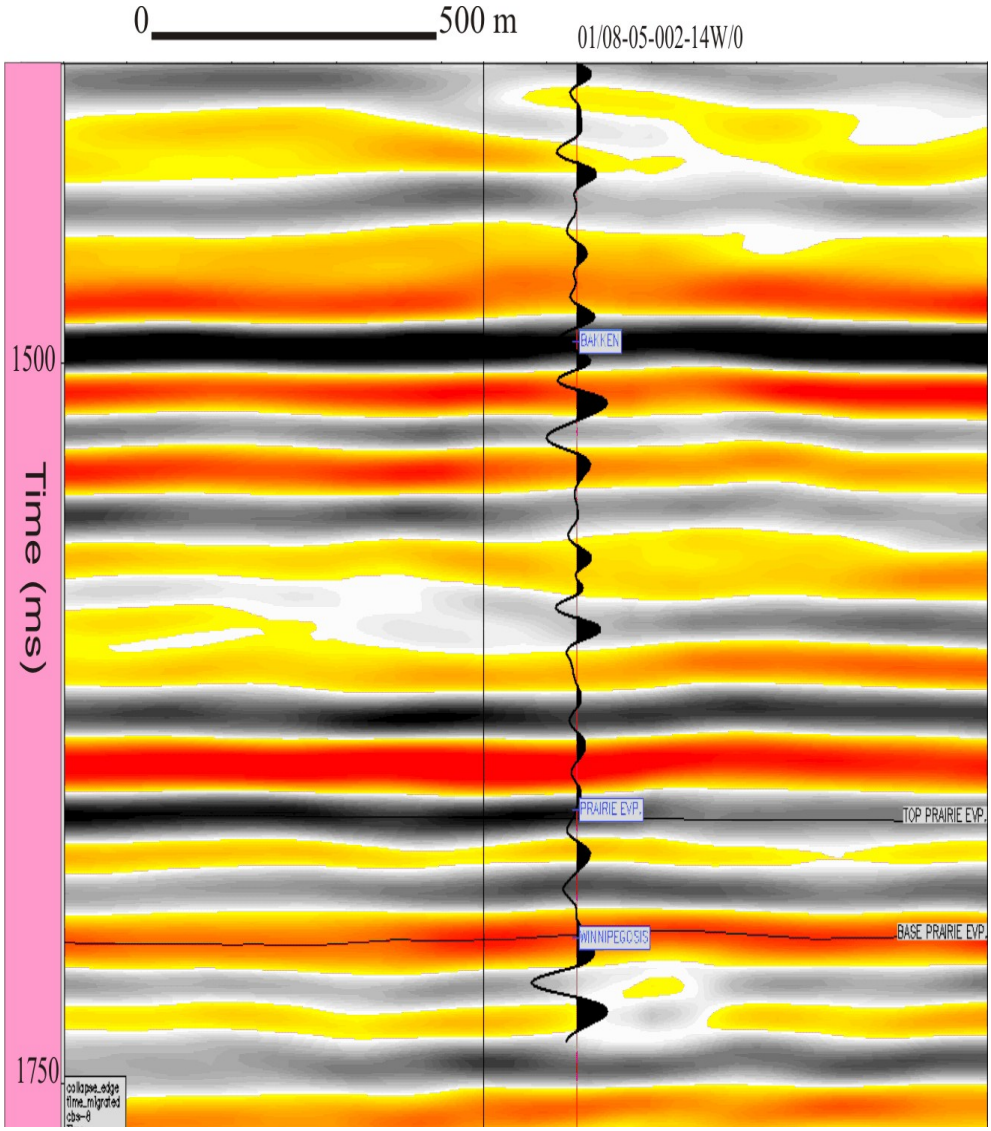

Figure 3.3 Correlation of synthetic seismogram of well no. 01/08-05-002-14W2/0 with seismic line J. Black colour indicates negative amplitudes and red shows positive amplitudes.

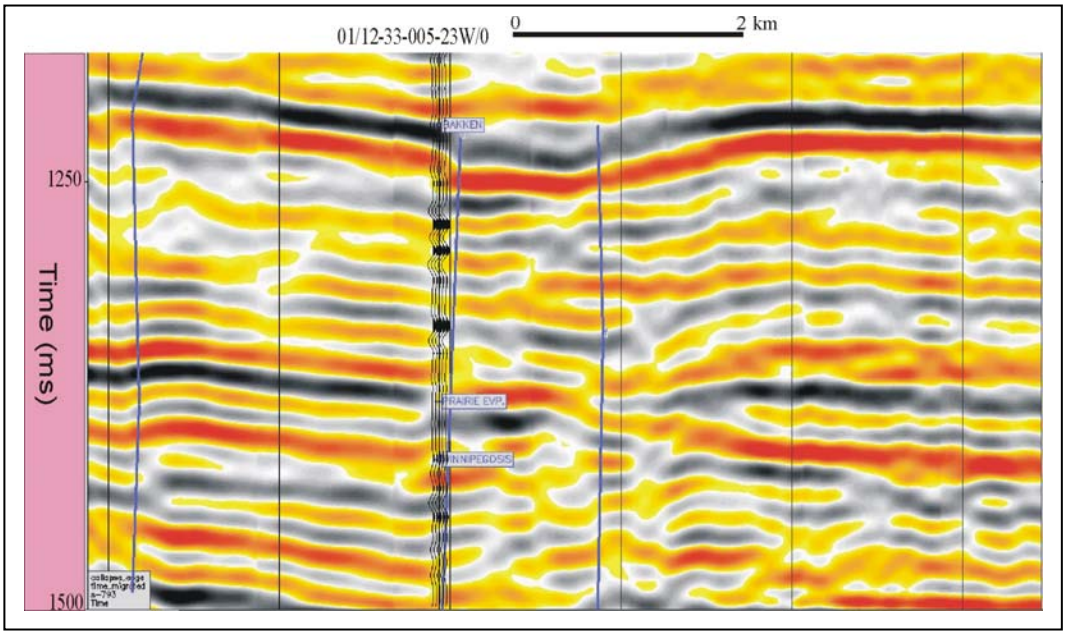

Figure 3.4 Correlation of synthetic seismogram of well no. 01/12-33-005-23W2/0 with seismic line M. Black colour indicates negative amplitudes and red shows positive amplitudes.

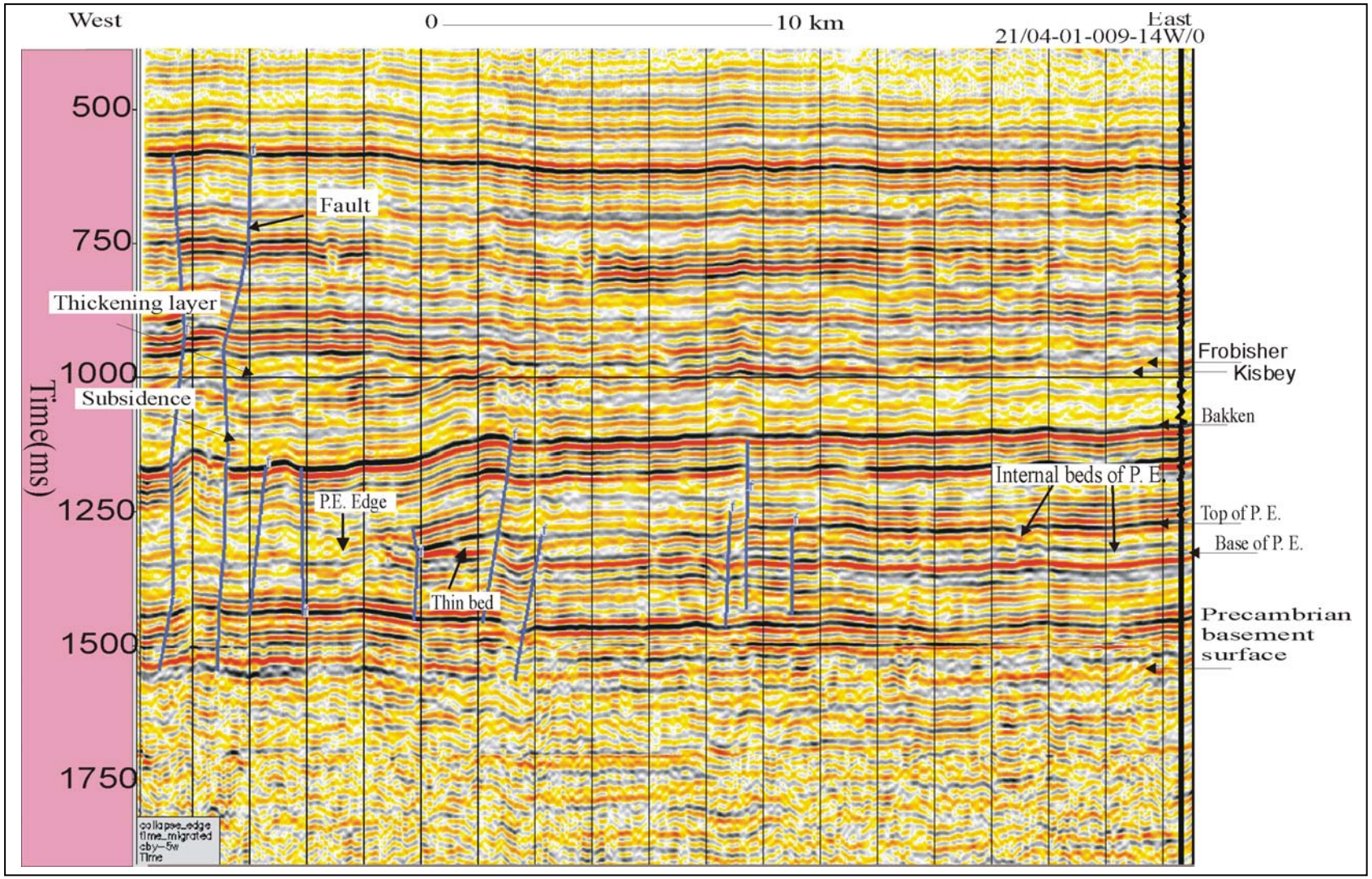

Figure 3.5 Salt-dissolution induced subsidence that did not affect the strata shallower than about ~980 ms (seismic line E). P.E.-Prairie Evaporite. Black colour indicates negative amplitudes and red shows positive amplitudes.

The image from line E indicates that the Prairie Evaporite Formation decreases in thickness from 110 m in the east to zero near the western part of the section. All layers above the Prairie Evaporite appear to be collapsed, including the Late Devonian Bakken Formation, whereas the layers above the Bakken formation between ~980 to 1100 ms are thickened. These thickened layers represent the Mississippian Frobisher formation.

The above reflection character suggests that the salt was dissolved and removed during the deposition of Frobisher. The dissolution thus apparently took place during the Mississippian. The existence of the faults on the seismic line E supports earlier suggestions that the dissolution of the P.E. shown on the seismic data was probably initiated by regional faulting and fracturing. The fault/fracture often provides vertical and lateral fluid conduits between the evaporite layers and over or below aquifers resulting in salt dissolution and subsidence of overlying strata (Anderson, 1992; Anderson et el., 1988).

Seismic lines G, H and M (Figures 3.6, 3.7 and 3.8) represent a salt collapse that may have occurred more recently. Lines G and H display a depression that appears to have affected all the seismic horizons above the Prairie Evaporite. This salt dissolution could occur more recently than those discussed above. Seismic lines G and H (Figures 3.6 and 3.7) also show basement subsidence related to the Regina Trough, suggesting that Regina Trough could be associated with faults rooted in the basement. The salt dissolution has no indication of thickening layer in the seismic sections. However, thickening could also occur in the upper Cretaceous or Cenozoic layers which are not imaged in these seismic sections.

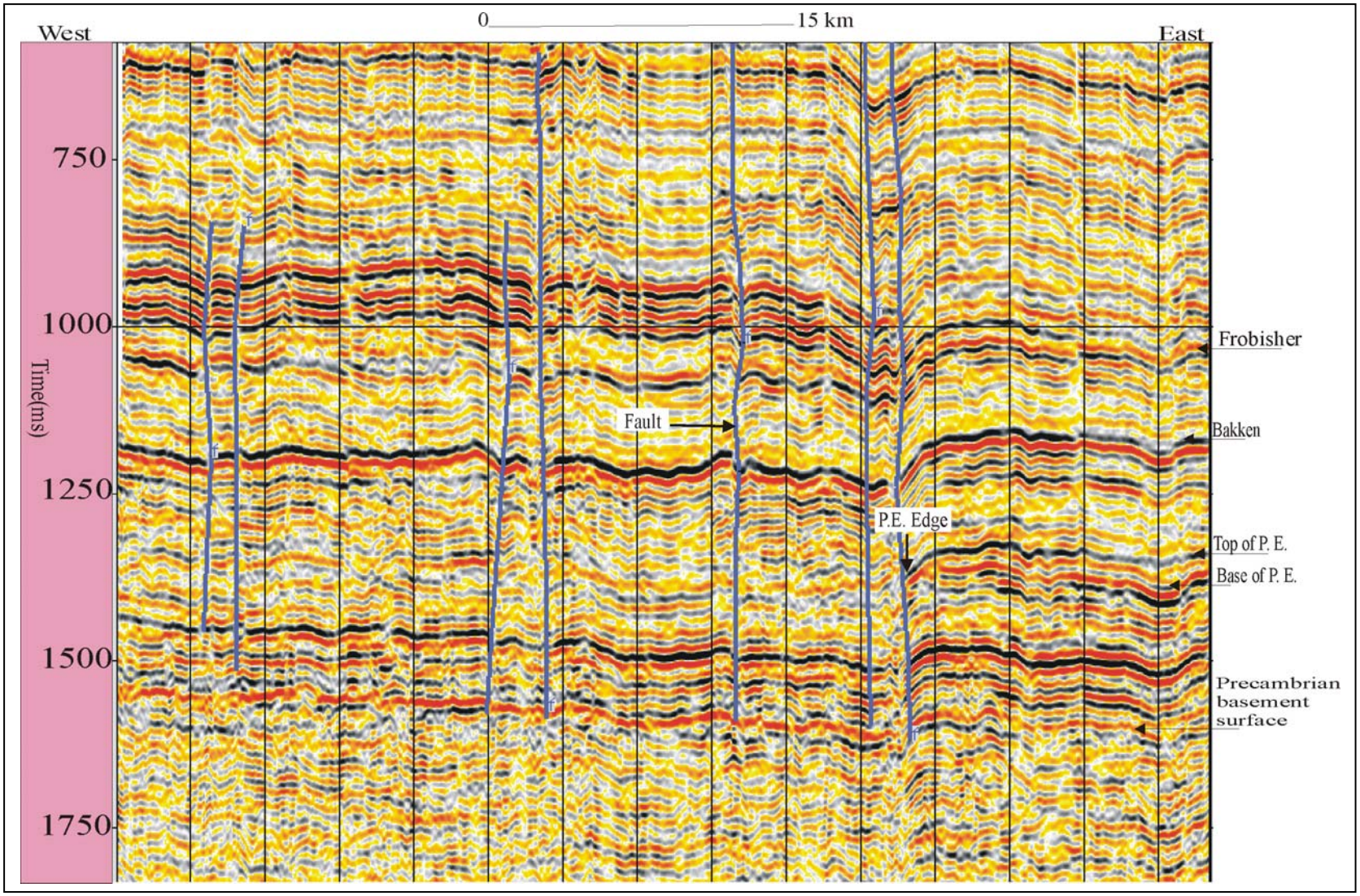

Figure 3.6 Effect of a salt collapse on seismic events (Line G). Note that compared to the collapse feature shown in Figure 3.5, this collapse structure must have formed more recently as it disturbs all of the overlying strata. P.E.-Prairie Evaporite. Black colour indicates negative amplitude and red shows positive amplitude.

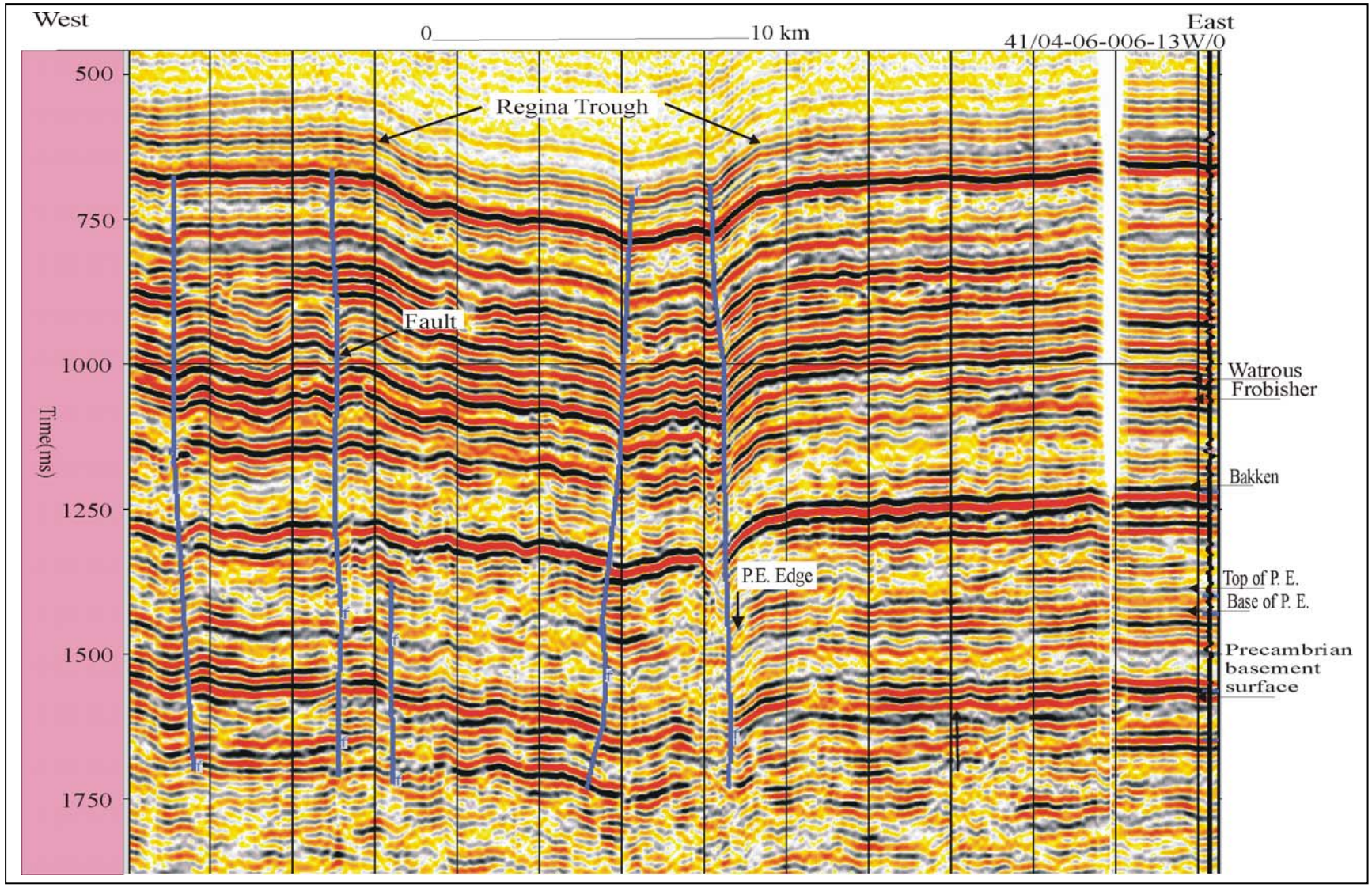

Figure 3.7 Seismic Line H shows Regina Trough. P.E.-Prairie Evaporite Black colour indicates negative amplitude and red shows positive amplitude.

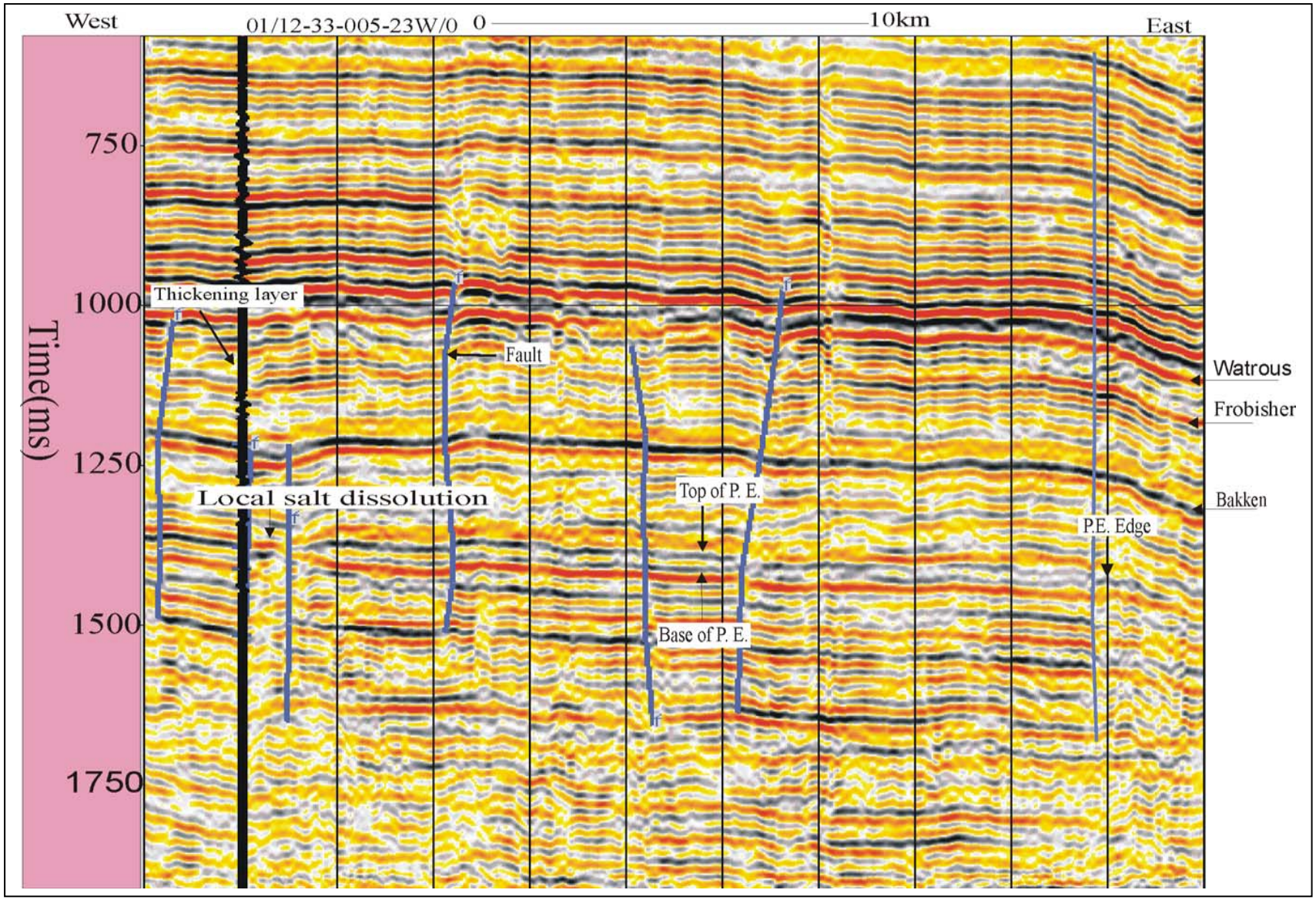

Figure 3.8 Seismic Line M displays both regional and local salt dissolution of the Prairie Evaporite formation. P.E.-Prairie Evaporite. Black colour indicates negative amplitude and red shows positive amplitude.

Seismic line M (Figure 3.8) shows a regional salt dissolution located off-salt (in the eastern part of the seismic section) and localized salt collapse of ~800 m in diameter exists within the body of Prairie Evaporite within the western part of the seismic section. Compared to the localized salt collapse in the western part, the regional dissolution may have occurred more recently, as it has disturbed all the overlying layers. Thickening of the Mississippian Frobisher Formation over the localized salt collapse indicated that salt dissolution took place during the Mississippian. Seismic lines show that the regional salt dissolution edge is relatively sharp, with thickness changing from ~70 to ~0 m across about 800 m. Such steep dissolution relief could be an indication of its association with activated faults.

Lines J and K (Figures 3.9 and 3.10) represent salt dissolution that occurred in the Triassic and Jurassic periods. Features which generally can be seen in the section and related to the salt dissolution are faulting and disruption of the normal Phanerozoic column in the Williston basin. Variations in thickness of the Prairie Evaporate and overlaying layer sediments are essential to set a time when salt dissolution occurred. The initial stages of salt dissolution and removal from the Prairie Evaporite are observed in the western part of the seismic lines. Thickening of the Mesozoic Watrous Formation compensated the different amounts of salt removal from the middle Devonian P.E. in each of seismic sections. This observation suggests that the salt dissolution took place at the same time as Watrous was deposited. No evidence of further salt dissolution was found in these seismic sections.

The middle Devonian P.E. is interpreted to thicken gradually, but not necessary uniformly, to the east of the salt edge. These seismic lines have relatively wide salt front

compared to seismic line H. The potential reason is that the salt edge is gradational where the rate of leaching and lateral advance of salt dissolution edge is low.

Seismic line B lies 29.7 km N-S close and parallel to the salt dissolution edge in the northern part of the study area. It is also crossing seismic line E and G (Figure 1.1). The lack of well control close to this seismic line necessitates the use of the interpreted seismic line E and G to help identify whether or not P.E is existed along the seismic line B. Figures 3.11 and 3.12 show composite sections of seismic line B with E, and B with G respectively. Interpretation of the composite seismic sections shows that the P.E Formation is present along the seismic line B, with its thickness varying from 15-40 m.

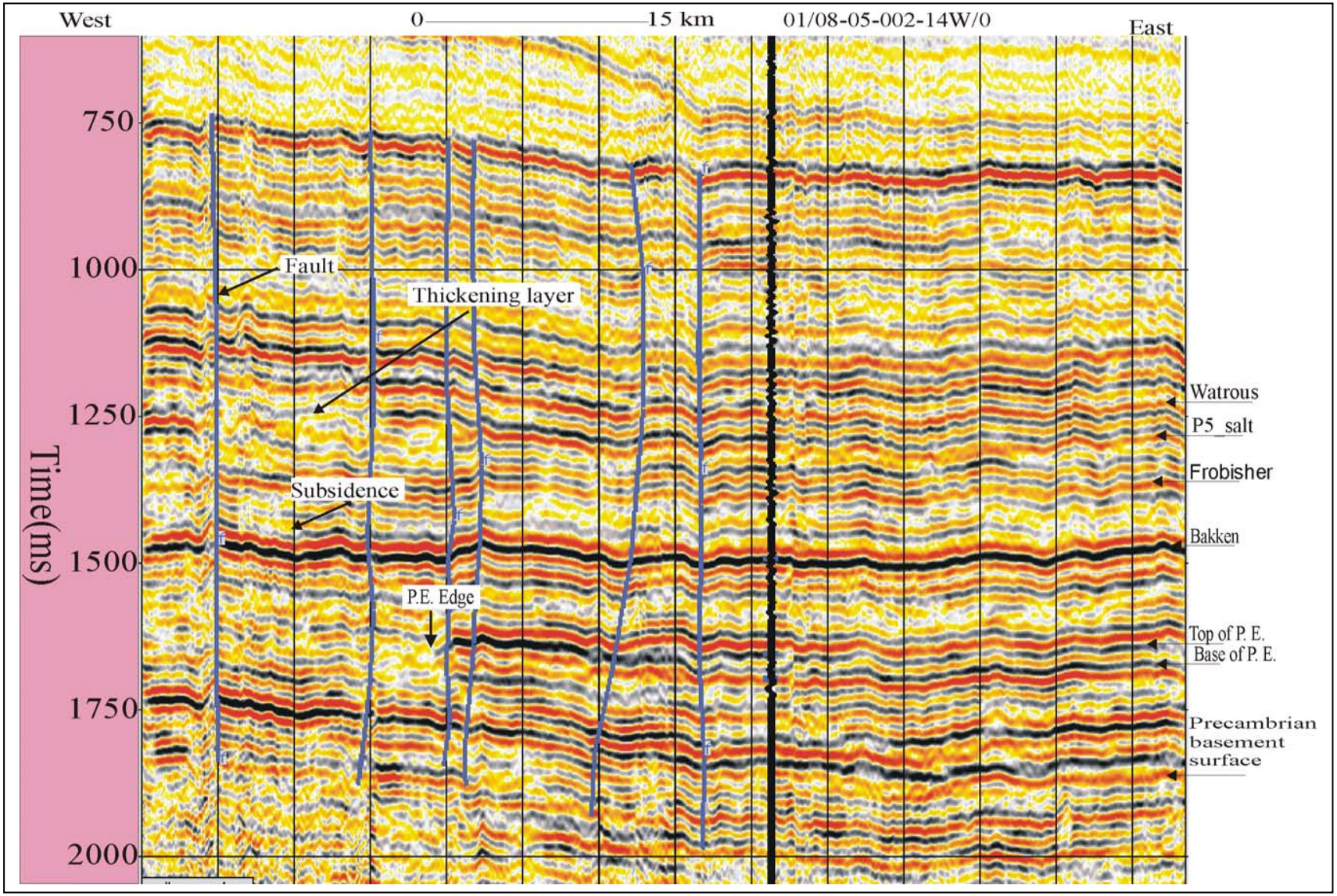

Figure 3.9 Strata slumping due to salt removal, basement uplift and several deep faults (Line J). P.E.-Prairie Evaporite Loss of the continuity in the west part is due to salt dissolution and faults. Black colour indicates negative amplitudes and red shows positive amplitudes.

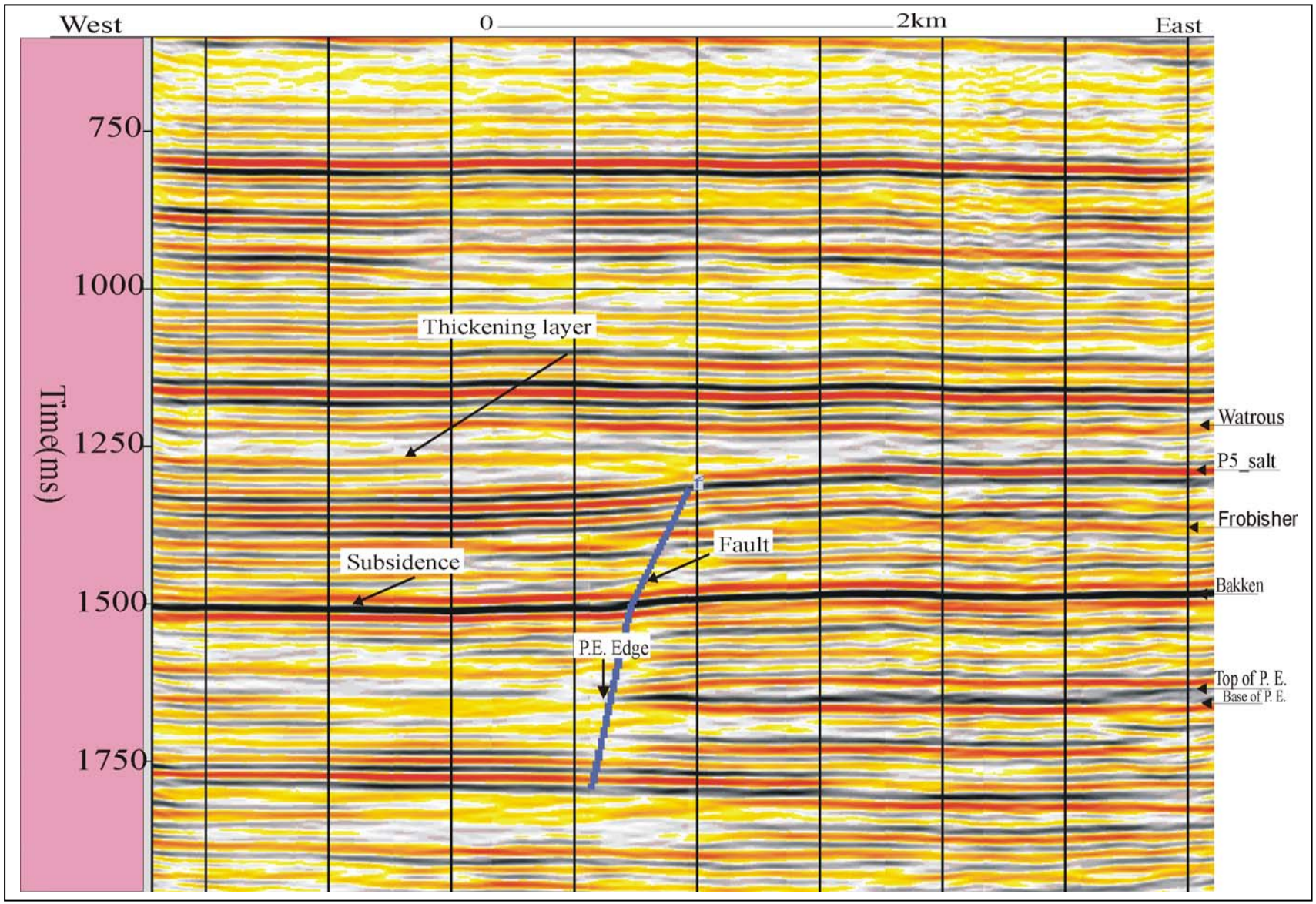

Figure 3.10 Line K shows salt collapse that may have occurred in Mesozoic. P.E.-Prairie Evaporite. Black colour indicates negative amplitudes and red shows positive amplitudes.

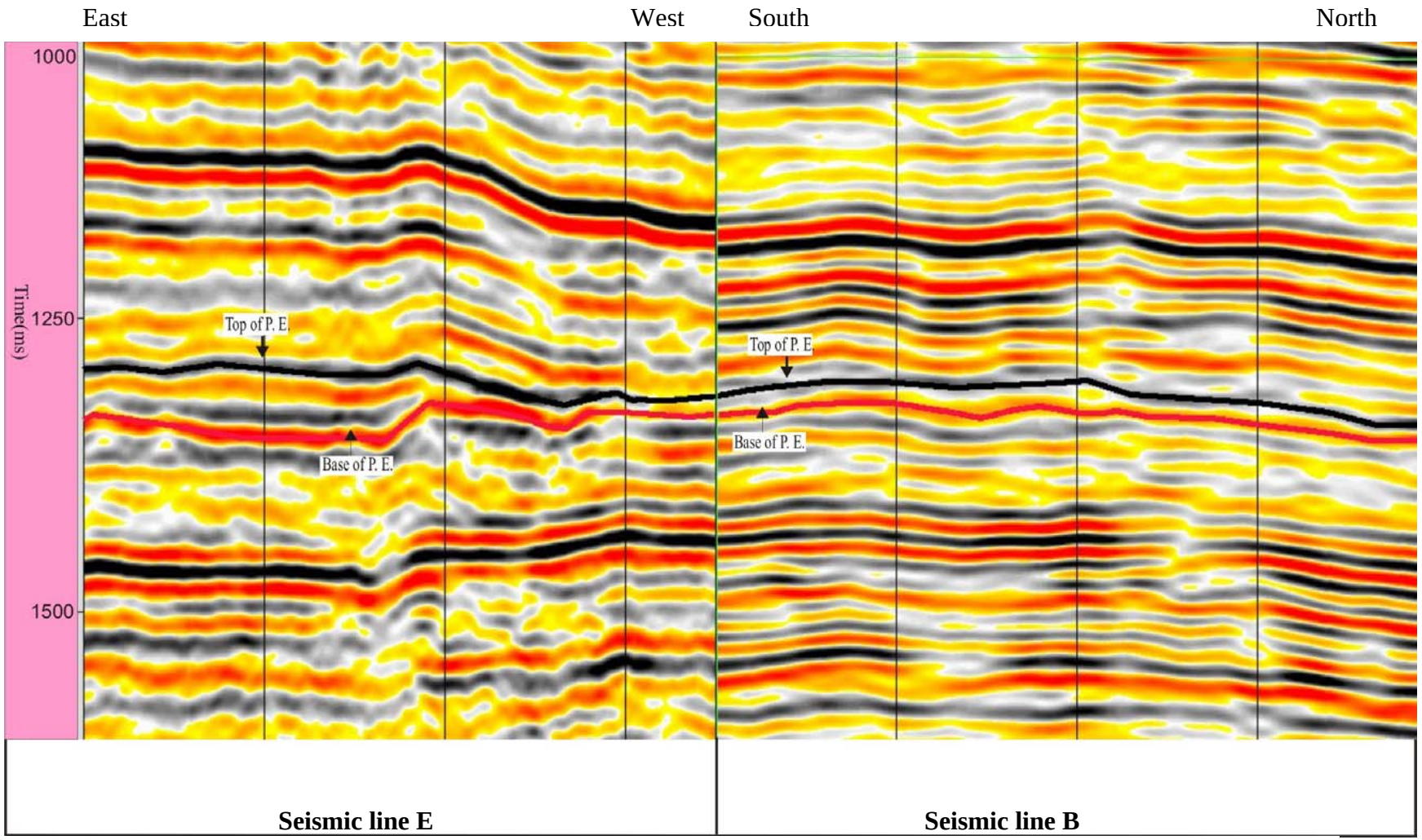

Figure 3.11 Interpretation of a composite cross-section from seismic lines E and B, northern part of the study area. Note that the Prairie Evaporite (P.E.) is present along the seismic line B. Black colour indicates negative amplitude and red shows positive amplitude.

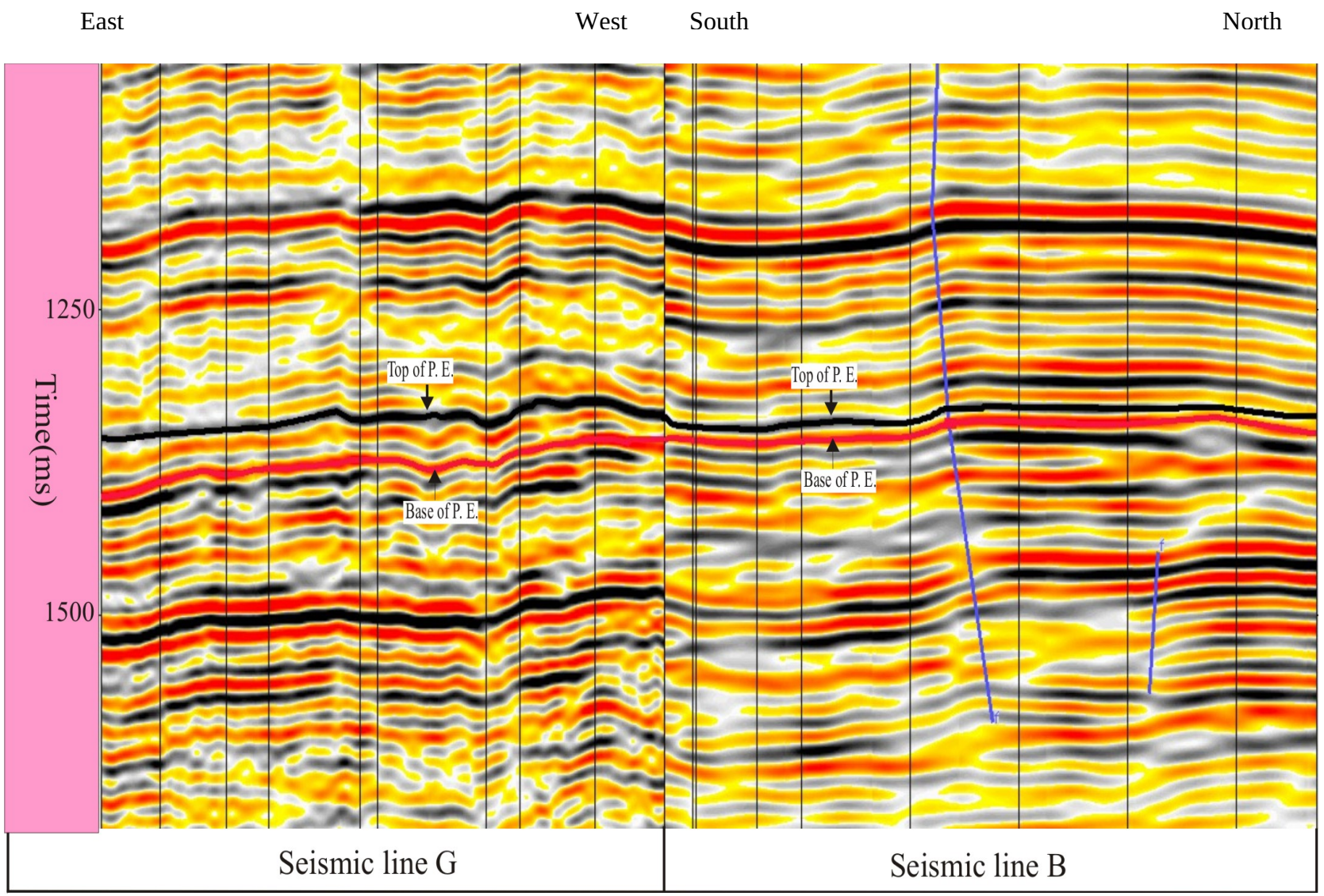

Figure 3.12 Composite cross-section from seismic lines G and B, northern part of the study area. Note that the Prairie Evaporite (P.E.) is present in the line B. Black colour indicates negative amplitudes and red shows positive amplitudes.

3.2 Subsurface Map Interpolation

Seismic and well-log observations provide linear or point spatial data that need to be interpolated to produce subsurface maps. However, with relatively sparsely spaced well log data set as in this study area, such interpolation depends on the method employed. This is particularly important where the data are interpolated or extrapolated in poorly constrained areas, such as the salt edges of this study. In order to evaluate the effectiveness of the interpolation techniques on the isopach contours, well picks of Middle Devonian strata in the IEA Weyburn CO_2 Monitoring and Storage Project area (Kreis et al., 2003) were used. Isopach maps of Prairie Evaporite created in spatial interpolation programs from Surfer, Matlab and Generic Mapping Tool (GMT) software packages were compared to evaluate the dependence of the resulting isopach map on the interpolation techniques. After several experiments, GMT was chosen as the preferred option. GMT programs offer a choice of "spline tension" parameter (described below), with tighter splines resulting in smoother maps (Smith and Wessel, 1990). Additional advantages of GMT are the free availability of the programs, possibilities of modifications, scalability, use of simple ASCII data formats, and high quality of PostScript images produced on a variety of cartographic projections.

Gridding the data using GMT was based on minimum-curvature. The method interpolates the data to be gridded with continuous second derivative and a minimal squared curvature over its surface. Smith and Wessel (1990) define the minimum-curvature tension interpolation by minimizing the total curvature given by:

$$\Phi\{z\} = \iint (\nabla^2 z)^2 dxdy \qquad (3.2)$$

where z is the interpolated function, *x* and *y* are the space variables, and ∇^2 is the partial derivative operator $(\partial^2/\partial x^2 + \partial^2/\partial y^2)$.

The functional (3.2) is minimized subject to the following boundary conditions along the edges of data coverage:

$$\frac{\partial(\nabla^2 z)}{\partial n} = 0, \tag{3.3}$$

where $\partial/\partial n$ denotes a derivative normal to the edge, and:

$$\frac{\partial^2 z}{\partial x \partial y} = 0 \tag{3.4}$$

at the corners.

A more general boundary condition is defined by introducing the tension parameter (T_B) for the boundary (Smith and Wessel, 1990). With parameter T_B ranges from 0 (free edge) to 1 (flat edge), this boundary condition requires that:

$$(1-T_B)\frac{\partial^2 z}{\partial n^2} + T_B \frac{\partial z}{\partial n} = 0 \tag{3.5}$$

along the edge of the surface.

To assess the sensitivity of interpretation to the choice of T_B, I used different values of spline tension T_B (Figures 3.13 and 3.14) to generate isopach maps of the Prairie Evaporite from the available well log and seismic picks. Figures 3.13 and 3.14 show that generally, as the value of T_B increases, the salt edge positions are shifted further to the west. The map with parameter T_B=0 shows data trends with minimal "bull's eye" artefacts around isolated data points and reasonable positions of the salt edge compared to the salt edge positions mapped on the seismic data. The value of T_B=0

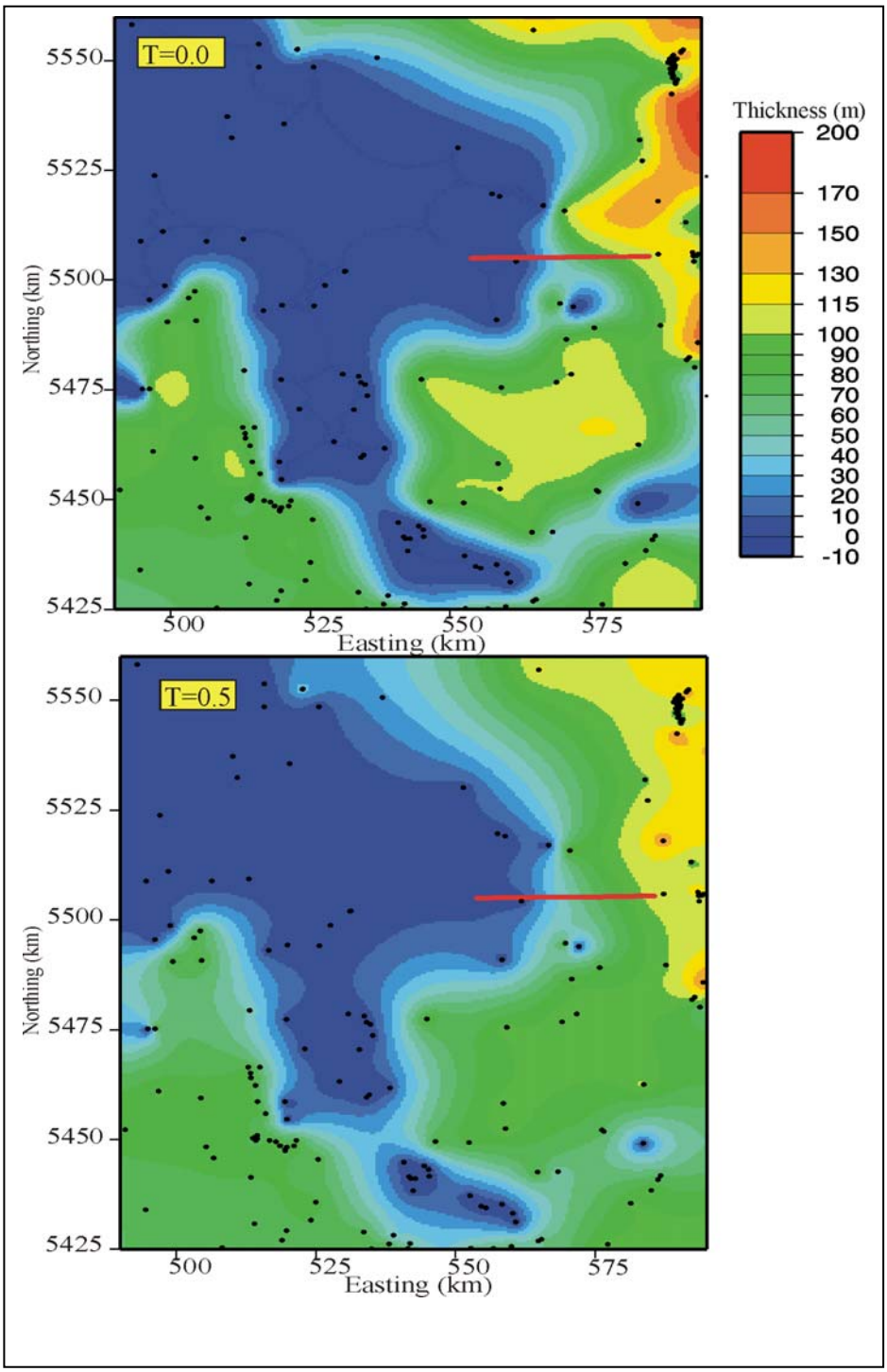

Figure 3.13. Prairie salt maps interpolated using GMT programs (Smith and Wessel, 1990), using two values of spline tension parameter T_B, as labelled. Black dots indicate the well readings used for interpolation. Note the differences between maps using different interpolation parameters. Coordinates are UTM in km; black dots indicate the wells used for mapping. Red line indicates the location of seismic line E.

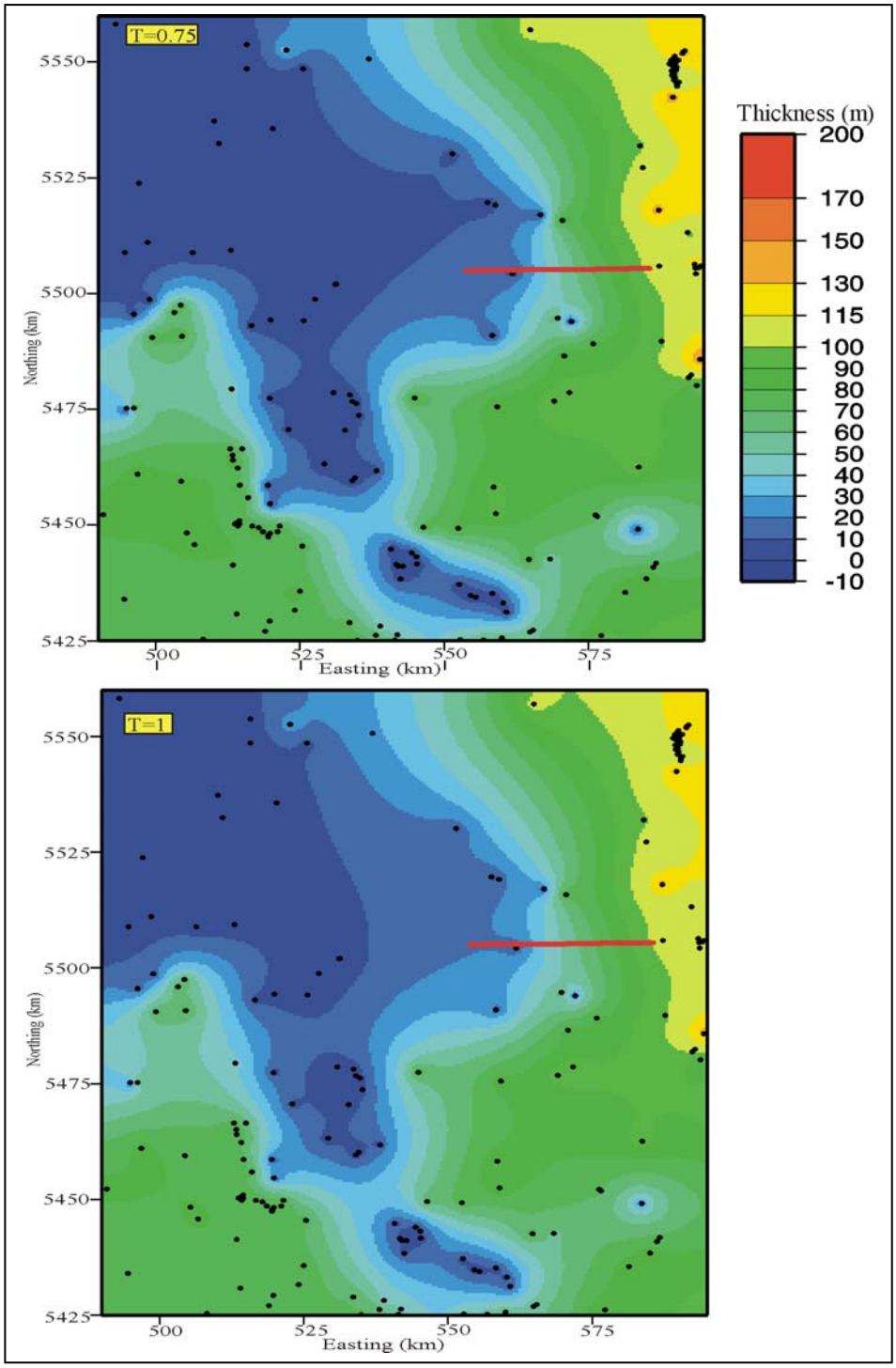

Figure 3.14. Prairie salt maps interpolated using T_B =0.75 and T_B =1.0. Red line indicates the location of seismic line E.

(i.e., the tightest spline) was finally chosen as the preferred mapping option, and a Prairie salt isopach map based on well data alone was created (Hamid et al., 2004). Appendix C shows the isopach maps of the Prairie Evaporite of the entire area interpolated using GMT with different values of spline tension parameter T_B.

Combining the well logs with seismic data allows the construction of a map, which is more detailed, and accurate in the areas crossed by the seismic lines (Figure 3.15). Appendix C contains the resulting isopach map of the Prairie Evaporite interpolated using the seismic and well log dada. Note that the results of seismic interpretations fill the gaps where well log data are not available.

The interpretations of the position of the salt dissolution edge of seismic lines E and G (Figure 1.1) indicate important deviations by as much as ~9 km from the previous interpretation by Kreis (2003). Connecting the positions of the salt edge of the two seismic lines is difficult because of the large distance between the seismic lines. However, the salt edge of the northern part of the study area can be estimated based on the interpretation of the seismic line B. Seismic interpretation indicated that the thickness of P. E. is ranging from ~15-40 m along the entire line. Assuming that the salt dissolution edge has a constant dip, the salt edge along the seismic line B could be extrapolated west of this line, as shown in Figure 2.16A.

In the southern part of the study area, the positions of the salt edge interpreted from seismic lines J and K generally agree with the interpretation by Kreis (2003), while in the south-western part seismic lines M and L show that the positions of the salt edge are shifted by ~2 km to the northeast (Figure 3.15). Thus inclusion of additional seismic

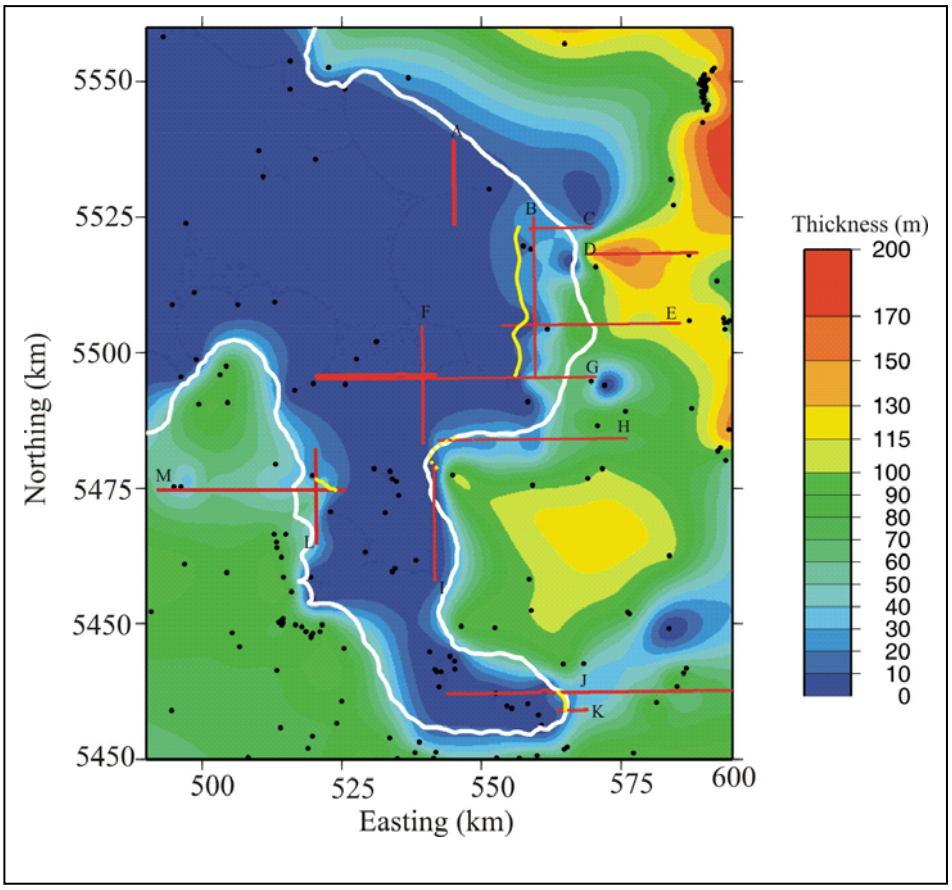

Figure 3.15 Interpolated isopach maps of the Prairie Evaporite Formation using both well and seismic data. Yellow and white contours show the salt edge of the Prairie Evaporite interpreted in this study and by Kreis et al. (2003), respectively. Yellow salt edge contour west of seismic line B was determined by extrapolation of PE thickness along this line. Seismic line I shows no salt and therefore the salt edge is likely passed east of it (dashed yellow line). Note that the differences of this interpretation from the previous study not using the seismic data shown here. Coordinates are UTM in km.

information significantly improves mapping of the Prairie Evaporite salt edge. Prairie Evaporite is not present along seismic lines I, F and A. Seismic line C shows that the thickness of the Prairie Evaporite varies from ~ 20-30 m, while seismic line D shows Prairie Evaporite thickness ranging from ~120-150 m.

3.3 Gravity Inversion and Interpretation

The gravity inversion addressed to complementary objectives: 1) to explain the regional gravity anomaly observed along gravity profile (A-A' in Figure 3.17) and also 2) to provide a detailed examination of the gravity in the vicinity and at the scale of a seismic line (line H; gravity profile B-B' in Figure 3.19) targeting comparative analysis of the contributions from the different lithological units well-constrained from the seismic data.

Although salt collapses contribute very little (~2 mgal) to the amplitude of the total Bouguer anomalies in the study area (35 mgal), gravity modeling is still important from two perspectives: 1) to gain understanding of the regional architecture of the basement of the Williston Basin and its relation to salt deposition and dissolution; and 2) to evaluate whether additional, very high-resolution gravity studies could be useful in identification and delineation of salt collapses.

3.3.1 Regional Gravity Profile A-A'

From the interpolated 2D gravity grid obtained from the Geological Survey of Canada, a ~350 km E-W profile across the Williston Basin was extracted (A-A' in Figure 3.16). It traverses a large segment of the northeastern Williston Basin and crosses a known salt collapse and the Wyoming-Trans-Hudson boundary. From borehole and seismic data, basement depths along the profile range from 2000 to 2300 m. Basement densities were assigned based on the studies by Leclair et al. (1993, 1994) and increased from 2.73 $g \cdot cm^{-3}$ in the west (the granitic complex of the Wyoming Craton) to 2.82-3.03 $g \cdot cm^{-3}$ in the east (within the Trans-Hudson Orogen). The gravity profile (Figure 3.17)

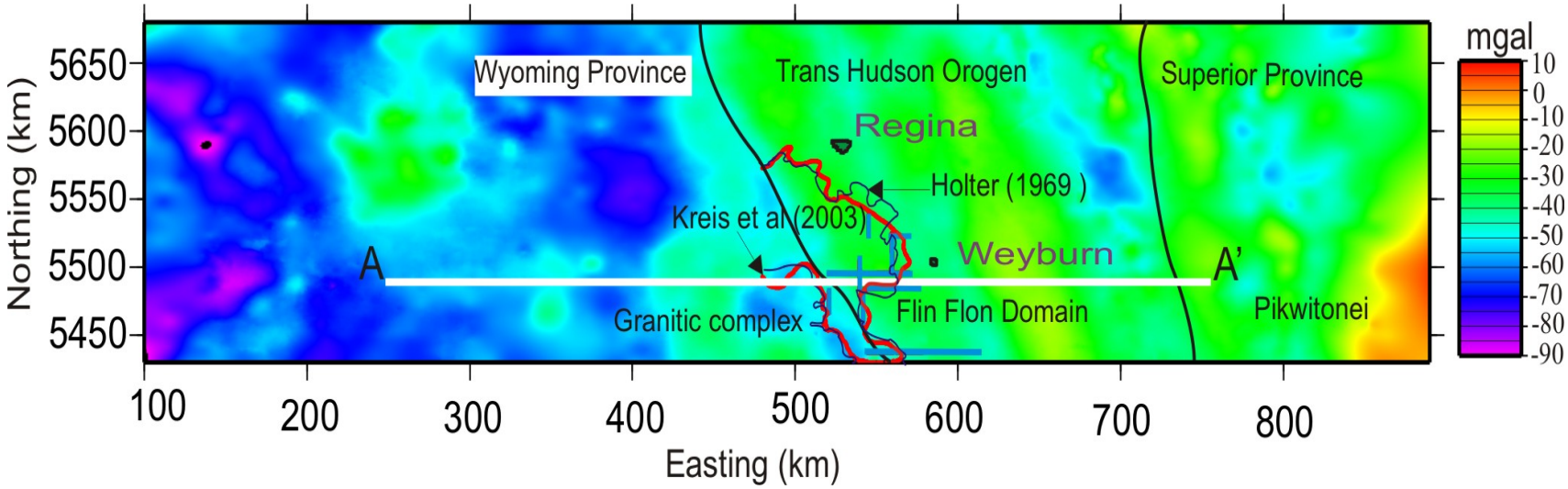

Figure 3.16 Bouguer anomaly map of Saskatchewan obtained using GMT (minimum-curvature spline with T_B =0) interpolation of gravity readings from the Geological Survey of Canada database. Black and red contours show the edge of the Prairie Evaporite interpreted by Holter (1969) and Kreis et al. (2003), respectively (Figure 1). A-A' is the line of the gravity cross-section extracted from the data and modeled in Figure 3.17. The major tectonic domains are indicated. Coordinates are UTM in km.

The Bouguer gravity profile (Figure 3.17) shows that the gravity field decreases from about -20 mgal in the east to -55 mgal in the west, an approximately 35 mgal change over its total length

The gravity map across the study area is characterized by two groups of anomalies:

1) A broad, high-amplitude anomaly in the east (over the Trans-Hudson Orogen), and a low-gravity anomaly occupying the western half of the study area (Wyoming Province); generally the density within the basement decreases from the east (2.82 to 3.03 $g \cdot cm^{-3}$ within the Trans-Hudson Orogen) to the west (2.73 $g \cdot cm^{-3}$ for the granitic complex of the Wyoming Craton) (Leclair et al. 1993, 1994); and
2) Localized, low- and high-amplitude anomalies (labelled L and H, respectively, in Figure 3.17) are superimposed on the first group; their amplitudes do not exceed 10 mgal and they have widths of ~15 to 16 km. One anomaly of this kind is in the Trans-Hudson Orogen, and another is in the Wyoming Province.

Preliminary 2D modeling of the gravity data was performed using the GM-SYS software. A polygonal gravity model was designed based on known lithologies, deep boreholes, densities, previous studies and nearby seismic work. The accuracy of this modeling depends on several assumptions, such as: 1) the density of the Williston Basin sedimentary rocks (chosen as 2.61 gm/cc); and 2) the density of basement rocks. However, it is unlikely that variations of these properties affect the first-order observations outlined below.

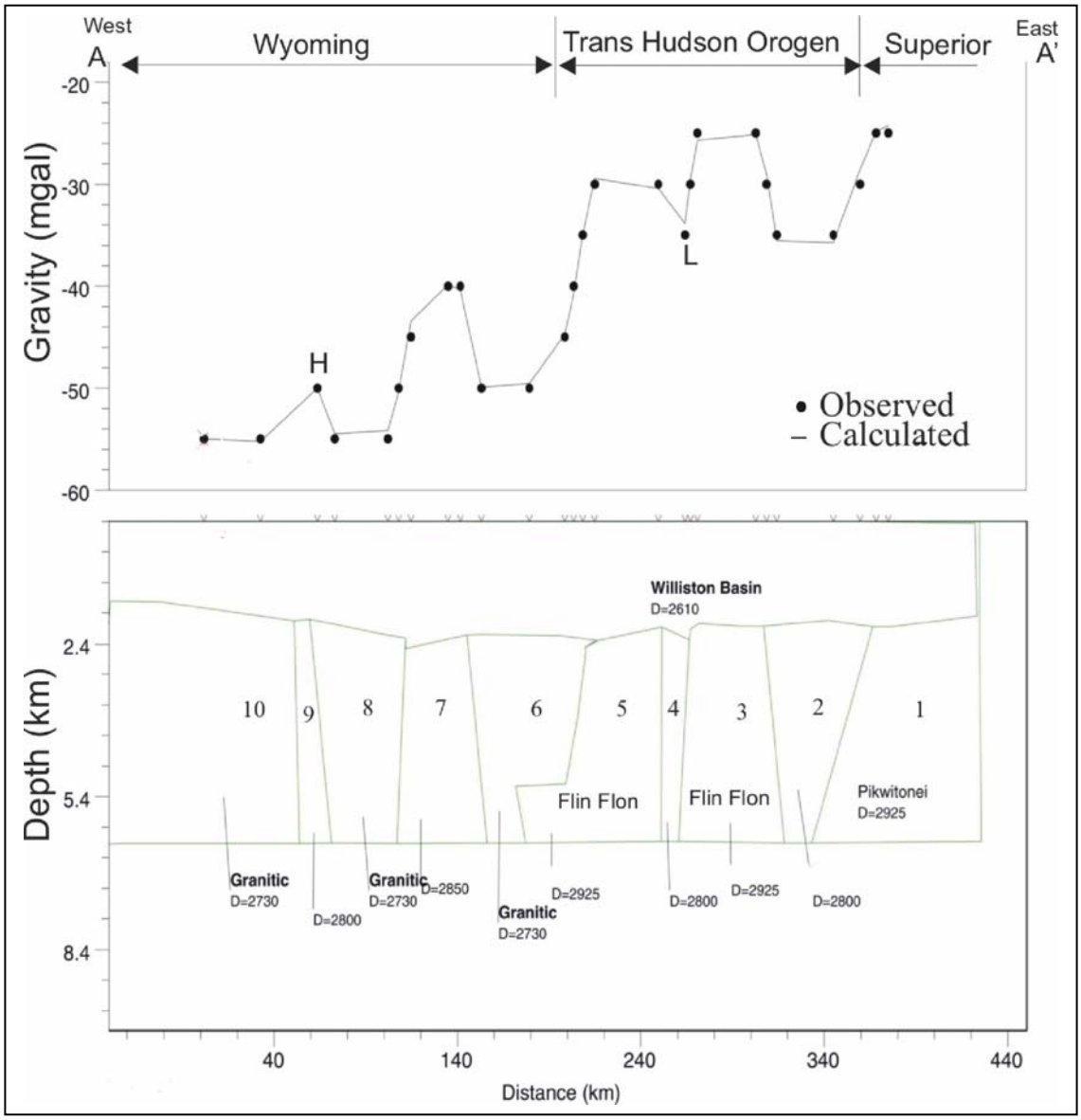

Figure 3.17 Gravity model along the cross-section A-A' in Figure 3.16. Note that the regional gravity anomalies require deep-rooted (~6 to 7 km deep) density variations within the basement. L and H indicate the localized gravity low and high, respectively, referred to in the text. Note that the gravity is modeled at the same points which were picked from ~10 mgal gravity map contours.

Trans-Hudson anomaly

The Trans-Hudson anomaly has a width of about 200 km and extends across several lithotectonic units, represented by polygons 3-6 in our gravity model (Figure 3.17). The approximate locations of these features were taken from the magnetic map of Saskatchewan (Miles et al., 1997).

The easternmost polygon represents the granulitic Pikwitonei Gneiss unit, which is marked by gravity high corresponding to density of 2.93 $g \cdot cm^{-3}$. Polygons 2, 3,4, and 5 in our model are assumed to be the extension of the Flin Flon domain (characterized by low metamorphic grade, mafic volcanic and granitoid rocks with density ranging between 2.8 and 2.93 $g \cdot cm^{-3}$). The contact between Pikwitonei and Flin Flon lithotectonic units (polygons 1 and 2) dips west, and the regional gravity field was found to decrease at a rate of 0.3 mgal/km toward the west. Bodies 3 and 5 are separated by a narrow gravity low about 15 km wide labelled L in Figure 3.17 (top). This anomaly is associated with a low-density polygon 4 that could be related to the extension of the Tabbernor Fault Zone, which is marked by a steep magnetic gradient in the centre of the Trans-Hudson Orogen (Miles et al., 1997).

Wyoming anomaly

The crustal transition from the Trans-Hudson Orogen to the Wyoming Province is marked by a sharply decreasing gravity field (0.6 mgal/km) that is spatially coincident with the eastern margin of the Hummingbird Trough, a salt-dissolution area. The Wyoming anomaly is characterized by the presence of a complex anomaly represented by polygon 6 in our model (Figure 3.17). This block may correspond to a granitic intrusion with density of 2.73 $g \cdot cm^{-3}$ located beneath the Hummingbird Trough. The

positive anomaly west of this possible intrusion represents basement rocks with a density of 2.85 gm/cc positioned beneath the Roncott anticlinorium (polygon 7). Farther west, the gravity field is represented by alternating gravity lows (polygons 8 and 10) and highs (polygon 9) with small amplitudes (~5 mgal) and widths of ~16 km. These features are generally associated with the granitic complex of the Wyoming Province.

Gravity modeling indicates that the observed regional gravity pattern is dominantly affected by deep-seated structures (about 6 to 7 km deep). Gravity signatures of salt collapse structures are significantly weaker and therefore almost irresolvable at this scale.

3.3.2 Detailed Gravity Profile B-B'

In addition to the regional profile A-A', I also attempted to investigate the relationship between the basement structures, sedimentary units, and salt collapses of the Prairie Evaporite in more detail. The gravity data have high density in the eastern and northwestern parts of the study area while the centre is poorly covered by only a few scattered gravity readings. From the interpolated 2D gravity grid, a ~33 km E-W profile just south of the centre of 3D gravity anomaly was extracted (Figure 3.18). The profile is parallel to the seismic line H and lies ~2 km to the north of it. The location of the profile was chosen because it is well covered with gravity readings, and it is near the seismic line H (Figure 3.18).

2-D modeling of gravity data was performed using GM-SYS software (Figure 3.19). Gravity model was constructed using the seismic interpretation of seismic line H (this study) and assumptions of the average densities of the Williston basin sedimentary column and basement rocks.

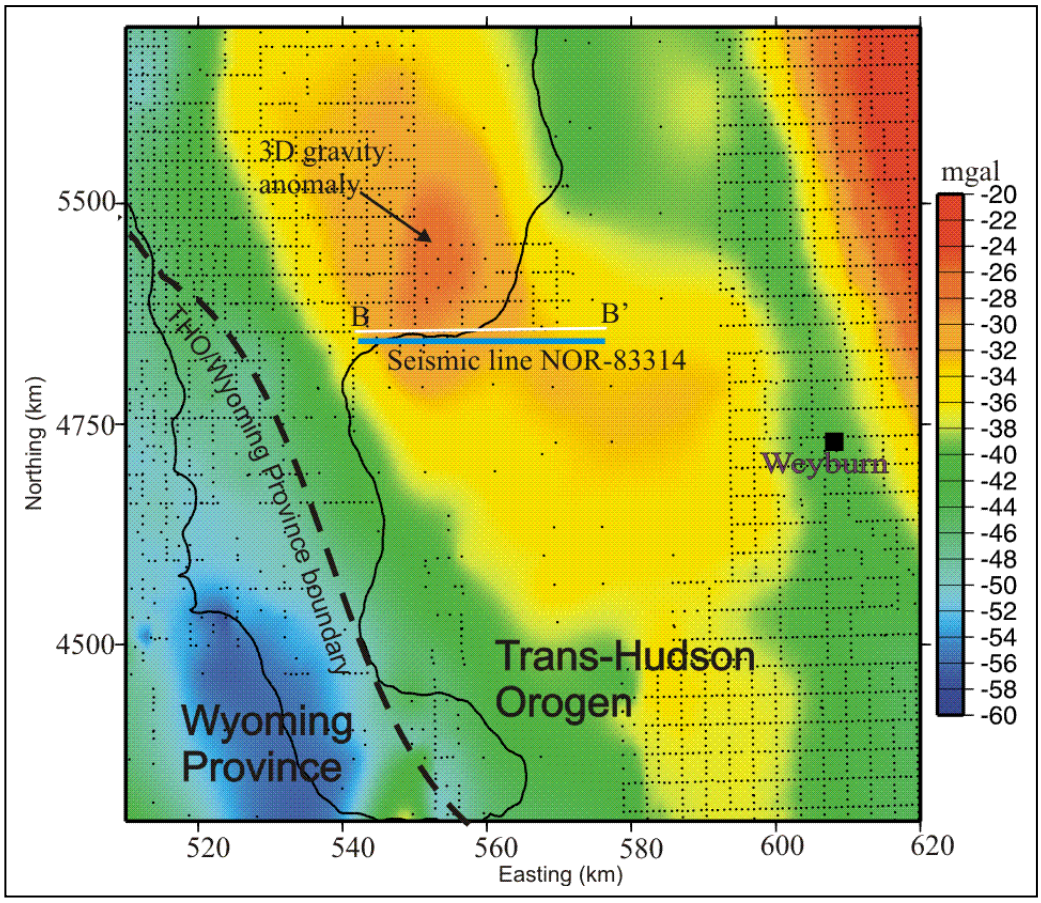

Figure 3.18 The observed gravity profile shows a major positive anomaly (~4 mgal) occurring in the vicinity of a known salt collapse west of the gravity profile. At a more regional scale, the observed gravity decreases sharply near the margin of the Trans-Hudson Orogen and Wyoming province. Black contour shows the edge of the Prairie Evaporite interpreted by Kreis et al. (2003) (Figure 1). B-B' is the line of the gravity cross-section extracted from the data and modeled in Figure 3.19. Black dots indicate the locations of gravity readings. Seismic line H is shown in white. Coordinates are UTM in km.

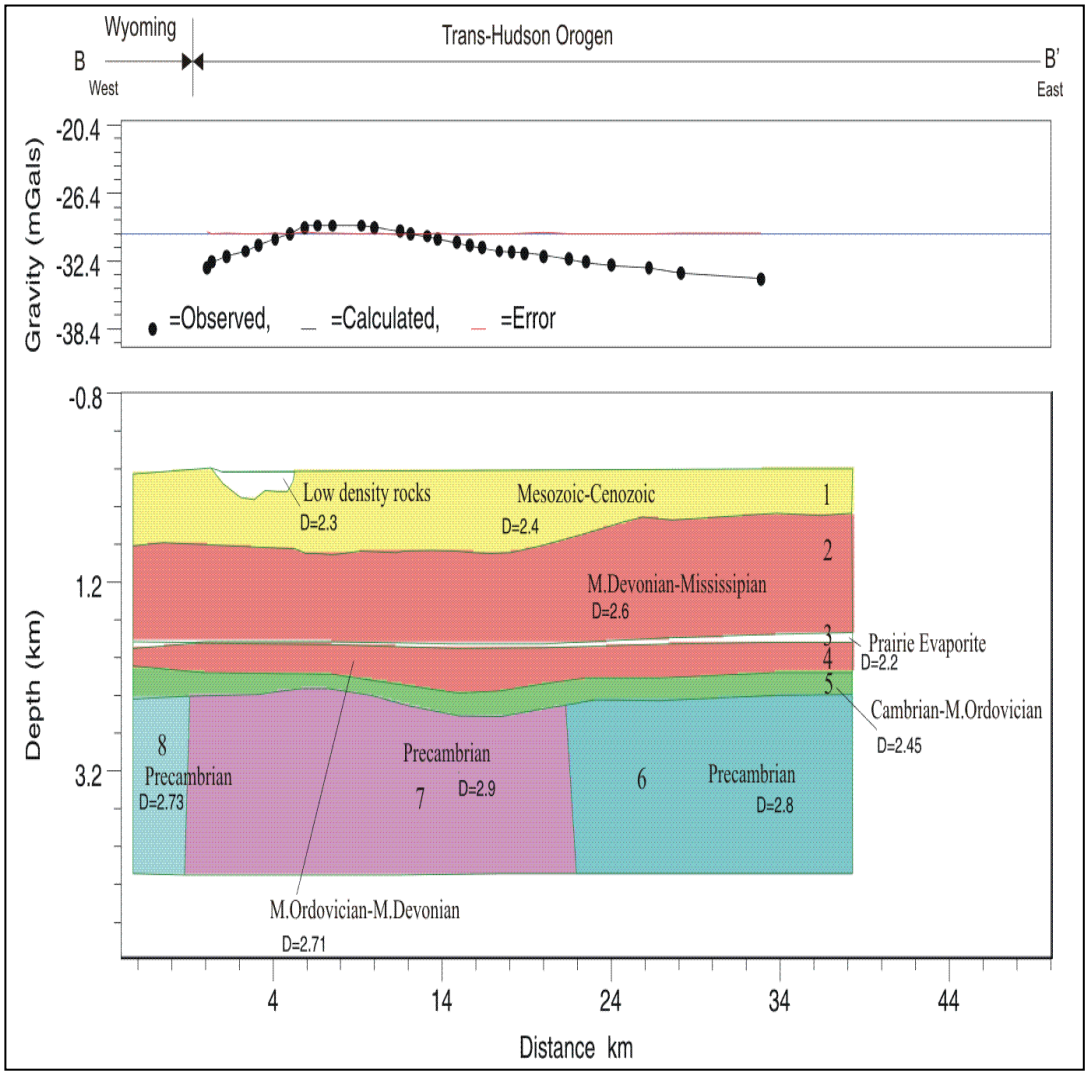

Figure 3.19 Gravity model along the ~33 km gravity profile across the salt collapse (Figure 3.18). Note the strong density contrast within the Precambrian basement below ~2.1 km depth.

Assigning densities to the formations using well logs information was considerably complicated because of the high density variability within the formations (Figure 3.20). In order to facilitate the interpretation, the average densities of the various formations were estimated from the density logs while also taking into account the ages and physical properties of the rocks. Five main blocks were established within the Phanerozoic rocks (Figure 3.19), with blocks 1, 2, 3, 4, and 5 representing the Mesozoic-Cenozoic (2.4 $g \cdot cm^{-3}$), M. Devonian-Mississippian (2.6 $g \cdot cm^{-3}$), M. Devonian Prairie Evaporite (2.2 $g \cdot cm^{-3}$), M. Ordovician-M. Devonian (2.71 $g \cdot cm^{-3}$) and Cambrian-M. Ordovician rocks (2.45 $g \cdot cm^{-3}$) respectively. Modeling of the observed anomaly also suggested adding a small low-density sub-block (2.30 $g \cdot cm^{-3}$) within the first block (Figure 3.19).

Mesozoic rocks show highly variable densities when compared to the more consistent densities of the other formations. A closer look at the logs shows that the Mesozoic densities vary from 1.9 to 2.6 $g \cdot cm^{-3}$. Therefore, using 2.3 and 2.4 $g.cm^{-3}$ for the average is suitable density for the purposes of gravity modeling. However, the scatter is quite large suggesting that there could be significant density variation within the shallow subsurface.

The Precambrian basement represented by blocks 6, 7 and 8 with densities ranging from 2.73 to 2.9 $g \cdot cm^{-3}$. Blocks 6 and 7 refer to the Trans-Hudson Orogen while block 8 represents the Wyoming Province. The observed gravity data were fitted by adjusting the densities of the Phanerozoic strata, Precambrian basement and the position of the bottom of the Precambrian basement block. The observed gravity profile shows a major positive anomaly (~4 mgal) occurring in the vicinity of a known salt collapse west of the gravity profile. At a more regional scale, the observed gravity decreases sharply

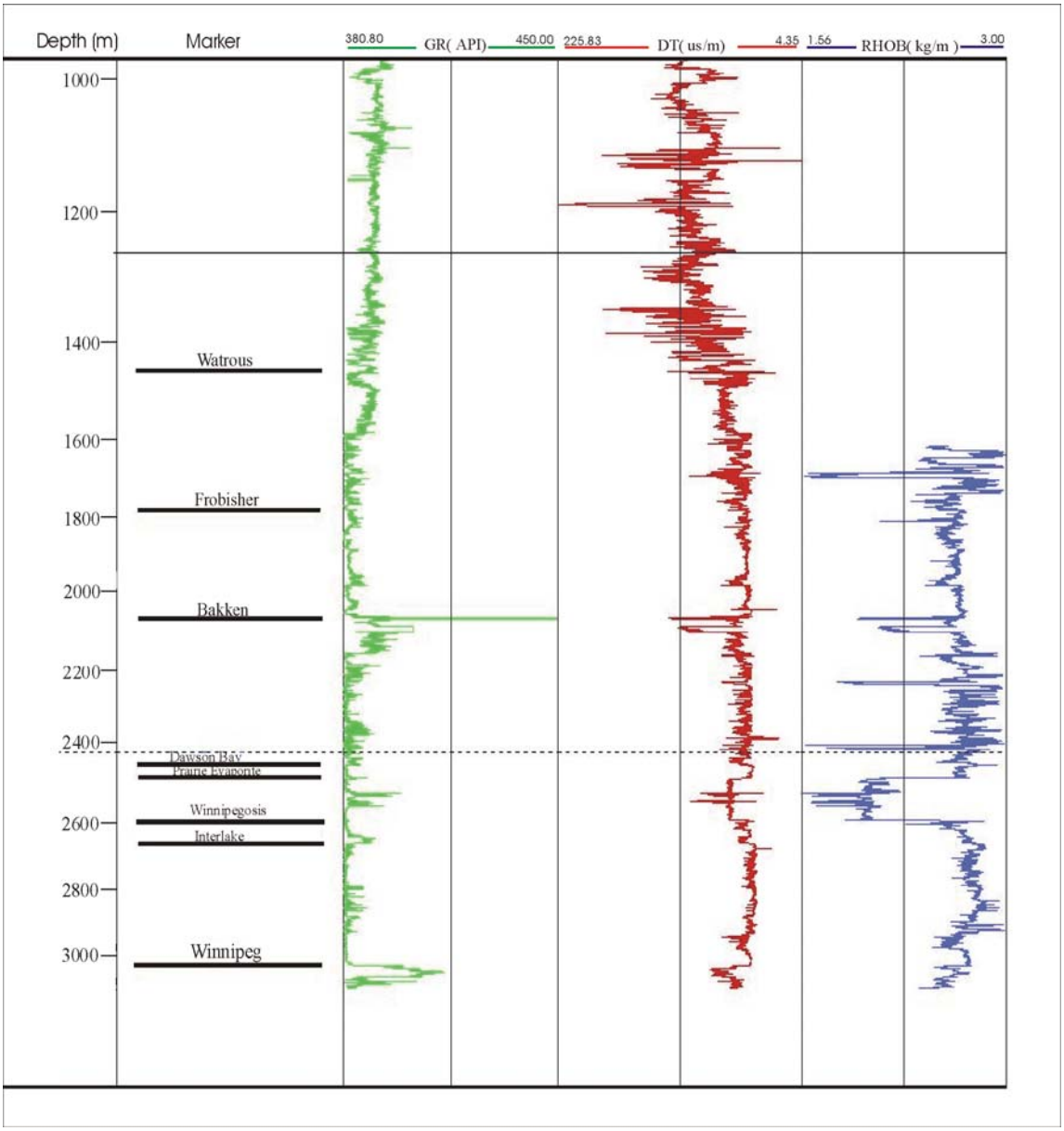

Figure 3.20 Gamma (green), sonic (red), and density (blue) logs, and the formation tops of well no. (01/08-05-002-14W/0). Note the strong variability of density within the formations.

near the margin of the Trans-Hudson Orogen and Wyoming Province (Figure 3.19; see also Hamid et al., 2004).

Modeling of the observed anomaly reveals a depression in the basement rock, which affects all of the sedimentary layers (Figure 3.19). After careful application of the constraints from detailed seismic imaging of the sedimentary cover, gravity modeling reveals strong density contrasts within the Precambrian basement (Figure 3.19). Potentially (although somewhat speculatively), the interpreted high-density basement between km 0 - 22 of our gravity profile could be associated with the localized gravity high observed N-NW of the profile (Figure 3.18). Because of their proximity of to both the Prairie Evaporate and salt collapse, such strong density contrast could make detection of the gravity signatures of the salts problematic.

Although the gravity anomaly is caused mainly by high densities within the crystalline crust (with the spatial wavelength exceeding ~40 km likely associated with the varying crustal thickness), the effect of the Phanerozoic cover was also examined. Seismic interpretation of line H and well log data was used to determine the effect of the Phanerozoic cover and especially of the salt dissolution edge of the Prairie Evaporite. As the interpretation of seismic line H indicated that the maximum thickness of P. E. is ~60 m, modeling shows that the Prairie salts have an effect of 0.4 mgal, or ~10% of the total anomaly. Thus, given the uncertainties in characterization of its overburden, and particularly in the Precambrian basement, unambiguous recognition of the Prairie salts gravity signature appears hardly possible. However, high-resolution gravity surveys with station spacing of 100 - 200 m might still constrain this overburden and help detect salt collapses and thin beds in the study area.

4. CONCLUSIONS

Seismic sections contribute critical information to help accurately locate salt dissolution edges. Achieving sufficiently high seismic frequencies is the key factor in detection of thin beds and salt dissolution edges of the Prairie Evaporite Formation. To enhance the high frequencies, post-stack spectral whitening was applied followed by *f*-x deconvolution, resulting in marked improvements in the resolution of thin beds and salt dissolution edges. In terms of the dominant frequency, these operations lead to an improvement from ~30 Hz to ~50 Hz, thereby improving the estimated depth resolution from 25 to 15 m at the formation depth.

Two types of salt collapses were identified rorm the newly re-processed seismic data: salt dissolution located off-salt, and local salt dissolutions located on-salt within the Prairie Evaporite. Salt dissolutions affected the overlying sediments and were apparently related to periodic movement along faults rooted in the Precambrian basement.

The interpretation shows that the timing and extents of subsurface dissolution of the P.E. was not uniform throughout the examined part of the Williston Basin. Significant differences in the nature of the dissolution may occur within the relatively restricted areas. Removal of material through dissolution of the salts of the middle Devonian P.E Formation caused localized thickening of the sediments deposited during the periods when the dissolution took place. Thickening of these sediments provides a

clue to the timing of dissolution and the possible thickness of layers potentially affected by the removal of the salt. Within the study area, indications of Mississippian, Mesozoic and of a more recent salt collapse event were observed.

The interpretations of the positions of the Prairie Evaporite edge in the seismic lines analysed in this study generally agree with the previous interpretations by Kreis et al (2003) and Holter (1969) in the southern part of the study area, but also indicate important differences. In the northern and southwestern parts parts of the study area, the newly mapped P.E. edges differ from those known from the previous studies by ~2-9 km.

The effects of of map interpolation techniques on the resulting isopach maps of the P.E formation were studied by varying the spline tension parameter in the Generaic Mapping Tools (GMT) software. The resulting maps show marked differences, especially near the edge of the salt where its thickness is small. The value of spline tension of 0 was recommended, and a Prairie salt isopach map based on seismic and well data was created (Figure 1.1).

Gravity interpretation shows that strong, larger-scale regional gravity anomalies within the study area are mostly related to density contrasts within the deep crust or mantle. However, the effects of Phanerozoic sedimentary cover were also noted. An interpretation of one of the seismic lines (H in Figure 3.7) and well log data were used to determine the effect of the Phanerozoic cover and especially of the salt dissolution edge of the Prairie Evaporite. As the maximum thickness of Prairie Evaporite is 60 m, modeling shows that the Prairie salts have an effect of 0.4 mgal, or ~10% of the total gravity anomaly. High-resolution gravity surveying in combination with seismic imaging, could still potentially be useful in detecting salt collapses in the study area.

REFERENCES

Anderson, N.L., 1992, Dissolution of the Wabamun Group salt: Exploration implication, in Cavanaugh, T.D., Ed., Integrated exploration case histories, North America: The Geophys.Soc. Tulsa, OK, 179-210.

Anderson, N.L., Brown, R.J., 1991, Black Creek and Wabamun salt collapse features, Western Canadian Sedimentary Basin: Geophysics, 56, 518-527.

Anderson, N.L., Brown, R.J., 1992, Dissolution and Deformation of Rock Salt, Stettler area, southeastern, Alberta: Can.J.Expl.Geophys., 28, no. 2, 129-137.

Anderson, N.L., Brown, R.J., and Hints, R.C., 1988, Geophysical aspect of Wabamun salt dissolution in southern Alberta: Can.J. Expl. Geophys., 166-178.

Anderson, N.L. and Cederwall, D.A., 1993, Westhazel General Petroleum Pool: Case history of a salt- dissolution trap in west-central Saskatchewan, Canada; Geophys., v58, no6, 889-897.

Baillie, A.D., 1953, Devonian System of the Williston Basin area; Man. Dept. Mines and Nat. Res., Mines Branch Publ. 52-5, 105p.

Baird, D.J., Nelson, K.D., Walters, J.J., and Brown, L.D., 1995, A comparison of crustal structure along strike in the Trans-Hudson Orogen from LITHOPROBE and COCORP transects; in Hajnal Z. and Lewry, J. (ed.) LITHOPROBE Trans-Hudson Orogen Transect, Rep. No.48, p47-65.

Bikford, M.E., Van Schmus, W.R., Collerson,K.D. and Macdonald, R.,1987, U-pb Zircon geochronology project: New Result and Interpretation, Summary of Inves, Sask.Geol.Surv., Miscell.Rept. 87-4, 76-79.

Bishop, R.A., 1954, Saskatchewan exploration progress and problem; *in* L.M. Clark (ed.), Western Canada Sedimentary Basin Symposium, American Association of Petroleum Geologists Ralph Leslie Rutherford Memorial Volume, p474-485.

Camfield, P.A., and Gough, D.I., 977, A possible Proterozoic plate boundary in North America; Can.J. Earth Sci., v14, 1229-1238.

Christiansen, E.A, 1967, collapse structures near Saskatoon, Saskatchewan, Canada, Canadian Journal of Earth Sciences, v.4, 757-767.

Christiansen, E.A, 1971a, Geology of groundwater resources of the Regina area (721), Saskatchewan, v Research Council Map 13, 1:250,000.

Christiansen, E.A, 1971b, Geology of Crater Lake collapse structure in southeastern Saskatchewan, Canadian Journal of Earth Sciences, v.8, 1505-1513.

Christiansen, E.A., and Sauer, E.K., 2001, Stratigraphy and structure of a Late Wisconsinan salt collapse in the Saskatoon, south of Saskatoon, Saskatchewan, Canada. Canadian Journal of earth Sciences 38: 1601-1613.

Christopher, J.E., 1961, Transitional Devonian-Mississippian formations of southern Saskatchewan; Sask. Dept. Mineral Resources, Report No. 66, 103p.

Davis, T.L., 1972, Velocity variations around Leduc reefs, Alberta; Geophys. v3, no4, 584-604.

DeMille, G, Shouldice, J.R., and Nelson, H.W., 1964, Collapse structure related to evaporites of the Prairie Formation, Saskatchewan; Geological Society of America Bulletin, v75, 307-316.

Dietrich, J.R and Magnusson, D.H., 1998, In: eighth International Williston Basin Symposium, Christopher, J.E., Gilboy, c., Patterson, D and Bend, S. (Eds). Sask.Geol.Soc., Regina, 166-174.

Edmunds, R.H. (1980): Salt removal and oil entrapment, Can. Soc. Petr. Geol., Mem. 6, 988.

Emery, D., and Myers, K.J., 1996, Sequences stratigraphy. Balckwell Science, 297p.

Fu, Qilong, 2005, Diagenesis of the Middle Devonian Winnipegosis and Ratner deposits in southern Saskatchewan, Canada, Unpublished M.Sc. thesis, University of Regina, Regina, Saskatchewan.

Fuzesy, A., 1982, Potash in Saskatchewan, Saskatchewan Energy and Mines Report 181, Saskatchewan Geological Survey.

Gendzwill, D.J., 1978, Winnipegosis mounds and Prairie Evaporite Formation of Saskatchewan – seismic study; American Association of Petroleum Geologists Bulletin. v62, 73-86.

Gendzwill, D.J. and Martin, M., 1996, Flooding and loss of the Patience Lake Potash Mine; CIM Bulletin. v89, no. 1000, 62-73.

Gibson, R.I., 1995, Basement tectonic and hydrocarbon production in the Williston Basin: An interpretive overview; in Hunter, L.D. and Schalla, R.A.(eds.), Seventh International Williston Basin Symposium, Sask. Geol. Soc., Spec. Publ.No.12, 3-9.

Gordon, A., 1979, Geology of Saskatchewan: A historical approach; western Extension College Educational Publishers, Saskatoon.

Grayston, L.D., Sherwin, D.R., and Allan, J.F., 1964, Middle Devonian, in McCrossan, R.G. and Glaister, R.P.eds.: Geological History of Western Canada, Alb. Sco. Pet. Geol., ch5, 49-59.

Green, A.G., Weber, W., and Hijnal, Z., 1985a, Evolution of Proterozoic terrians beneath the Williston Basin; Geol., v13, 624-628.

Green, A.G., Weber, W., and Hijnal, Z., 1985b, an evolution model of the western Churchill Province and western margin of the Superior Province in Canada and the north-central United States; Tectonophysics, v116, 281-322.

Hamid, H., Morozov,I.,M and Kreis, K., 2004, Seismic Delineation of the Southern Margin of the Middle Devonian Prairie Evaporite in the Elk Point Basin, southeastern Saskatchewan; in Summary of Investigations, volume 1, Saskatchewan Geological Survey, Sask. Industry Resources, Misc. Rep. 2004-4.1, Paper A-5, 9p.

Hatton, L., Worthington, M.W, and Makin, J., 1986, Seismic data processing: theory and practice: Blackwell Scientific.

Hoffman, P.F., 1981, Autopsy of Athapuscow Aulacogen: a failed arm affected by three collisions. In Campbell, F.H.A, edit., Proterozoic Basin of Canada, Geol.Surv.Can.Paper, 81-10, 97-102.

Holter, M.E., 1969, The Middle Devonian Prairie Evaporite of Saskatchewan; Sask. Dept. Mineral Resources, Report No. 123, 134p.

Houston, R.S., Karlstrom,K. E., Hills,F.A., and Smithson,S.B.,1979, The Cheyenne belt: Geological Society of America, Abstracts with Programs, v.11,p.446.

Jin, J., and Bergman, K.M., 1999, Sequence Stratigraphy of the Devonian Winnipegosis carbonate - Prairie Evaporite transition Southern Elk Point Basin, Carbonates and Evaporites, v14, 64-83.

Jones, L., 1965, The Middle Devonian Winnipegosis Formation of Saskatchewan; DMR Rep 98, 101p.

Jordan S.P., 1968, Will Zama be duplicated at Quill lake, Saskatchewan; oilweek, v19, no.9, 10-12.

Kalweit, R.S., and Wood, L.C., 1982, The limits of resolution of zero-phase wavelets. Geophysics, 47: 421-39.

Kent, D.M., 1968, The geology of Upper Devonian Saskatchewan Group and equivalent rocks in western Saskatchewan and adjacent areas, Saskatchewan Department of mineral Resources, Report No. 99.

Kent, D.M, 1974, The relationship between hydrocarbon accumulations and basement structural elements in the northern Williston basin; in Parslow, G.R. (ed.), Fuels: A Geological Appraisal, Sask. Geol. Soc., Special Publication 2, 63-79.

Kent, D.M., 1987, Palaeozoic controls on sedimentation in the northern Williston Basin, Saskatchewan; in Longman M.W. (ed.), Williston Basin: Anatomy of a Cratonic Oil Province, Rocky Mtn.Assoc.Geol., Denver, 45-56.

Kreis, L.K. and Kent, D.M., 2000, Basement Controls on Red River Sedimentation and Hydrocarbon Production in Southeastern Saskatchewan; in Summary of Investigations 2000; Saskatchewan Geological Survey; Saskatchewan Energy and Mines; Misc. Report 2000-4.1.

Kreis, L.K., Thomas, P.L., Burke, R.B., and Whittaker, S.G., 2003, Prairie Salt Isopach (Prairie Formation), in: Devonian Isopach and Structure Maps, IEA Weyburn CO_2

Monitoring and Storage Project Area (Test version), CD ROM, Saskatchewan Industry and Resources and North Dakota Geological Survey.

Leclair, A.D., Scott, R.G., and Lucas, S.B., 1993,Sub-Paleozoic geology of the Flin Flon Belt from integrated drill core and potential field data, Cormorant Lake area, Manitoba and Saskatchewan; *in* Current Research, Part C. Geological Survey of Canada, Paper 93-1C, 249-258.

Leclair, A.D., Lucas, S.B., Scott, R.G., Viljoen, D., and Broome, H.J., 1994, Regional geology and geophysics of the sub-Phanerozoic Precambrian basement south of the Flin Flon – Snow Lake – Hanson Lake Belt, Manitoba – Saskatchewan; *in* Current Research, Part-C, Geological Survey of Canada, Paper 94-1C, 215-224.

Lefever, J.A. and Lefever, R.D., 1995, Relationship of salt patterns to hydrocarbon accumulations, North Dakota Williston Basin; *in* L.D.V. Hunter and R.A. Schalla (eds.), Seventh International Williston Basin Symposium Guidebook, Montana Geological Society, 69-88.

Lewry, J.F., 1981, lower Proterozoic arc-microcontinent collisional tectonics in the westernChurchill Province, Nature, 294, 69-72.

Lewry, J.F. and collerson, K.D., 1990, The Trans-Hudson Orogen; extend, subdivision and problems. In; J.F. Lewry and M.R. Stauffer (Editors), The Early Proterozoic Trans-Hudson Orogen of North America. Geol. Assoc. Can.Spec. Pap., 37:1-4.

Lidiak, E.G., 1971, Buried Precambrian rocks of South Dakota, Geological Society of America Bulletin, 82, 1411-1420.

Macdonald, R., and Broughton, P., 1980, Geological map of Saskatchewan, provisional edition; Sask. Geol. Survey.

Majorowicz, J.A., jones, F.W., and Osadetz, K.G., 1988, Heat flow environment of the electrical conductivity in the Williston Basin, and occurrence of hydrocarbon; Bull.Can.Pet.Geol, v36, 86-90.

McTavish, G.J., 1990, Salt dissolution and tectonics, south-central Saskatchewan, Unpublished M.Sc. thesis, University of Regina, Regina, Saskatchewan.

McTavish, G.J., 1991, Role of salt dissolution in controlling outcrop ditribution in south-central Saskatchewan; in Christopher, J.E. and Haidl, F.(eds.), sixth International Williston Basin Symposium.

McTavish, G.J. and Vigrass, L.W., 1987, Salt dissolution and tectonics, south-central Saskatchewan; *in* C.G. Carlson and J.E. Christopher (eds.) Fifth International Williston Basin Symposium, Regina, Saskatchewan Geological Society Special Publication Number 9, 157-168.

Meijer Drees, N.C., 1986, Evaporite deposit of western Canada. Geological survey of Canada Paper 85-20, 118p

Miles, M., Stone, P.E., and Thomas, M.D., 1997, Magnetic and Gravity Maps with Interpreted Precambrian Basement, Saskatchewan; Geological Survey of Canada, Open File 3488, 5 sheets, scale 1:1 500 000.

Mossop, G.D., 1972, Origin of the peripheral rim water reef, Alberta: Bull. Canadian Petroleum ogy, v. 20, 238-280.

Norris, A., W., Uyeno, T.T., and MaCabe, H.R., 1982, Devonian of the Lake Winnipegosis-Lake Manitoba outcrop belt, Manitoba: Geological Survey of Canada Memoir # 392. Manitoba Mineral Resources Division Publication # 771, 280p.

Oglesby, C.A., 1988, Deposition and dissolution of the Middle Devonian Prairie Evaporite, Williston Basin, North Dakota and Montana: M.Sc. Thesis, Colorado school of Mines, 79p.

Parker, J.M., 1967, Salt solution and subsidence structures, Wyoming, North Dakota and Mountana; AAPG Bull., v51, 1929-1947.

Porter, J.W., Price, R.A., and McCrossan, R.G., 1982, Western Canada Sedimentary Basin: Philosophical Transaction of the Royal Society of London, Series A 305, p. 169-192.

Reasnor, M.D., 2001, Forward modeling and interpretation of multicomponent seismic data for fracture characterization, Weyburn field, Saskatchewan, M.Sc. Thesis, Colorado School of Mines, and Golden, Colorado.

Reinson, G.E., and Wardlaw, N.C, 1972, Nomenclature and stratigraphic relationships, Winnipegosis and Prairie Evaporite formations, central Saskatchewan; Bulletin of Canadian petroleum Geology, v20, 301-320.

Ricker, N., 1953, Wavelet contraction, wavelet expansion, and the control of seismic resolution: Geophysics, 18, 769-792.

Sask. Dept. of Mineral Resources. , 1961, Structure Contour Maps E-166 to 173.

Sawatzky, H.B., Agarwal, R.G., and Wilson, W., 1960, Helium Prospects in Southwest Saskatchewan; Sask. Dept.Min.Resources, Report No.49, 26p.

Sheriff, R.E. and Geldart, L.P., 1995, Exploration Seismology (second edition); Cambridge University Press. Cambridge, New York, Melbourne; 592p.

Sims, P.K., and Peterman, Z.E., 1986, Eraly Proterozoic Central Plains Orgen, a major buried structure in the north-central United State. Geology, 14, 488-491.

Simson, F., 1982, Sedimentlogy, paleecology and economic geology of Lower Colorado strata of west central Saskatchewan; Sask. Energy and mines, Rep.150.

Sjogren, B., 1984, Shallow refraction seismic: Seismic Chapman and Hall.

Smith, D.G. and Pullen, J.R., 1976, Hummingbird structure of southeast Saskatchewan; Bull. of Canadian Petrol. Geology, v15, 468-482.

Smith, W.H.F. and Wessel, P., 1990, Gridding with continuous curvature splines in tension; Geophysics 55, 293-305.

Telford, W.M., L.P. Geldart, and R.E. Sheriff, 1990, Applied Geophysics, Second edition. Cambridge University Press, 770p.

Too, D.C. and Toth, J., 1995, Hydrogeochemical Characterization of Formation Waters Using Ionic Ratios, South-Central Saskatchewan; in Hunter, L.D. and Schalla, R.A. (eds.), Seventh International Williston Basin Symposium, Sask. Geol. Soc., Spec. Pub. No.12, 313-319.

VanHees, H., 1956, Elk Point Group, Notes on a Subsurface Cross Section extending from East Central Alberta through Saskatchewan to Western Manitoba; Jour., Alberta Soc.Petrol.Geol., vol.4, No.2, 29-39.

Wardlaw, N.C. and Reinson, G.E., 1971, Carbonate and evaporite deposition and digenesis, Middle Devonian Winnipegosis and Prairie Evaporite formations of south-central Saskatchewan; AAPG Bulletin, v55, 1759-1786.

Widess, M.B., 1973, How thin is a thin bed?: Geophysics, 38, 1176-1180.

Wilson, N., 1985, A study of the Upper Winnpegosis mounds in south-central Saskatchewan, Unpublished M.Sc. Thesis, University of Saskatchewan, 98p.

Wilson, N.L., 1984, The Winnipegosis Formation of south-central Saskatchewan, in Oil and Gas in Saskatchewan: Saskatchewan Geological Society Special Publication Number 7, 13-15.

Wilson, W., Surjik, D.L., and Sawatzky, H.B., 1963, Hydrocarbon potential of the south Regina area, Saskatchewan; Sask. Dept. Min. Resour., Rep. 76, 15p.

Yilmaz, O., 1987, Seismic Data Processing, ed. S.M. Doherty, Society of Exploration Geophysicists, Tulsa, 526p.

Zharkov, M.A., 1984, Paleozoic Salt Bearing Formations of the World, New York, Springer, 427p.

Zharkov, M.A., 1988, Devonian Evaporite Basin. In: McMillan, N.J., Embry, A.F., and Glass, D.J. (eds.). Devonian of the world. Proceedings of the second international symposium on the Devonian system; v2, sedimentation. Canadian Society of Petroleum Geologist Memoir, 14, 415-427.

APPENDIX A

RE-PROCESSED SEISMIC LINES

Plots below show the stacked and migrated seismic sections from all lines re-processed in this study. Line labels and acquisition parameters are given in Table 2.1, and the processing sequence is shown in Table 2.2. Locations of the lines are shown in Figure 1.1.

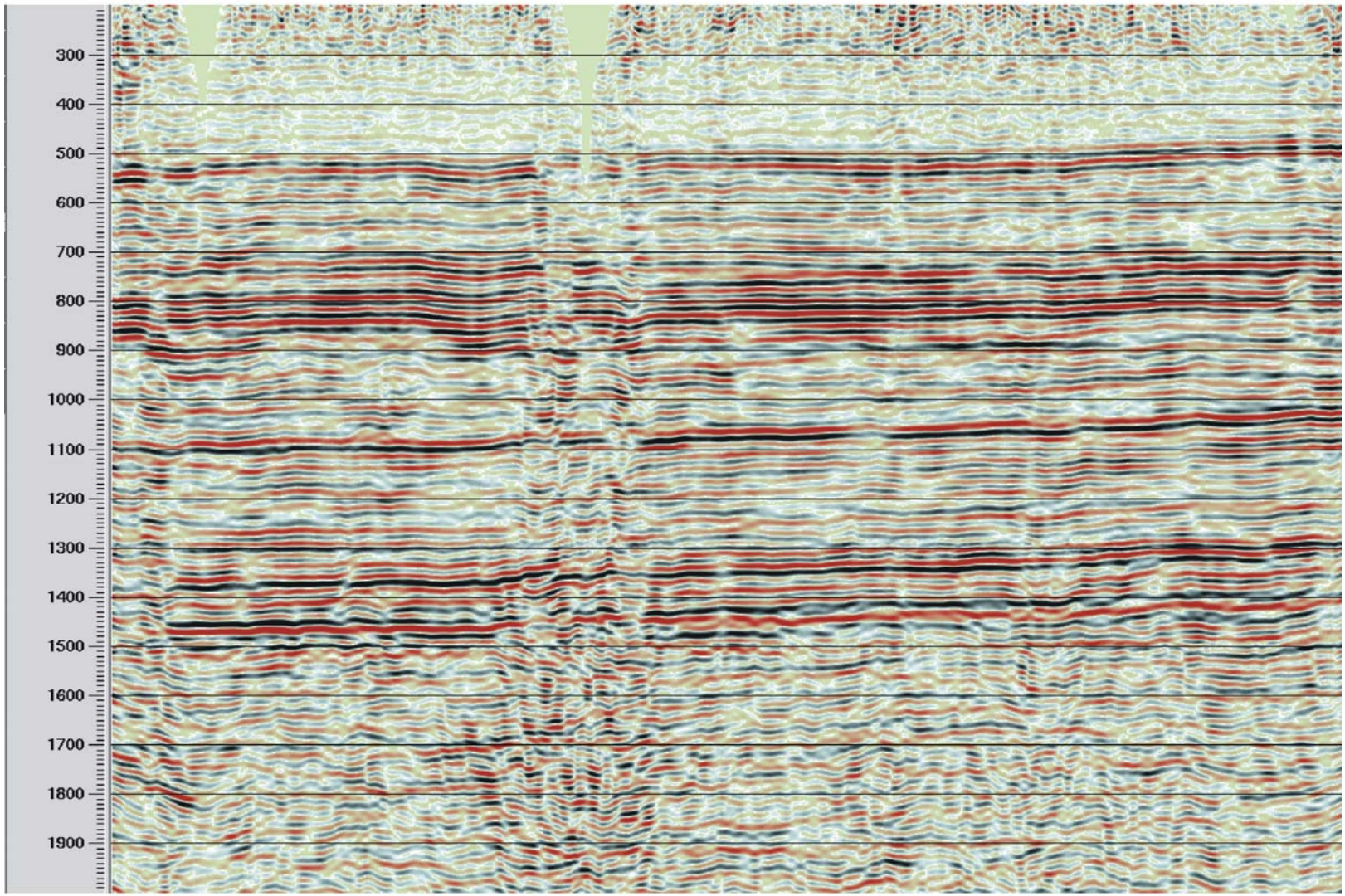

Figure A.1 Seismic Line A

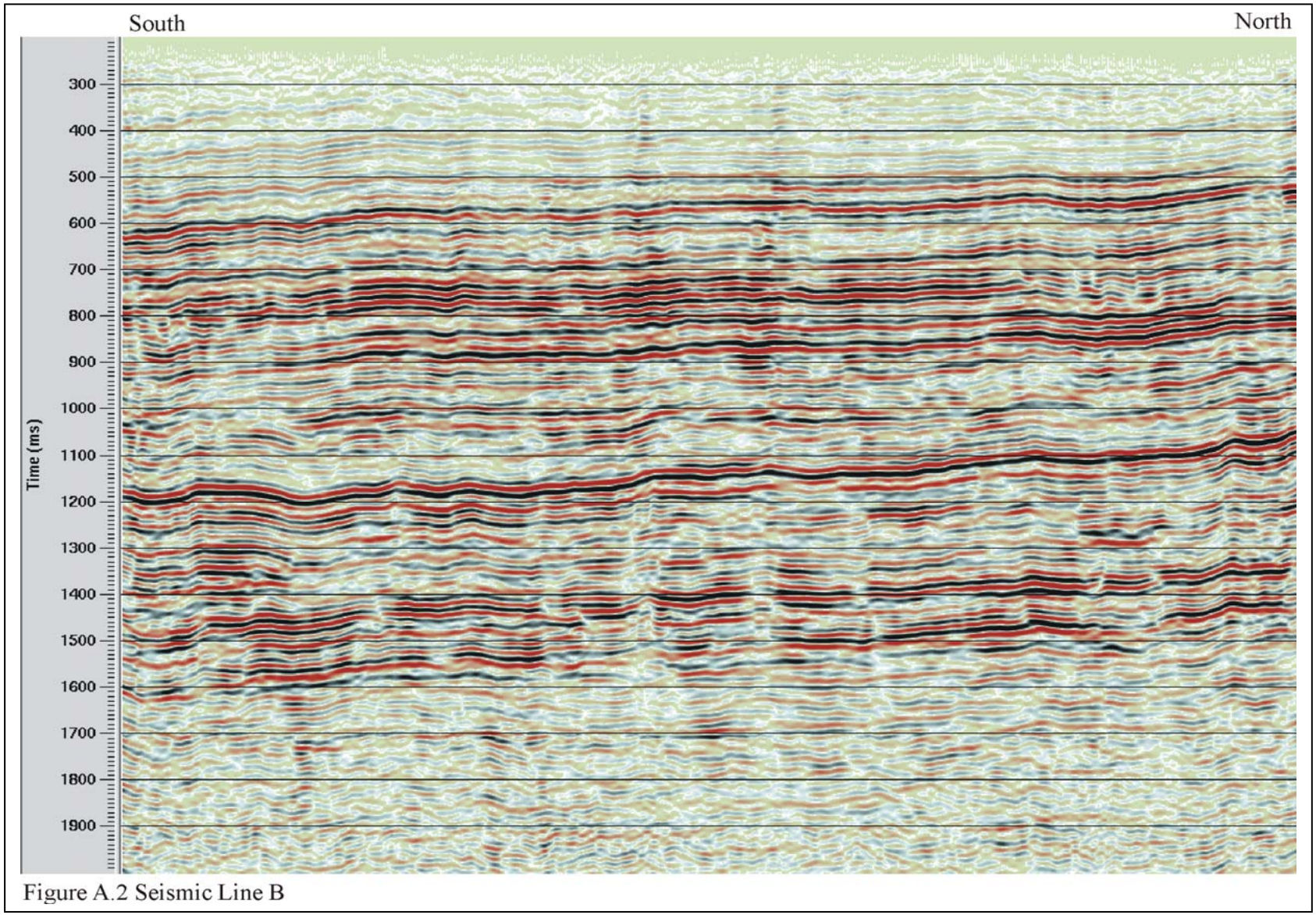

Figure A.2 Seismic Line B

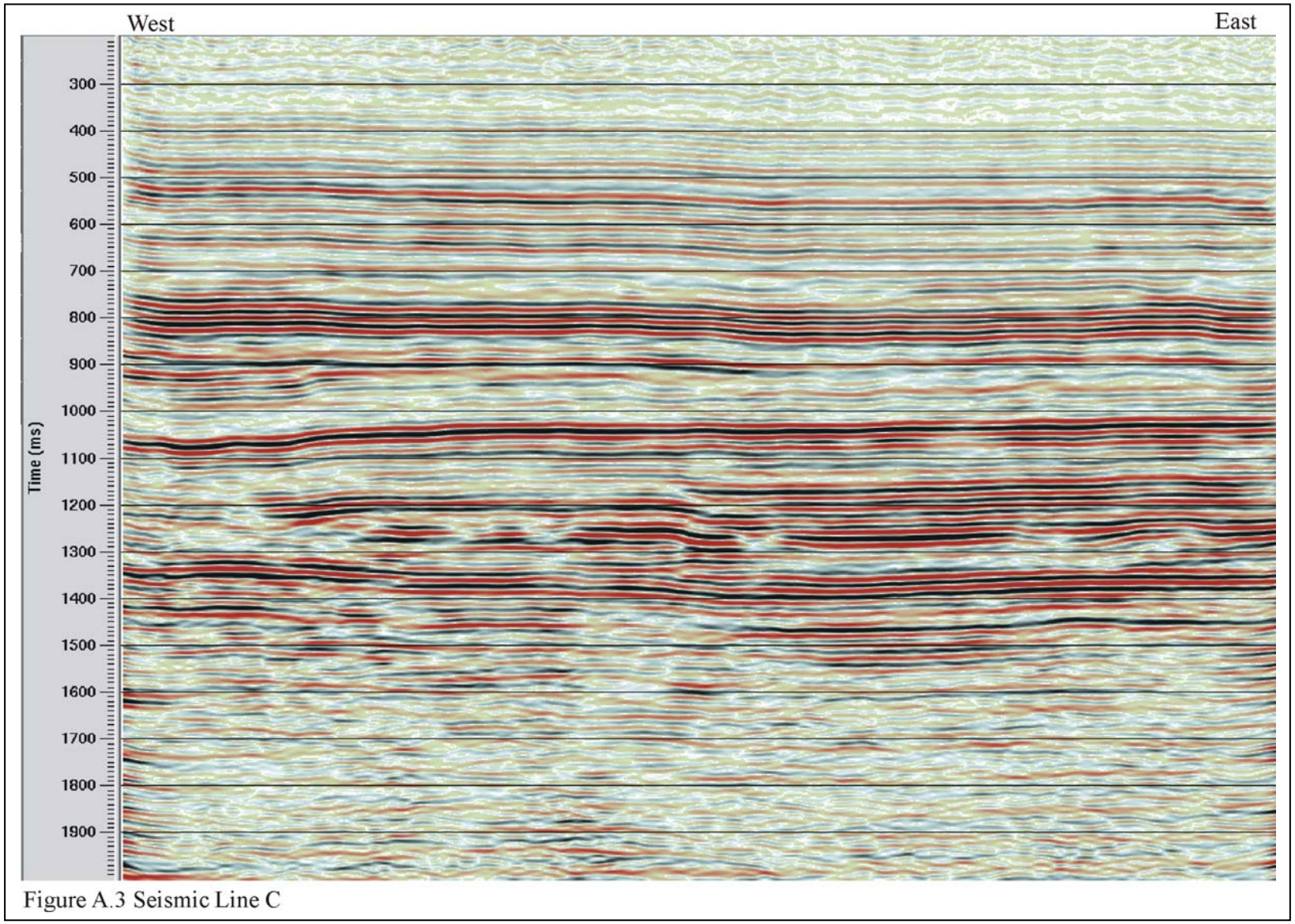

Figure A.3 Seismic Line C

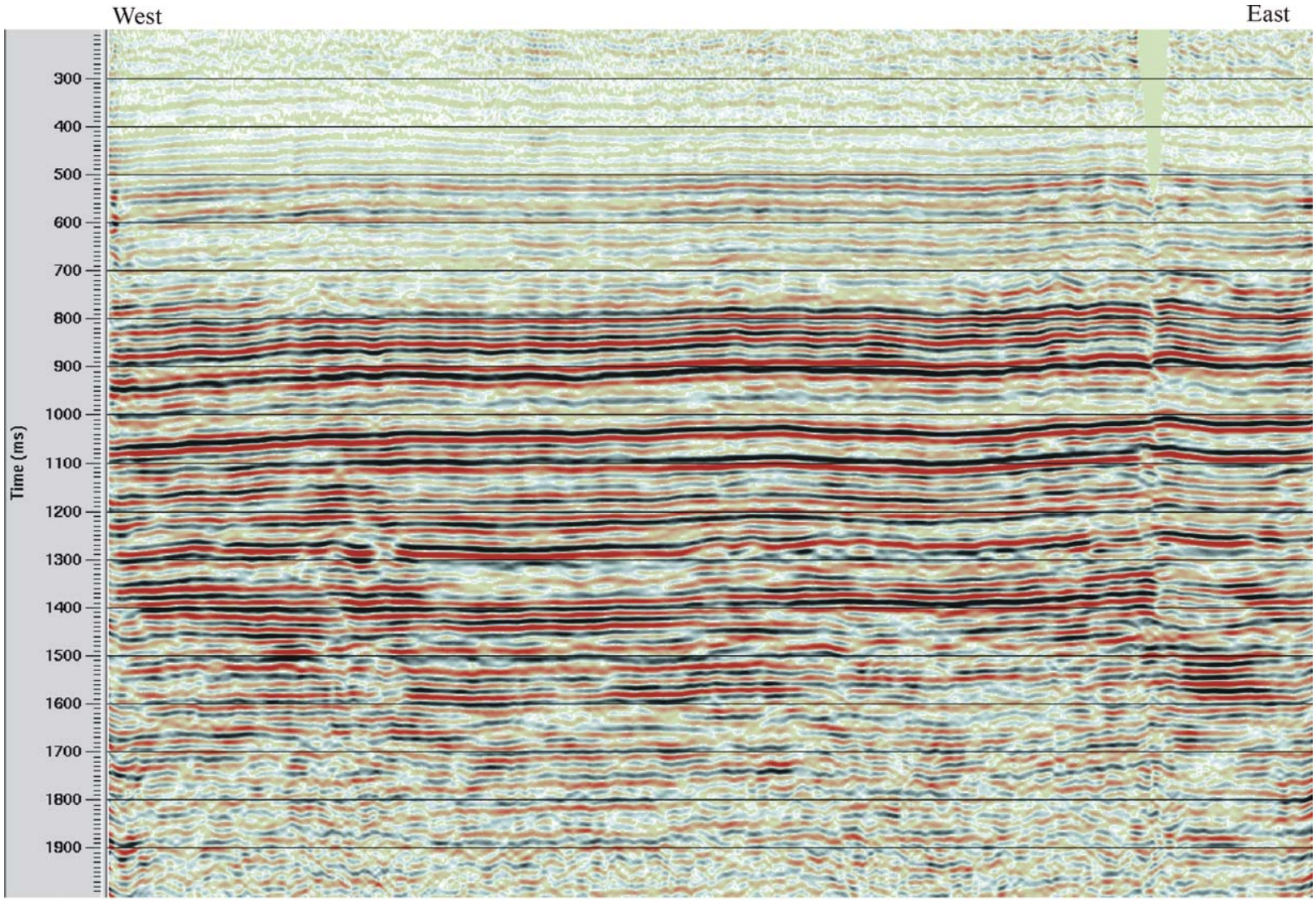

Figure A.4 Seismic Line D

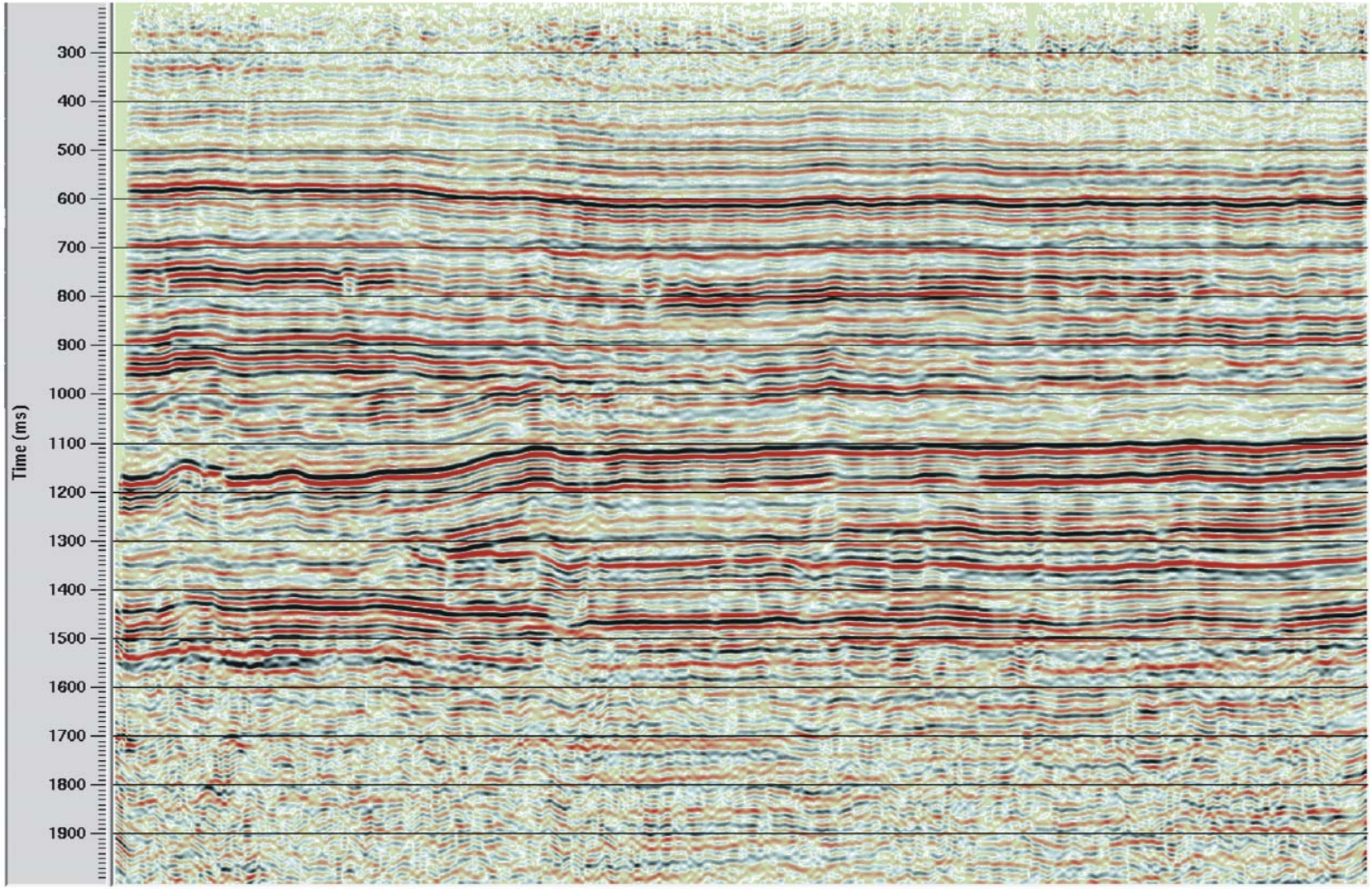

Figure A.5 Seismic Line E

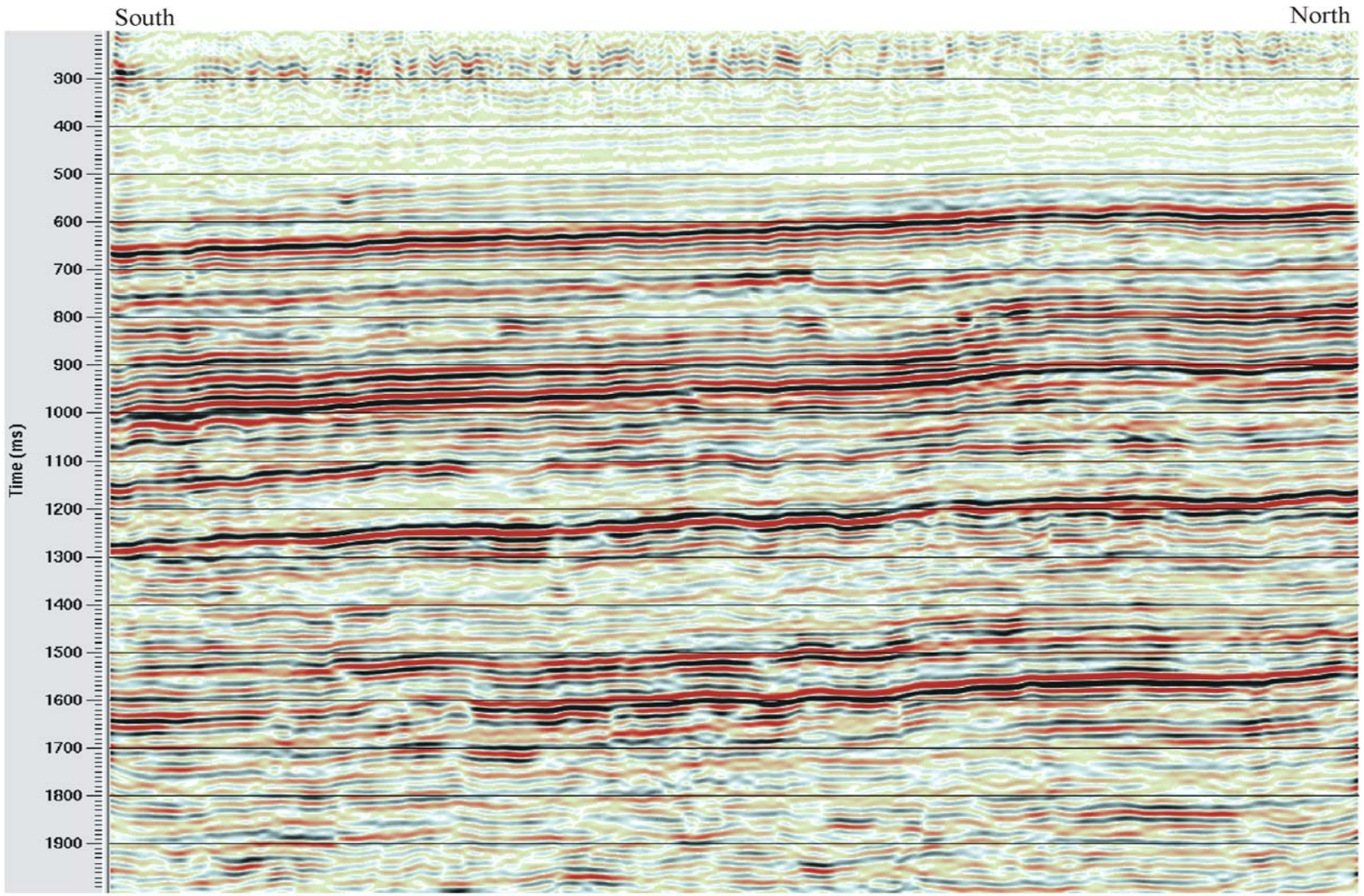

Figure A.6 Seismic Line F

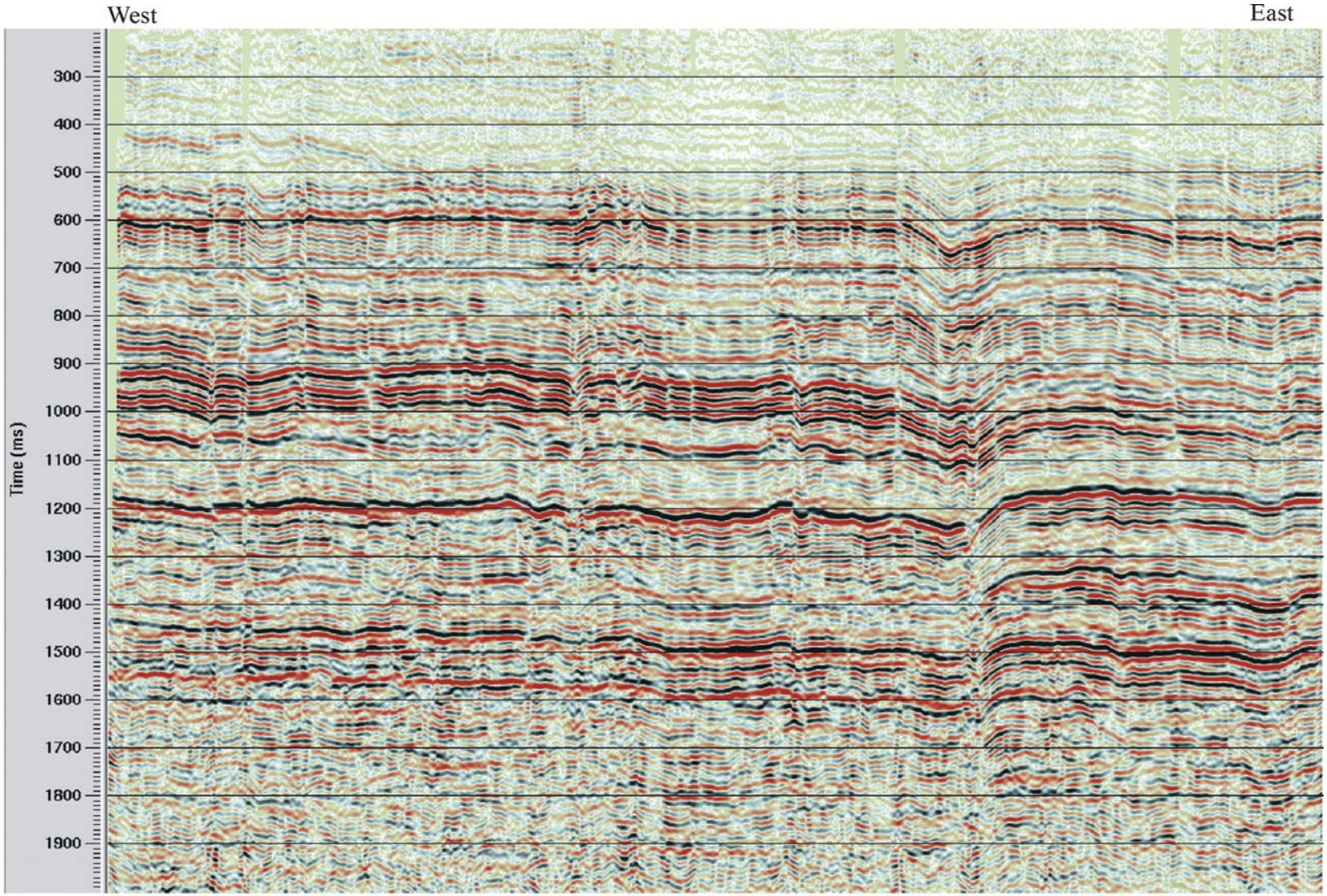

Figure A.7 Seismic Line G

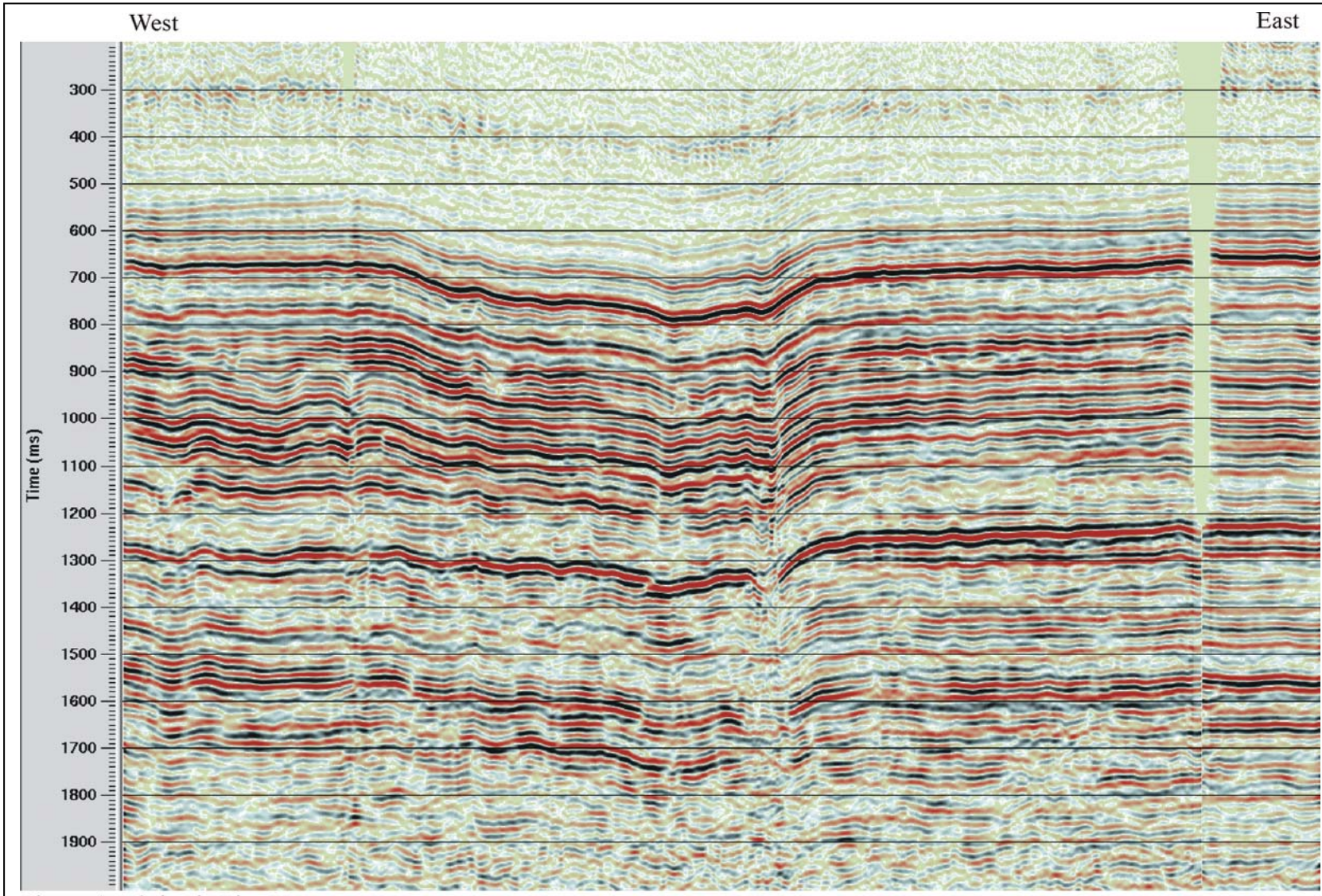

Figure A.8 Seismic Line H

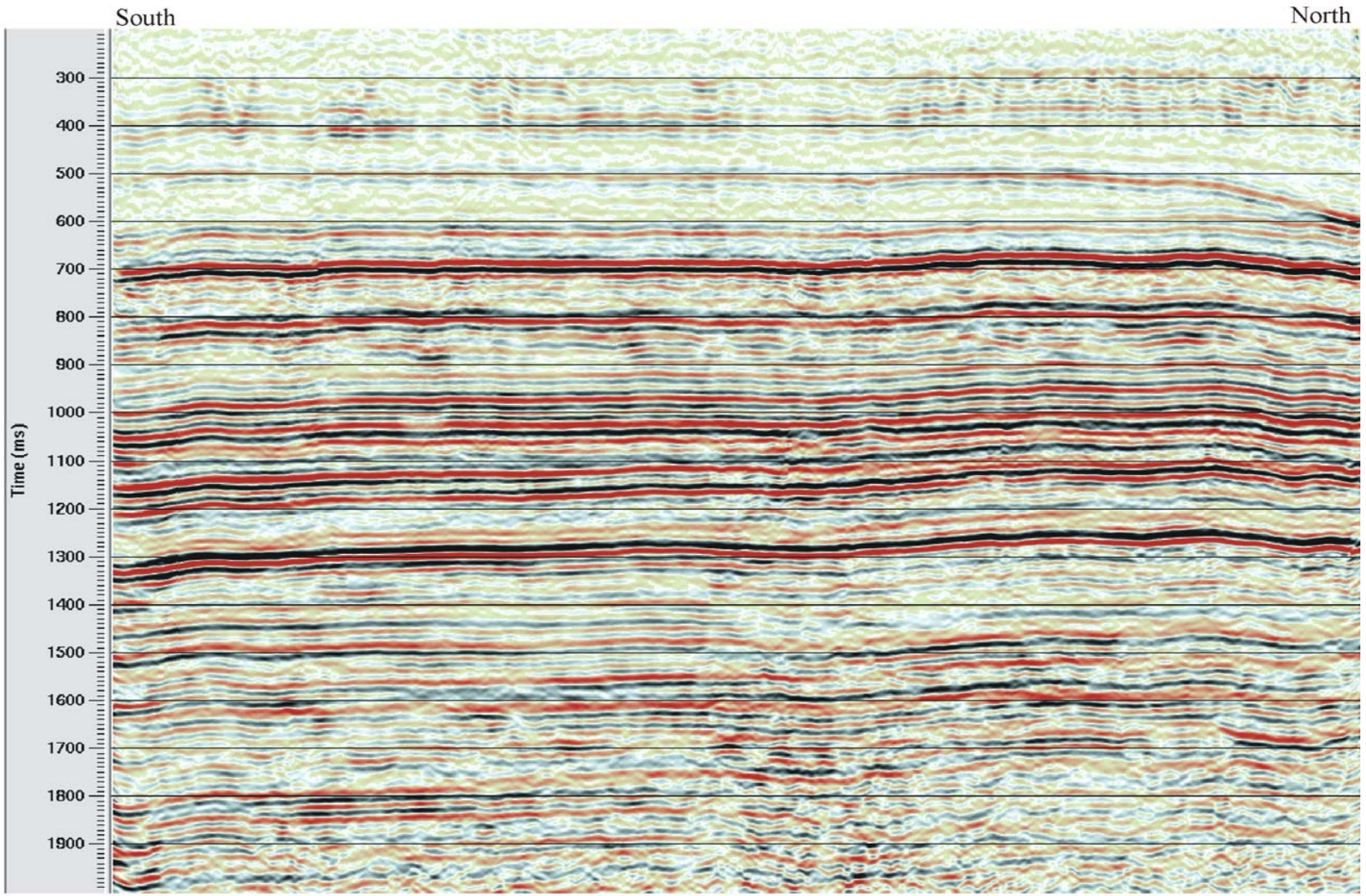

Figure A.9 Seismic Line I

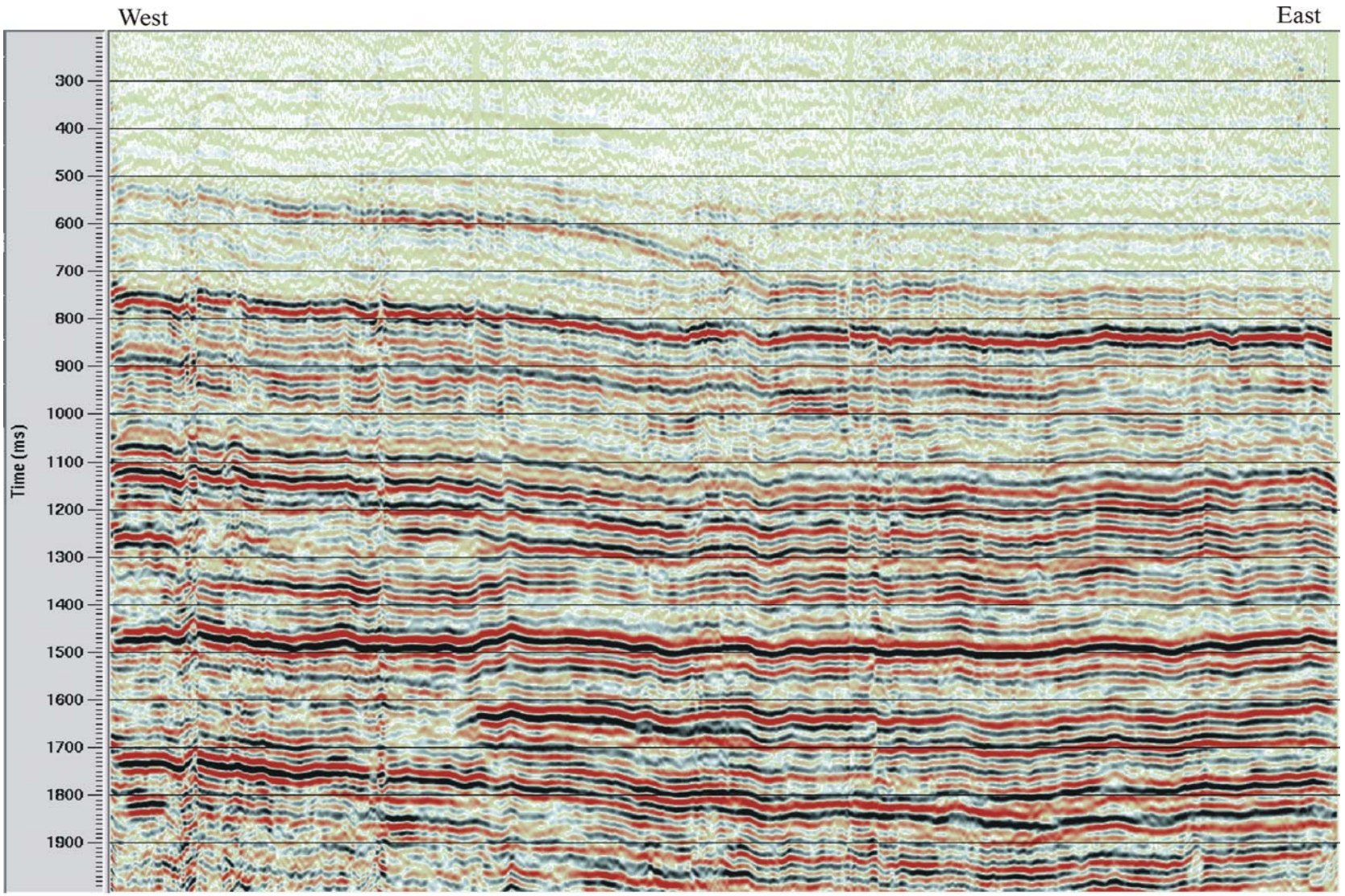

Figure A.10 Seismic Line J

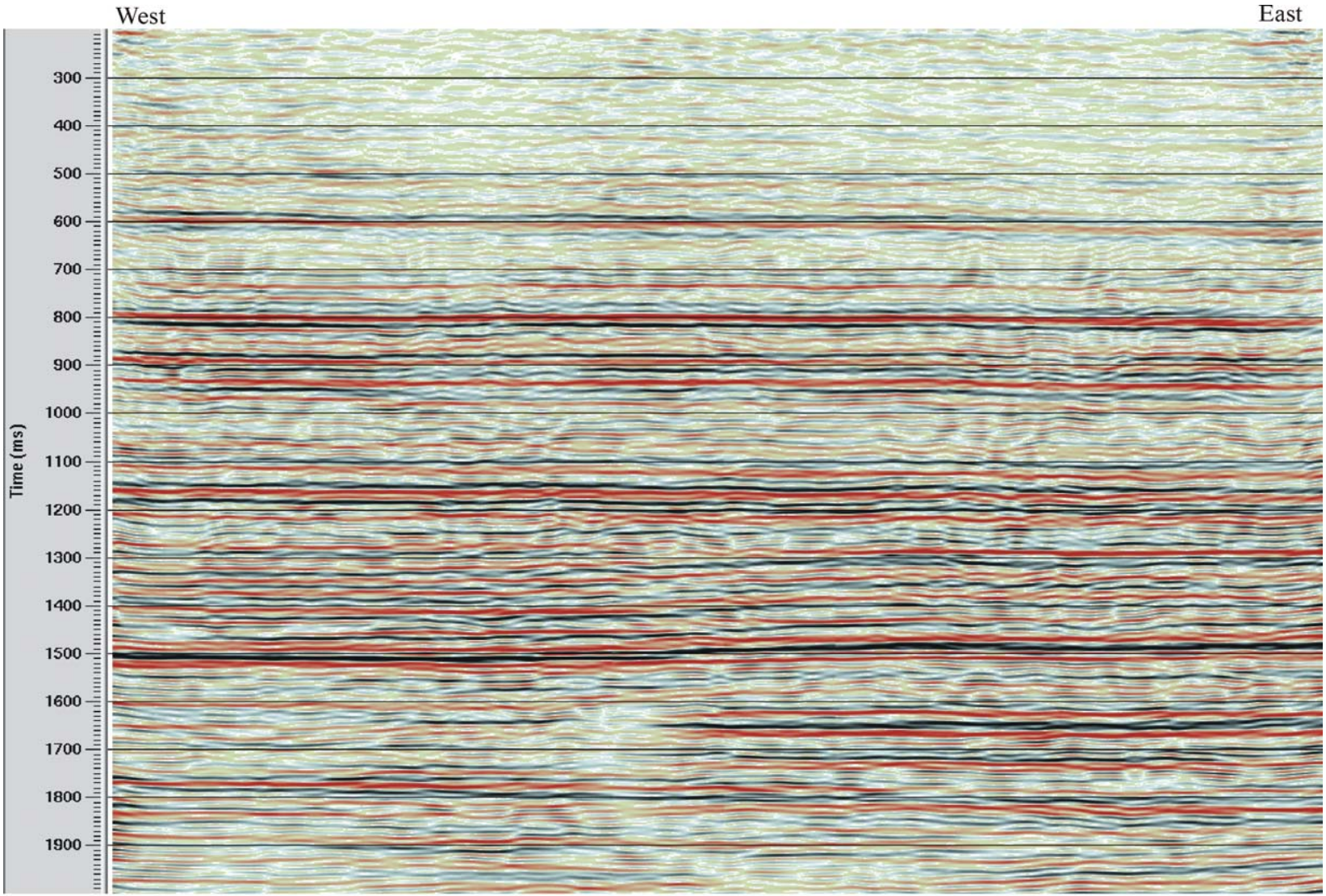

Figure A.11 Seismic Line K

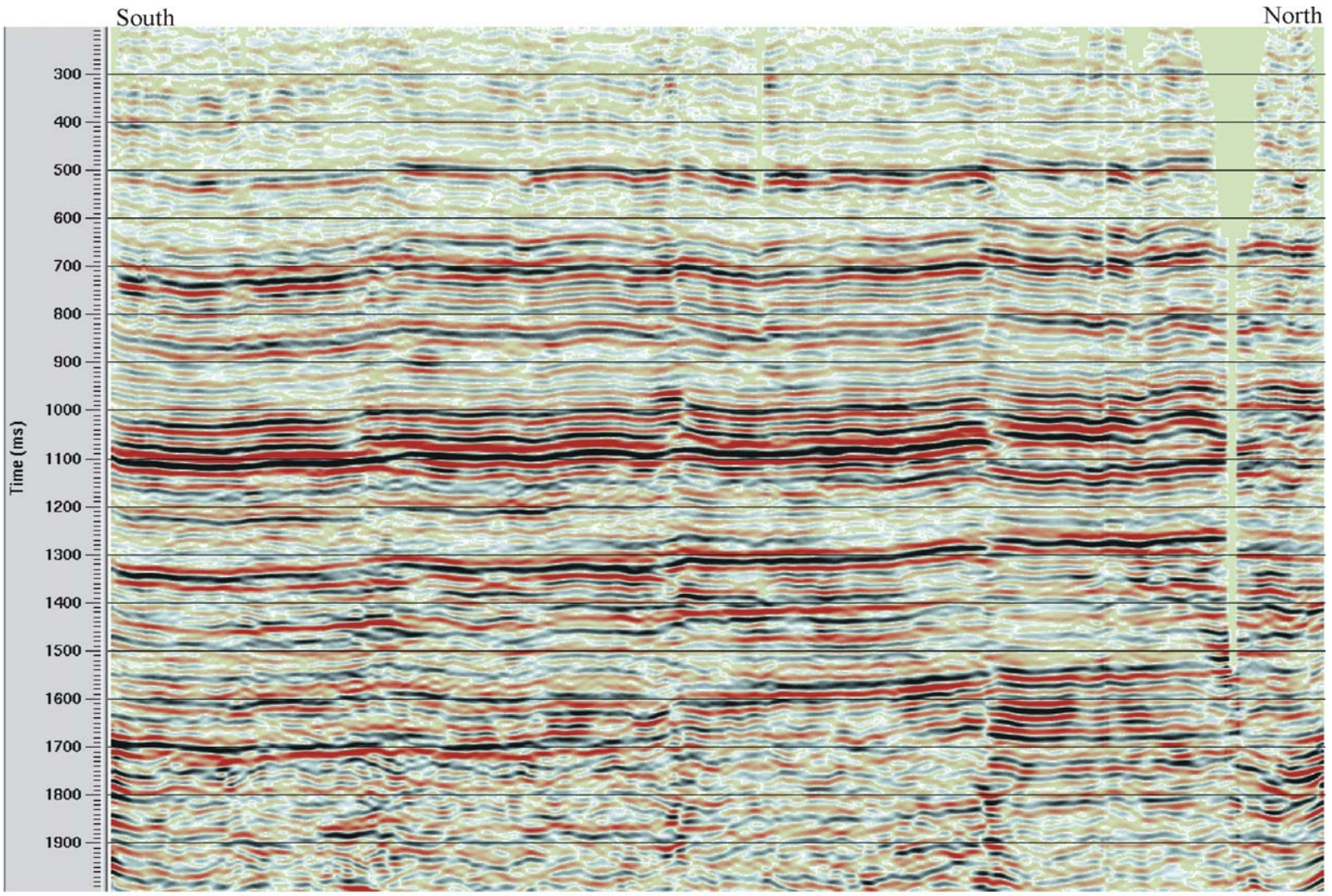

Figure A.12 Seismic Line L

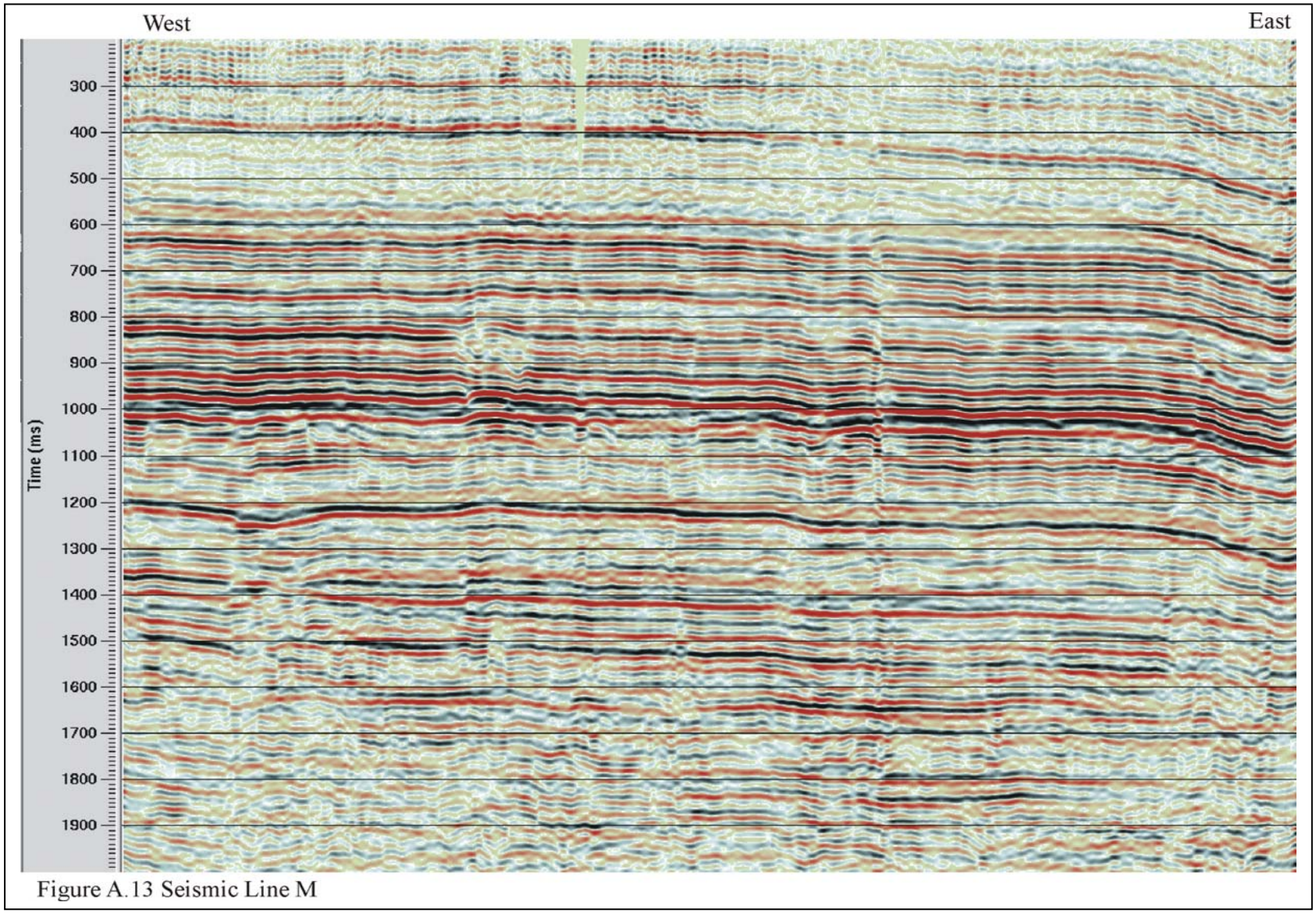

Figure A.13 Seismic Line M

APPENDIX B

TIME-VARIANT SPECTRAL WHITENING (TVSW) ALGORITHM

In the Time-Variant Spectral Whitening approach used in this work, a series of overlapping bandpass filters is first applied to a copy of each trace. Each of these filter panels has the same pass-band width specified by the user. In order to define four corner frequencies of each of these filter panels, the low-cut, high- pass and the high-cut frequencies have to be computed. The low-cut frequency is obtained by subtracting the panel width from the low-pass frequency which is defined by the user, while the high-cut frequency calculated by adding twice the panel width to the low-pass frequency. The high-pass frequency is obtained by adding the value of the panel width to the low-pass frequency. Once the four corner frequencies are defined for the first panel, the second panel is determined by shifting these frequencies by twice the panel width, and so on. In other words, the high cut ramp for the first panel will become the low-cut ramp for the second and so forth until the frequency window reaches the high-pass frequency which is defined by the user.

For example, with the following input parameters:

1) Low-pass frequency = 20 Hz.,
2) High-pass frequency = 90 Hz.,
3) Panel width = 10 Hz,

the following band-pass filter panels will be generated:

1) 10-20-30-40;
2) 30-40-50-60;
3) 50-60-70-80;

4) 70-80-90-100;

Within each of these frequency ranges, the trace is transformed into the frequency domain, multiplied by the filter response function, and transformed back into the time domain. These operations are performed by class FILTER in the code example below and result in a band-pass filtered copy of the trace.

Further, an Automatic Gain Control (AGC) is applied to each of the filtered traces. In order to apply AGC scalar, the average Root Mean Square (RMS).amplitude is computed within a given AGC window sliding along the trace. The program moves the window down the trace sample-by-sample and calculates the average amplitude at each location.

While applying the AGC, its scalars are also stored and summed in the end to produce a cumulative AGC scalar trace. To restore the true amplitude while equalizing the spectral amplitudes at any part of the trace, the resulting filtered and AGC'd traces are summed and multiplied by the AGC scalar. This procedure results in a record with the average amplitude-time dependence the same as in the original trace and the frequency spectrum approximately flat within any time window within the trace.

The implementation is based on the seismic processing package SIA developed by Prof. I. Morozov and relies on its parameter and data input/output, and also on data management and filtering functions. With minor modifications, the code currently uis included as a time-variant spectral whitening tool in this package (see http://seisweb.usask.ca/SIA/www/index/index.html). The C++ code of the module is shown below.

```
/*      tvsw_ep.C            */
/*************************************************************
      SIA - system for advanced seismic data analysis
```

```
      Copyright (c) 1995-2004, I. B. Morozov
*****************************************************************/

//#define DEBUG

#include "tvsw.h"

/*== initializer ===*/

extern "C"
{
void *tvsw_init( int active )
{
  return new TVSW;
}
}

/*== this function returns the name of the program for the GUI ===*/

CHARSTR TVSW::module_name( int active )
{
  if ( active )
  {
    read_params();
    return "Sample 1-trace process";
  }
  return "> tvsw <";
}

/*================================================================
      Constructor; reads the global parameter list
================================================================*/

TVSW::TVSW()
      : SIA_MODULE()
{
}

void TVSW::read_params()
{
  /*--- read parameters from the job file or GUI ----*/

  f1.read("F1",REAL);
  f2.read("F2",REAL);
  panelw.read("Panelw",REAL);
  agcw.read("AGCW",REAL);
}

/*================================================================
      Edit phase - called once to load the parameters of the tool
================================================================*/

int TVSW::edit()
{
```

```
  read_params();  // read module parameters
  return NORMAL_MODULE;
      // normal return status for a trace-in-trace-out module
}

/*****************************************************************
      SIA - system for advanced seismic data analysis
      Copyright (c) 1995-2003, I. B. Morozov
*****************************************************************/

//#define DEBUG

#include "sia_module.C.h"
#include  "filter/filter.h"
#include "tvsw.h"
#include "stdio.h"
#include "iostream.h"

boolean TVSW::proc(TRACE *t )
{
  // this obtains parameter value from t

  int ns = t->num_samples();        // number of trace data samples
  double si = t->sample_interval(), // sampling interval
       ts = t->time_start();

  DATA_SAMPLE     *d = t->data_start();
  TRACE_TRANSFORM trans(t);

//=============================================================
int i=0;
int AGCW = (int) agcw.value(t);
            // the average moving window in milliseconds

int Window=AGCW*2;  // number of trace data sample in the moving window

double  F1 = f1.value(t),
      F2 = f2.value(t),
      Panelw = panelw.value(t);

double lo_cut, lo_pass, hi_pass, hi_cut;
double *AGC = new double[ns];

//=============================================================

// initialize all elements in the AGC array to zero

for ( i=0; i<ns; i++)
      AGC[i] = 0;

double fPanelw=(F1-Panelw);   // obtain the low-cut Frequency
 if ( fPanelw < 0)            // in case of  panel width is
                              // larger than F1,
 fPanelw=fPanelw*(-1);        // get the low_cut Frequency
```

```
                              // as a positive value

while ( fPanelw < F2-Panelw)
{

  //====== make a Copy of the trace=============
      TRACE *tcopy = trans.copy();
      DATA_SAMPLE   *dcopy = tcopy->data_start();

  //==== Filter the copy============================

  lo_cut=fPanelw;
  lo_pass=lo_cut+Panelw;
  hi_pass=lo_pass+Panelw;
  hi_cut=hi_pass+Panelw; // obtain  four corner
                         //frequencies for each filter panel

  // build and apply the filter

  FILTER f( lo_cut, lo_pass, hi_pass, hi_cut);
  f.build(tcopy);
  f.apply(tcopy);

    //========= Apply AGC==========================

  ComputeAGC ( d, dcopy, AGC, Window, ns);

  fPanelw += Panelw*2;           //  frequency scaling factor
  delete tcopy;
}

  return OK;
}

void TVSW::ComputeAGC( DATA_SAMPLE *d, DATA_SAMPLE *dcopy,
                       double *AGC, int Window, int ns)
{
      double *S;
      S = new double[ns+1];
      S[0] = 0.0f;

      for(int i=0; i<ns; i++ )
            S[i+1] = S[i] + sqr(dcopy[i]);
                  //  this perfromes the summation of the square
                  //  value of each sample of the trace

  double factor;
  double Amp;
  int ws=0;

  for (int i=0; i < ns; i++)
  {
    Amp = sqrt( ( S[ws+Window]- S[ws]) / Window);
      // compute the RMS amplitude as the window moves down the trace
```

```
    if ( Amp > 1.0e-10 )
      AGC[i] += (double) dcopy[i] / Amp;   // apply  AGC factor

  d[i]=d[i]*Amp; //  restore the original  amplitude
  }

  if ( i > Window/2 && i < (ns-Window/2) )
           //The first and the last valid caculation of RMS amplitude
           //are extended to the ends of the trace.

   ws++;
  }
}


/*============================================================
      Process phase - called every time the
      system tries to produce an output
      (e.g., when there is a trace in the input gather)
============================================================*/

boolean TVSW::process()
{
  /*-- the following passes one trace from the input to
      the output gather and
      performs the required processing on it -----*/

  TRACE     *t = SIA.input()->pass_trace(SIA.output());

  return t ? proc(t) : FAIL;
}
```

APPENDIX C

ISOPACH MAPS OF THE PRAIRIE EVAPORITE FORMATION

Below, I present Prairie Evaporate isopach maps produced from the same well log data using the GMT *surface* program (Smith and Wessel, 1990) with spline tension parameter varying from 0.0 to 1.0 (Figures C1-4). Figure C5 shows an interpolated map using the recommended spline tension of 0.0 and incorporating all the available (well log and seismic) data.

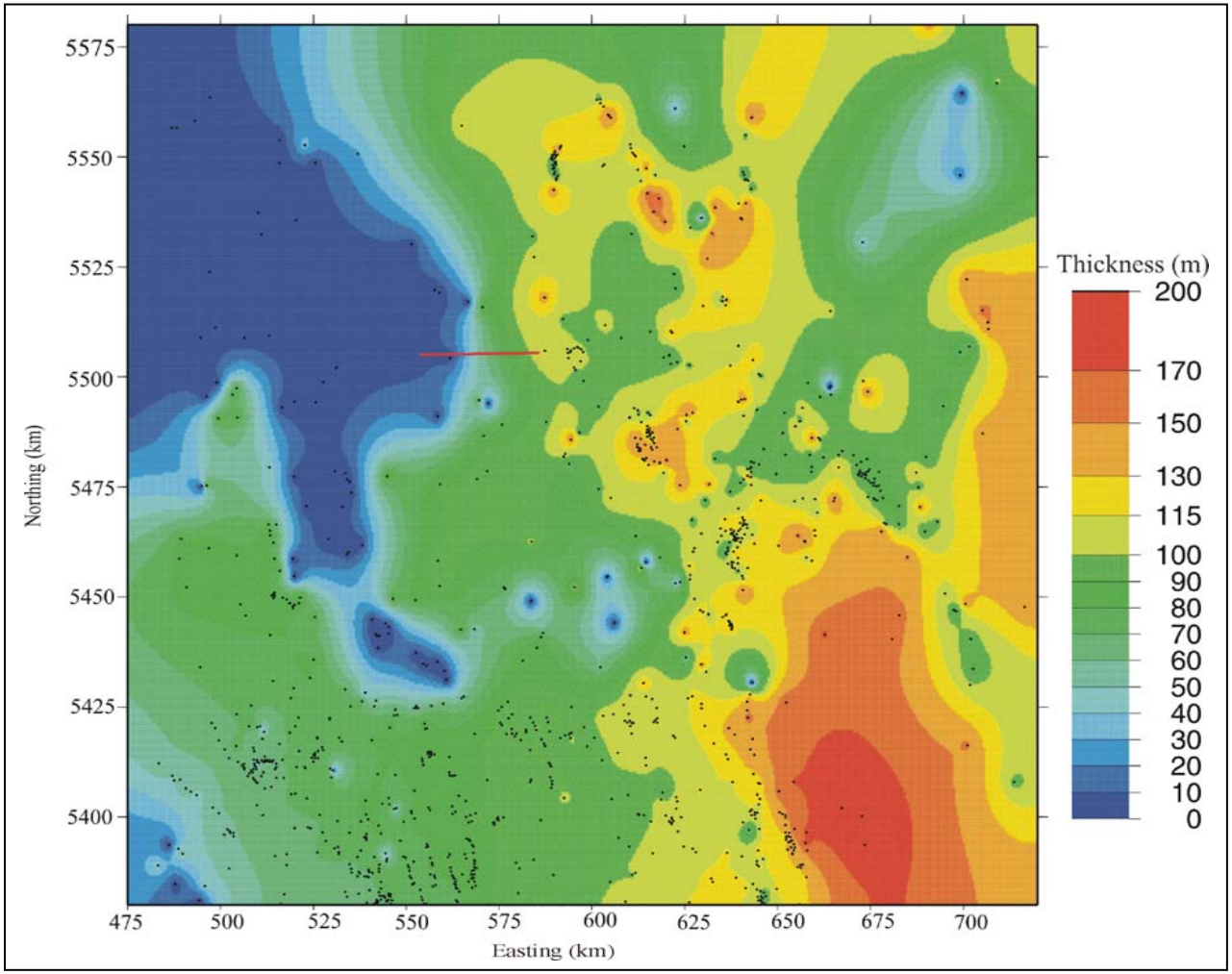

Figure C.1 Isopach map of the Prairie Evaporite Formation created using GMT (Smith and Wessel, 1990) with spline tension parameter T_B = 0.0. Black dots indicate the well readings used for interpolation, Coordinates are UTM in km; Red line indicates the location of seismic line E.

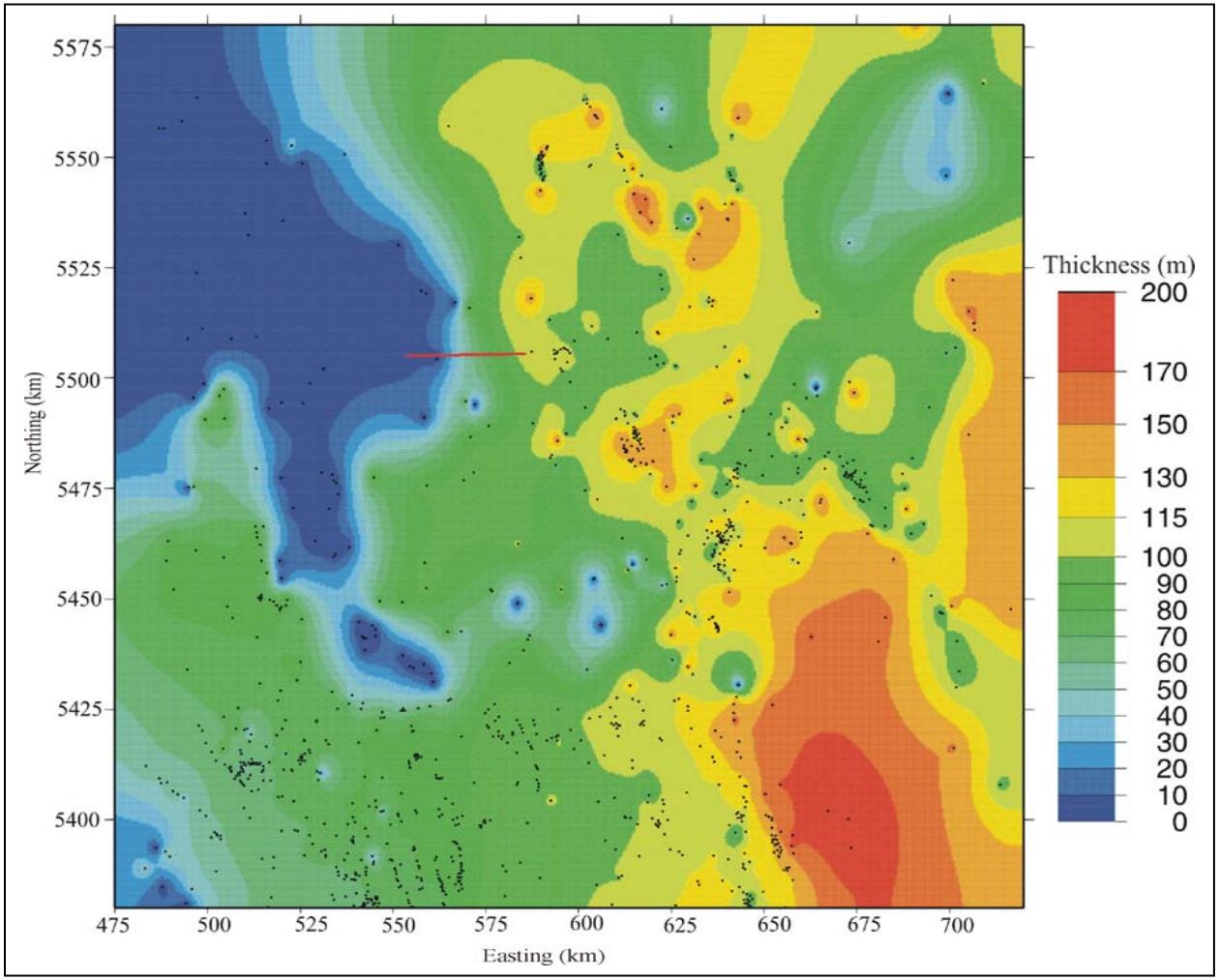

Figure C.2 Interpolated isopach map of the Prairie Evaporite Formation using GMT (Smith and Wessel, 1990) with spline tension parameter T_B = 0.5. Black dots indicate the well readings used for interpolation, Coordinates are UTM in km; Red line indicates the location of seismic line E.

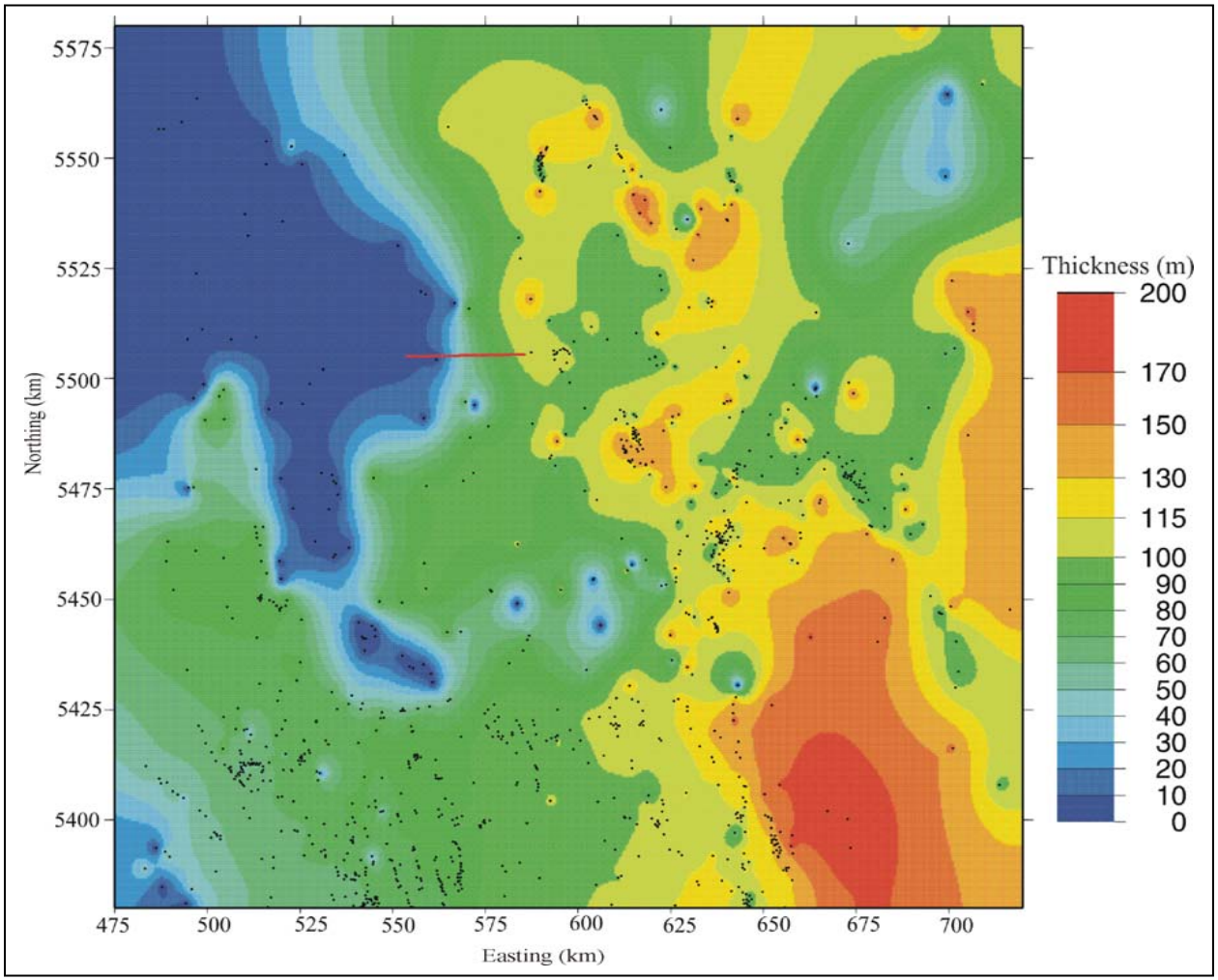

Figure C.3 Interpolated isopach map of the Prairie Evaporite Formation using GMT (Smith and Wessel, 1990) with spline tension parameter T_B = 0.75. Black dots indicate the well readings used for interpolation, Coordinates are UTM in km; Red line indicates the location of seismic line E.

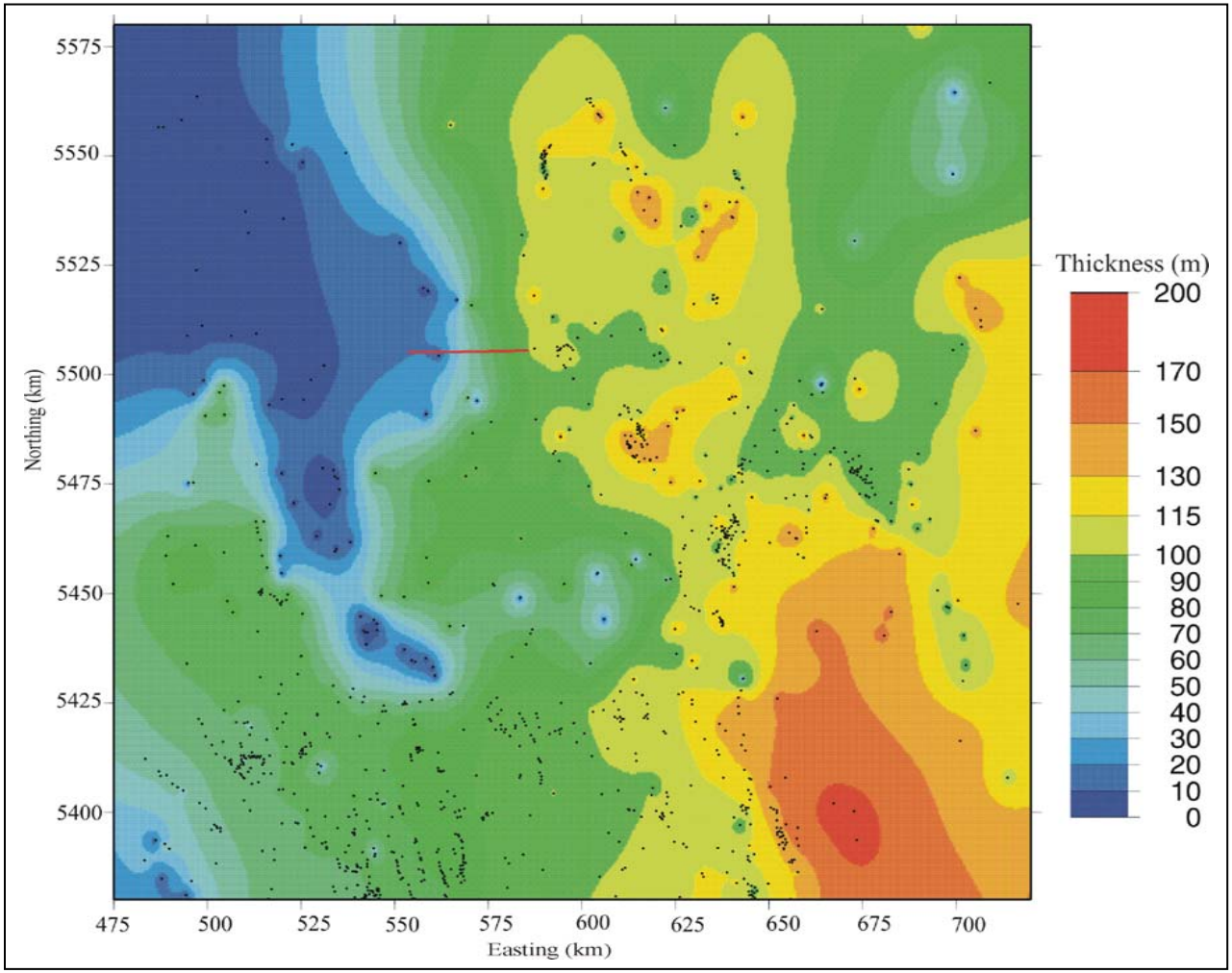

Figure C.4 Interpolated isopach map of the Prairie Evaporite Formation using GMT (Smith and Wessel, 1990) with spline tension parameter T_B = 1.0. Black dots indicate the well readings used for interpolation, Coordinates are UTM in km; Red line indicates the location of seismic line E.

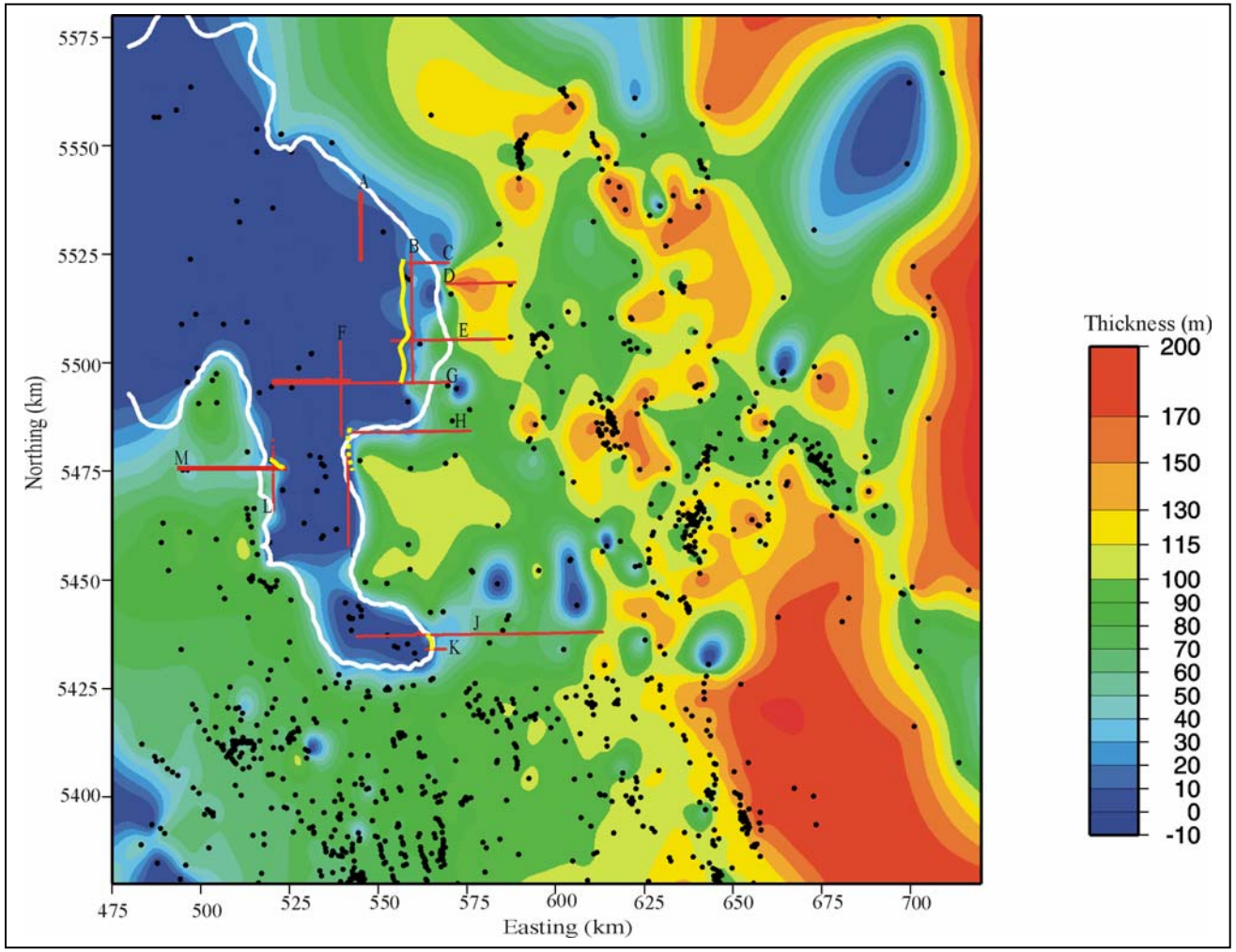

Figure C.5 Interpolated isopach maps of the Prairie Evaporite Formation using both well and seismic data. Yellow and white contours show the salt edge of the Prairie Evaporite interpreted in this study and Kreis et al. (2003), respectively. Note that the differences of this interpretation from the previous study not using the seismic data shown here. Coordinates are UTM in km.